Perception and memories in the fly brain

Dissertation

zur

Erlangung des Doktorgrades (Dr. rer. nat.)

der

Mathematisch-Naturwissenschaftlichen Fakultät

der

Rheinischen Friedrich-Wilhelms-Universität Bonn

vorgelegt von

Luigi Prisco

aus Tradate

Bonn, November 2021

Angefertigt mit Genehmigung der Mathematisch-Naturwissenschaftlichen Fakultät der Rheinischen Friedrich-Wilhelms-Universität Bonn

1. Gutachterin: Prof. Dr. Gaia Tavosanis
2. Gutachter: Prof. Dr. Walter Witke

Tag der Promotion: 14.01.2022
Erscheinungsjahr: 2022

Based on my doctoral studies, the following articles have been published:

Baltruschat*, L., **Prisco, L.***, Ranft, P.*, Lauritzen, J.S., Fiala, A., Bock, D.D., Tavosanis, G. (2021). Circuit reorganization in the Drosophila mushroom body calyx accompanies memory consolidation. Cell Rep. 34(11): 108871, doi: doi.org/10.1016/j.celrep.2021.108871

Luigi Prisco, Stephan Hubertus Deimel, Hanna Yeliseyeva, André Fiala, Gaia Tavosanis, (2021). The anterior paired lateral neuron normalizes odour-evoked activity at the mushroom body calyx. BiorXiv, doi: https://doi.org/10.1101/2021.09.20.461071

***Equal contribution**

Abstract

The brain is an extremely complex organ that controls thoughts, memories, motor skills and every process that is required to maintain our body alive and healthy. Although this is common knowledge, the mechanisms by which the brain performs these tasks are currently not fully understood.

In this thesis, I focused on how sensory information is represented in higher brain regions, and how these representations are used to create and consolidate memories related to them. Precisely, using *Drosophila melanogaster* as a model, I investigated the circuitry of the mushroom body calyx, the input region of a neuropil involved in stimuli discrimination and memory formation in the fly brain. In the calyx, olfactory projection neurons synapse onto mushroom body intrinsic cells, the Kenyon cells, via synaptic complexes known as microglomeruli. Each microglomerulus is a microcircuit of his own, constituted by a central projection neuron presynaptic bouton surrounded by several dendritic endings of different Kenyon cells. This structural organization is believed to facilitate stimuli discrimination by transforming highly overlapping representations at the level of the projection neurons into sparse, decorrelated responses at the Kenyon cells one. Moreover, structural changes at the microglomerular level following associative memory formation have been reported in insect brains over the years. Nevertheless, the exact processes underlying such phenomena have not been described yet.

Here, I show that memory consolidation induces structural plasticity in a stimulus-specific way in the calyx. Specifically, I found that the microglomeruli involved in the representation of the stimulus presented in the behavioural task increased in number after long-term memory formation. This increase in microglomeruli was protein synthesis dependent and strictly linked to the consolidation of the memory, as control flies and mutants unable to consolidate memories did not show structural changes within the same time frame.

Furthermore, in this thesis I analyse the role of inhibitory synapses in microglomeruli of the calyx. Inhibition at the mushroom bodies is provided by the APL neuron, whose presence is required to maintain Kenyon cells odour responses sparse, hence facilitating odours discrimination in the fly. Here, I show that via inhibitory and reciprocal synapses targeting both projection neurons boutons and Kenyon cells dendrites, APL normalizes odour-evoked representations in microglomeruli of the calyx. In particular, I observed that APL inhibition scaled with the inputs strength and localized to the regions where those inputs were located within the calyx, leading to more homogenous responses in Kenyon cells dendrites. I confirmed this hypothesis by inhibiting output from the APL, which led to more variable activities in Kenyon cells dendrites.

Altoghether, this thesis provides insights on how stimuli are processed, represented and used to create associative memories in the fly brain. As similar network organizations can be found in brains of other species including humans, I believe that the principles here described can be potentially applied to all brain regions sharing conformational features with the *Drosophila* mushroom body.

Table of Contents

Table of Figures

List of abbreviations

AL	antennal lobe
APL	anterior paired lateral neuron
ARM	anaesthesia resistant memory
AZ	active zone
Brp	Bruchpilot
CaM	calmodulin
cpEGFP	circular permutated enhanced GFP
CS	conditioned stimulus
cVA	cis-Vaccenyl Acetate
DAN	dopaminergic neuron
DLG	discs-large
ECFP	enhanced cyan flurescent protein
EYFP	enhanced yellow fluorescent protein
EM	electron microscopy
FAFB	female adult fly brain
FIB-SEM	focussed ion beam scanning electron microscope
FRET	Förster Resonance Energy Transfer
GABA	gamma-Aminobutyric acid
GECI	genetically encoded calcium indicator
GFP	green fluorescent protein
GGN	giant GABAergic neuron
Goc	Golgi cell
Grc	granule cell
KC	Kenyon cells
LTM	long-term memory
LTP	long-term potentiation
MB	mushroom body
MBON	mushroom body output neuron
MF	mossy fiber
MG	microglomerulus

MTM	mid-term memory
ORN	olfactory receptor neuron
PC	Purkinje cell
PN	projection neuron
PSD	post-synaptic density
RNAi	RNA interference
Syp	Synaptophysin
STM	short-term memory
TEM	transmission electron microscope
UAS	upstream activating sequence
US	unconditioned stimulus

1 Introduction

Odours can act like time machines. In my case, it is the smell of petrol that does it: road trips with my family, holidays, my first motorcycle and the sense of freedom that came with it, my first car. All these memories instantly popping up in my mind every time I come across that particular scent. We all have some sort of memories related to a particular odour, and it is interesting how such a simple phenomenon can be investigated by several different angles. A psychologist might ask why those particular recollections and not others, a chemist may want to know why petrol smells like petrol, whereas a neuroscientist like me will be more interested in how our brain is able to create associations between simple sensory stimuli as odours with complex notions such as emotions or episodes, and maintain these relationships stable over time.

More precisely, this question can be broken down in two more specific ones: how is our brain able to detect, represent and recognize a particular stimulus, even when the surroundings change? And how are memories related to that particular stimulus formed and maintained in the brain? These questions are as old as the neuroscience field itself and the aim of this thesis was to provide one further step towards the understanding of how organisms perceive and interact with the world around them.

1.1 Sensory representation in the brain

Sensory, proprioceptive and motor information is represented in the brain via firing patterns of neuronal populations. Typically, the path of information towards the brain starts at the periphery with reception. Here, sensory signals are detected and transduced to electrical impulses via specialized sensory neurons. From this point, electrical impulses in the shape of action potentials travel through neuronal layers until they reach their destination in the brain. Crucially, the code representing a specific stimulus is not invariant while being transmitted from one neuronal layer to the next one. Neuronal representations are typically dense and highly

overlapping at the periphery, reflecting rich and often similar inputs that are characteristic of natural environments. To make sense of this high amount of information and provide the ability to identify subtle changes in the external word, the brain must distinguish between similar patterns of neuronal activity. This is achieved by minimizing the overlap between patterns of neuronal activity while the information moves toward higher brain regions, through a process defined as "pattern separation" (Figure 1A) (Santoro, 2013). The concept of pattern separation applied to neuronal networks was already introduced by early independent work from theoretical scientists David Marr and James Albus, into what is nowadays referred as the Marr-Albus theory (Albus, 1971; Marr, 1969). The two were investigating the circuitry of the cerebellar cortex input layer, and concluded that the overlap between activated neurons is reduced by projecting activity patterns coming from the input mossy fibers onto a much larger population of sparsely active granule cells. Of notice, stimuli representation by sparse coding, where each stimulus evokes responses in only a small subset of the total neurons (Figure 1B), can be found in both vertebrates and invertebrates sensory systems (Hahnloser et al., 2002; Hromádka et al., 2008; Isaacson, 2010; Laurent, 2002; Rolls & Tovee, 1995; Turner et al., 2008b; Vinje & Gallant, 2000; Wolfe et al., 2010), and is thought to increase the storage capacity of associative networks, thereby supporting learning and classification tasks in otherwise noisy systems (Huerta et al., 2004; Jortner et al., 2007; Kanerva, 1988; Perez Vicente & Amit, 1989; Tsodyks & Feigel'man, 1988).

Since the formulation of the Albus-Marr theory, a great amount of theoretical work in support of it has been published (Babadi & Sompolinsky, 2014; Billings et al., 2014; Cayco-Gajic et al., 2017; Litwin-Kumar et al., 2017; Sahay et al., 2011; Schweighofer et al., 2001; Tyrrell & Willshaw, 1992). However, experimental evidence in support of these models in brain regions like the cerebellum is often lacking due to technical limitations when studying large neuronal populations in awake animals. Nevertheless, newly

developed methodologies such as two-photon microscopy, genetically encoded calcium indicators and semi-automated electron microscopy (EM) imaging/analysis are providing the tools to overcome such technical difficulties and, in this work, we were set to generate experimental data on how stimuli are efficiently discriminated in neuronal networks performing pattern separation.

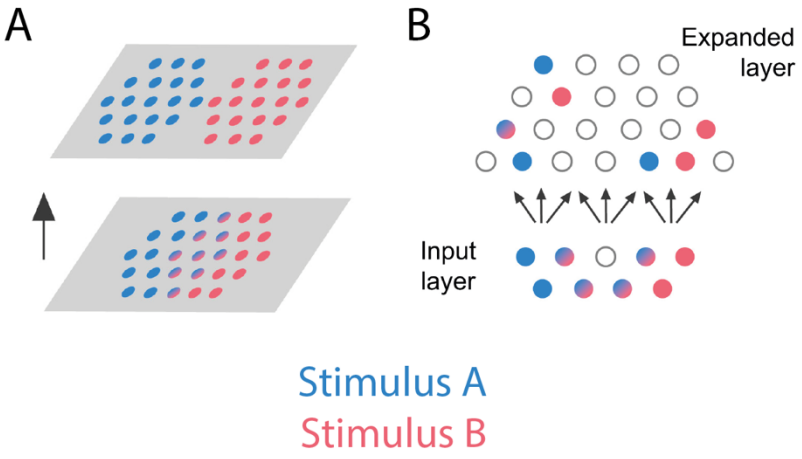

Figure 1. Pattern separation and sparse representations facilitate stimuli discrimination
A) Pattern separation: reducing the overlap between representations facilitates the brain to distinguish between similar patterns of activity. B) Schematic view of sparsening in sensory networks. Dense, overlapping representations are projected onto a larger population of sparsely active neurons, leading to reduced overlap and increased storage capacity of the network. Image adapted from Cayco-Gajic & Angus Silver, 2019.

1.2 The cerebellum

As mentioned above, the Marr-Albus theory was formulated based on features of the cerebellar cortex input layer. The cerebellum (latin for "little brain) is a major feature of the hindbrain of vertebrates (Figure 2A) (Hodos, 2009). In humans, it contains up to 80% of the total brain neurons (Herculano-Houzel, 2010). The cerebellum is classically considered to be involved in associative motor learning and motor control (Brooks et al., 2015; Wolpert et al., 1998), although recent work points to its role in non-motor cognitive functions as well (Buckner, 2013; Petersen et al., 1988).

From an anatomical point of view, the cerebellum can be divided into three cortical layers composed of highly regular arrays of neuronal units involving

five different cellular types (Figure 2B) (Apps & Garwicz, 2005; Roostaei et al., 2014). Purkinje cells are the most represented cell type and constitute the output neurons of the cerebellar cortex. Their cell bodies lay in the medial region of the cortex, hence referred to as the Purkinje layer, whereas their complex dendritic trees arborize in the level above, the molecular layer. The third cortical stratum, the granular layer, localizes below the Purkinje layer and is populated by granule cells and Golgi interneurons. The granular layer represents the input region of the cerebellum, as granule cells receive sensory and motor information directly from the afferent mossy fibers. Granule cells in turn project their axons to the molecular layer, where they bifurcate into parallel fibers and innervate dendrites of the Purkinje cells. The last cell type constituting the cerebellar cortex are the climbing fibers, which arise from the inferior olive in the caudal stem (Brodal & Kawamura, 1980) and make direct synapses with the Purkinje cells.

As the purpose of this thesis is to investigate perception and stimuli discrimination, I will particularly emphasize on the input component of the circuitry briefly described in this chapter, as this is the layer where highly correlating inputs are transformed into distinct representations.

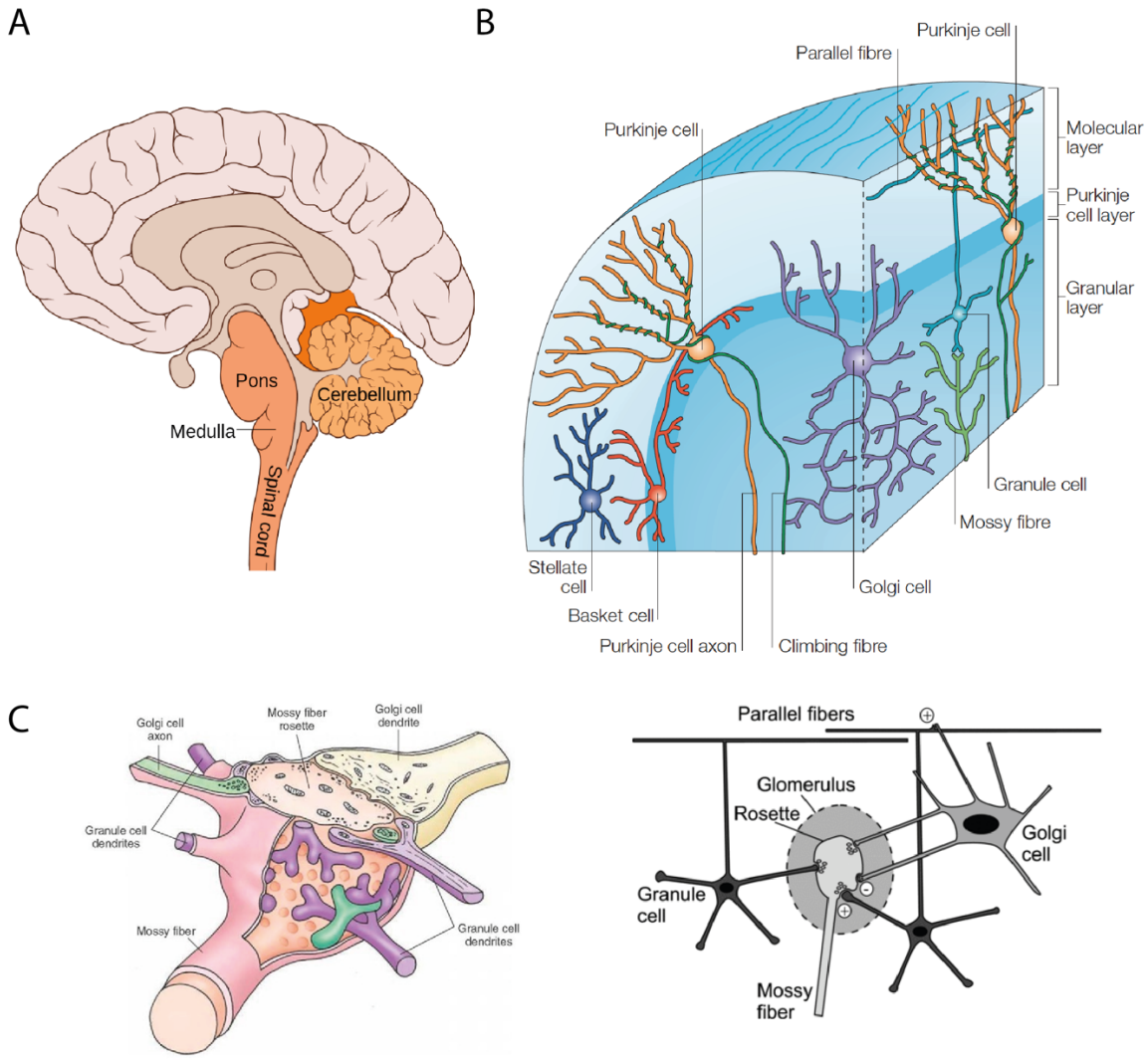

Figure 2. The cerebellar circuitry
A) The hindbrain is constituted by three main regions: pons, cerebellum and medulla oblongata. Image credit: Patrick J. Lynch, medical illustrator. B) Circuitry of the cerebellar cortex: The ascending axons of the granule cells, which receive input from the mossy fibers in the granular layer, branch in a T-shaped manner to form the parallel fibers. The latter, in turn, make excitatory synaptic contacts with Purkinje cells in the molecular layer. Purkinje cells also receive direct input from afferent climbing fibers. The circuitry is then completed by interneurons such as Golgi cells in the granular layer, stellate cells in the molecular layer and Basket cells in the Purkinje layer. Image adapted from Apps and Garwicz, 2005. C) Realistic (left) and schematic (right) drawings of the glomerular organization in the cerebellar cortex. Adapted from: what-when-how.com, Cambridge University press.

1.2.1 The cerebellar input layer: glomeruli and pattern separation

Theoretical work based on the Albus-Marr theory confirmed that the cerebellar cortex is well suited for pattern separation (Billings et al., 2014; Cayco-Gajic & Silver, 2019; Kanerva, 1988; Litwin-Kumar et al., 2017;

Tyrrell & Willshaw, 1992). In brief, these studies provided three requirements that a network needs to fulfil in order to perform pattern separation efficiently: *i*) expansion, in terms of number of units, from the input population onto the next layer´s "expanded population"; *ii*) sparse connectivity between the input and the expanded population; *iii*) presence of broad inhibition (Cayco-Gajic & Silver, 2019). Granule cells are the most abundant neurons in the vertebrate brain and therefore outnumber the mossy fiber population (ALTMAN & J., 1997). In the rat, around 7,000 mossy fibers and 209,000 granule cells are estimated to be presynaptic to a single Purkinje cell (Harvey & Napper, 1991; Tyrrell & Willshaw, 1992), for an expansion ratio, defined as number of units from the input population divided by the number of units in the expanded population, of 30 (Litwin-Kumar et al., 2017). Regarding the connectivity among these two cell types, mossy fibers afferents deliver sensory and motor information to the granule cells via synaptic structures known as cerebellar glomeruli in the granular layer (Figure 2C) (Arenz et al., 2008; Powell et al., 2015). In each glomerulus, single mossy fibers "en passant" presynaptic glutamatergic boutons (rosettes) (Cajal & Ramón y Cajal, 1909; Silver et al., 1992) are surrounded by several granule cells dendritic enlargements (claws) (Hámori & Somogyi, 1983). Each granule cell dendrite contacts different glomeruli, receiving inputs from different mossy fibers. However, the connectivity structure remains sparse, as every granule cell receives synaptic input from only four mossy fibers, on average (Eccles et al., 1966). Finally, inhibition is provided by Golgi cells, which participates in the glomerular structure with both dendrites and axons. Golgi cells receive excitatory synapses from granule cells in the molecular layer as well as from mossy fibers in the glomeruli at the granular layer, therefore inhibiting granule cells both via feedback and feedforward loop mechanisms (Duguid et al., 2015; Hámori & Somogyi, 1983; Vos et al., 1999).

Overall, the result of this glomerular connectivity is that stimuli representations are less overlapping and more decorrelated at the

expanded population level compared to the input one. Although this has been confirmed by substantial theoretical work on the cerebellar network, supporting experimental evidence has been lacking due to technical limitations. Additionally, recent experimental data obtained via state-of-the-art methodologies challenged some of these long-assumed dogmas (Gilmer & Person, 2018; Kawato et al., 2021). In other words, the mechanisms allowing for stimuli discrimination in the cerebellum is still under debate. Fortunately, the cerebellar cortex is not the only case of neuronal network performing patter separation. Indeed, nature offers other examples such as the dentate gyrus and the insect mushroom body. The latter, for a number of reasons that will be explained in detail in the next chapter, represents the most suitable system to generate experimental data on pattern separation and shine some light on the mechanisms by which stimuli discrimination is made possible.

1.3 *Drosophila melanogaster* as a model organism

Since its introduction to the field of biology by Thomas Hunt Morgan in the early 20th century, the fruit fly Drosophila melanogaster represents one of the most used animal models. There are several reasons why Drosophila was and is widely appreciated as a model. Some are purely practical reasons such as its ease of culture and manipulation, short generation time, small size and low cost of maintenance. *Drosophila*'s generation time is indeed around 10-12 days at 25 C. Female flies can lay up to 100 eggs/day, which will then go through three larval and a pupal stage before eclosing as adults. Finally, *Drosophila* stocks are usually harvested in either small tubes or large bottles containing enough food to supply each step of their life cycle.

Despite all this, however, the main reasons why the fly is such a powerful organism for research, especially in the field of neurobiology, is represented by its genetics and a simplified circuitry compared to higher organisms. Drosophila has a relatively simple genome, constituted by only 4 pairs of chromosomes: the X/Y sex chromosomes plus the autosomes 2, 3 and 4.

The genome of the fly is non-redundant, with about 165 million bases encoding for approximately 14,000 genes. On top of this, an incredibly high number of genetic tools, some of which are discussed later in this chapter, are available for *Drosophila*, allowing for specific expression of any transgenes of interest in any desired cellular target. Last but not least, the *Drosophila* brain is constituted by only ~100,000 neurons (Alivisatos et al., 2012; Raji & Potter, 2021), largely reconstructed at the EM Level (F. Li et al., 2020a; Zheng et al., 2018), hence representing one of the most powerful and comprehensive sources to investigate neuronal circuits and their functions.

1.3.1 Targeting specific cells: binary expression systems

In order to understand the function of specific cells, genes or genetic products, spatial and temporal control of transgenes expression is essential. Ectopic genes expression can be used to introduce fluorescent molecules and other reporter transgenes in a specific target, to overexpress or downregulate a particular gene via RNAi, to express cellular activators or inhibitors and various other applications. In *Drosophila*, the most common way to induce expression is via binary expression systems, such as the GAL4/UAS from *Saccharomyces cerevisiae* (Brand & Perrimon, 1993), *Escherichia coli´*s LexA/LexAop (Brent & Ptashne, 1985) and the Q-system from *Neurospora crassa* (Bello et al., 1998). All three systems share the same rationale: a transcriptional activator is able to bind DNA in presence of the respective effector sequence and drive transcription by itself (Figure 3A). Additionally, suppressors of the activator, as well as suppressors of the suppressor itself, can be introduced in the system to allow for a more precise control of the transgene expression (e.g., to restrict expression in a specific time window during development).

Typically, to induce ectopic genes expression in a selected cellular target, a transgenic driver line expressing the transcriptional activator in a characterized pattern is crossed to a second transgenic line carrying the transgene under the effector sequence. The progeny of such a cross will

express the transgene of interest wherever the activator is expressed (Figure 3B). Collections of transcriptional driver lines, each expressing the activator in a determined subset of cells, as well as lines carrying diverse transgenes under regulatory sequences are normally accessible via *Drosophila*'s stock centres spread around the world or by the laboratory that generated them upon specific request.

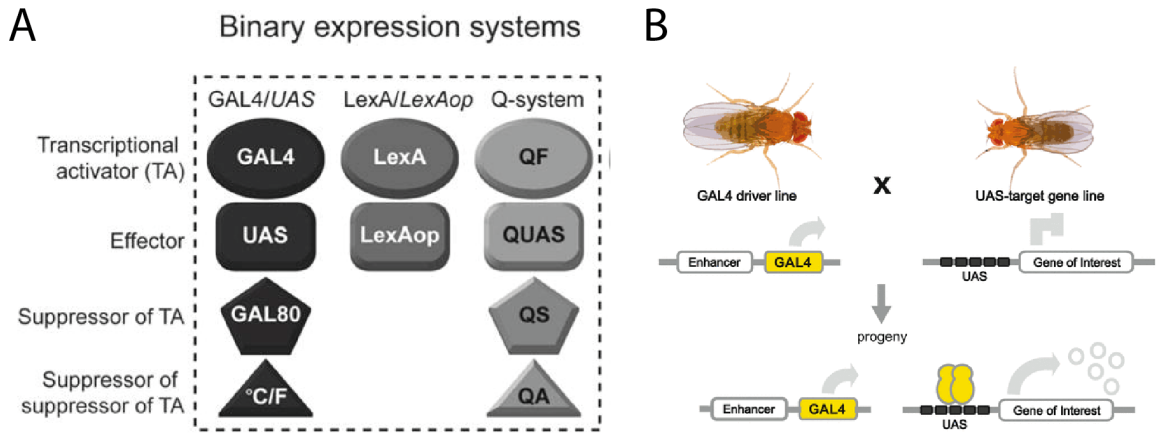

Figure 3. Binary expression systems in the fly
A) The most common expression systems used in Drosophila are represented in this scheme. Each system consists of a transcriptional activator, an effector sequence and additional suppressors, which can be in turn suppressed to allow for temporal control of the transgenes expression. Image adapted from Riabinina and Potter, 2016. B) example of targeted transgene expression using the GAL4/UAS system. GAL4 driver and UAS-transgene fly lines are generated and maintained as separate living stocks. Crossing a fly expressing GAL4 to a fly carrying a UAS-target genes results in targeted gene expression in the progeny of the cross. Image adapted from Caygill and Brand, 2016.

1.3.2 Tools to investigate neuronal functions in the fly

Fluorescent proteins

The use of fluorescent proteins as a marker in molecular biology was introduced by Martin Chalfie and colleagues in 1994 with their work on the Green Fluorescent Protein (GFP) for which they have been awarded with the 2008 Nobel Prize in Chemistry (M et al., 1994). GFP is a 238 amino acid protein isolated from the jellyfish Aequorea Victoria and characterized by the fact of being excited in the blue light range (excitation peak at 395 nm) while emitting at higher wavelengths in the green range (emission peak 509 nm). Nowadays, a large pool of optimized and alternative versions of Chalfie´s original GFP is available (Shaner et al., 2004), including red-

shifted fluorophores such as tdTomato (excitation peak: 554 nm, emission peak: 581 nm) or mCherry (excitation peak: 587 nm, emission peak: 610 nm), allowing for simple and inexpensive labelling of multiple targets within the same organism.

Protein-tags

To investigate specific proteins localization and modifications with subcellular resolution, fluorescent molecules are often fused to proteins of interest thus creating fluorescent tags. In *Drosophila*, several transgenic lines containing protein-tags are commercially available. Typically, these lines fall in two main categories: *i*) lines where an additional transgene, encoding for a selected protein fused with a fluorescent tag, is inserted in the genome under the control of an upstream regulatory sequence (e.g. *UAS-target_protein::GFP*) or *ii*) endogenously tagged flies, where a fluorescent tag is added downstream the endogenous gene encoding for the protein of interest. In this thesis, protein-tags including synaptic the presynaptic active zone (AZ) marker Bruchpilot-short::mCherry (Kremer et al., 2010) and the postsynaptic nicotinic acetylcholine receptor subunit Dalpha7::GFP (Leiss et al., 2009a) were utilized to simultaneously visualize pre- and postsynapses and their structural modifications over time (Baltruschat et al., 2021).

Genetically encoded calcium indicators (GECIs)

The ability to record and analyse neuronal activity is essential to understand their function. For many years, experiments to analyse physiological mechanisms were difficult to perform and mostly restricted to the periphery in an advantageous genetic model such as Drosophila, mainly due to its small size. Later, patch clamp recording from central neurons of the drosophila brain were successfully established (Wilson et al., 2004). The ability to track individual central neurons with electrophysiology resolution represents a milestone in the field of Drosophila neurobiology. However, as discussed in previous chapters of this thesis, sensory and motor information are often encoded as patterns of activity across neuronal population. Thus,

besides individual central neurons recordings, a method to monitor the activity across large populations in vivo is crucial. Once again, genetically encoded fluorescent proteins, combined with the ease of cell-type specific expression in Drosophila, proved to be solution to study mechanisms underlying brain functions, leading to the introduction of genetically encoded sensors of neuronal activity (Fiala et al., 2002).

Nowadays, the most common class of sensors is represented by genetically encoded calcium indicators (GECIs), a non-invasive method that provides sufficient signal-to-noise ratio and temporal resolution to study neuronal activity in intact preparations (Miyawaki et al., 1997). The underlying principle of calcium imaging relies on the fact that neuronal membrane depolarization is typically accompanied by intracellular calcium influx, which can propagate from the extracellular space via voltage-gated calcium channels as well as from internal reservoirs in the endoplasmic reticulum and mitochondria (Berridge, 1998). GECIs can be divided in two main groups: FRET-based GECIs and single fluorophore GECIs. FRET-based indicators such as Cameleon (Miyawaki et al., 1997) consist of a donor fluorophore, usually a cyan variant of GFP, and an acceptor fluorophore, usually a yellow variant of GFP, both fused to the calcium binding domain of a calmodulin (CaM) sequence. Calcium binding induces a conformational change in the calmodulin-binding peptide, which in turn enhances the Förster resonance energy transfer (FRET) from donor to acceptor and can therefore be measured as fluorescence in the emission range of the acceptor fluorophore (Figure 4A). Single fluorophore GECIs instead consists of modified GFP variants coupled to calcium binding sequencing. The most successful single fluorophore GECI is represented by GCaMP (Nakai et al., 2001). In GCaMP probes, the N terminus of a circularly permutated enhanced GFP (cpEGFP) was connected to the M13 fragment of myosin light chain kinase, which is a target sequence of CaM, whereas the C terminus of the cpEGFP was connected to CaM. When calcium binds to CaM, a conformational change triggered by the calcium-CaM-M13 interaction leads

in turn to a structural change in the GFP molecule, generating changes in the fluorescence intensity (Figure 4B). Since the first GCaMP molecule described in 2001, many laboratories worked towards improvements of the construct in order to achieve better baseline fluorescence, signal-to-noise ratio and temporal resolution (Chen et al., 2013; Tian et al., 2009). For example, the GCaMP6 family of calcium indicators, introduced in 2013, is available in fast (GCaMP6f), medium (GCaMP6m) or slow (GCaMP6s) variants depending on the desired kinetics decay speed (Chen et al., 2013). In addition to this, some subcellular localized versions of GCaMP have been created over the years, with the idea of analysing calcium kinetics in a particular region of the target cells. As an example, the pre- and post-synaptically tagged version of GCaMP3 Syp::GCaMP and homer::GCaMP (Pech et al., 2015) were used in this thesis to analyse odour-evoked activity in neuronal axon terminals and dendritic endings, respectively (Baltruschat et al., 2021; Prisco et al., 2021).

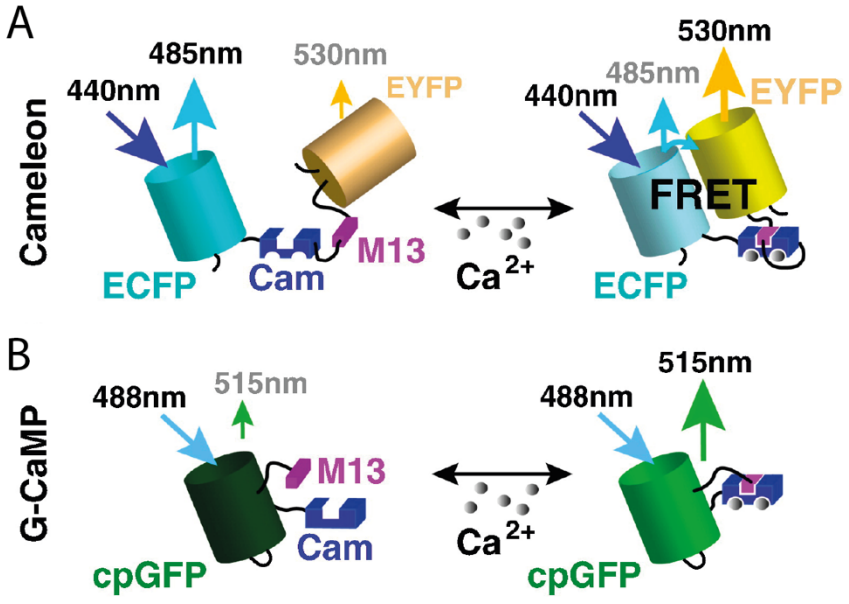

Figure 4. Different genetically encoded calcium indicators (GECIs) used in *Drosophila*
A) In FRET based sensors like Cameleon (Miyawaki et al 1997), a cyan fluorescence protein, e.g. ECFP, and a yellow fluorescence protein, e.g. EYFP, are interconnected by a calcium binding domain of calmodulin (CaM) and a CaM binding petide (M13). Calcium binding to CaM causes a conformational change bringing ECFP in closer proximity to EYFP, which enhances FRET from ECFP to EYFP. B) In GECIs that are based on circularly permutated GFP variants (cpGFP), like GCaMP (Nakai et al 2001), binding of calcium to CaM results in a change within

the barrel structure of the GFP, ultimately enhancing its fluorescence emission. Image adapted from Riemensperger et al 2012.

1.3.3 Connectomics

How brain circuits allow animals to implement complex behaviour is a key question of neurobiology. Connectomics is defined as the production and study of connectomes, maps of the synaptic connectivity between the neurons in a circuit (Lichtman et al., 2008). The term borrows the "-omics" suffix from genomics indicating the big data approach used to analyse these massive datasets produced by structural imaging of the brain or parts of it (Sughrue, 2019). In recent years, connectomes proved to be extremely helpful for understanding neuronal circuit functions (Ding et al., 2016; Jarrell et al., 2012; Kasthuri et al., 2015; Ohyama et al., 2015a; Takemura et al., 2017; Wanner et al., 2016), and the current increase in the speed and quality of imaging, segmentation and reconstruction of electron microscopy (EM), the major technique used to generate connectomics datasets, now allows for large-scale, dense connectomic studies of nervous systems. However, a major limitation is still represented by the fact that relatively small portions of brain can be imaged at once, while many neuronal circuitries are widespread among the brain. Whole-brain connectomes have been thus far limited to a few small organisms such as the nematode *Caenorhabditis elegans*, the *Drosophila melanogaster* larva and the larva of the tunicate *Ciona intestinalis* (Ohyama et al., 2015; Ryan et al., 2016; White et al., 1986).

Nevertheless, two independent working groups recently tackled this limitation via cutting edge methods (Figure 5A). With ~8 × 107 μm^3 and ~100,000 neurons (Alivisatos et al., 2012; Raji & Potter, 2021; Simpson, 2009), the brain of an adult fly is two orders of magnitude larger than that of the fruit fly larva and represent an unachievable barrier for classic volumetric EM. Therefore, new approaches exploiting high-speed acquisition and processing of serial section transmission EM (TEM) images or Focused Ion Beam Scanning Electron Microscopy (FIB-SEM) (both revised in Briggman & Bock, 2012) were established to image a whole fly

brain at synaptic resolution. The two resulting datasets comprise EM data on a full adult female fly brain (FAFB) (Zheng et al., 2018) and the central hemisphere of another female fly (Hemibrain) (F. Li et al., 2020b; Scheffer et al., 2020a). Regarding the latter, the imaged portion was chosen as it contains all critical regions of the central brain, including circuits involving associative learning in the mushroom body, navigation and sleep in the central complex and circadian rhythms among clock circuits (Figure 5B) (Scheffer et al., 2020b).

In this thesis, data from both adult fly brain EM datasets were extracted and analysed in order to understand how distinct neuronal population interact with each other and formulate predictions on the functionality of those interactions, some of which were later confirmed via *in vivo* calcium imaging experiments (Baltruschat et al., 2021; Prisco et al., 2021).

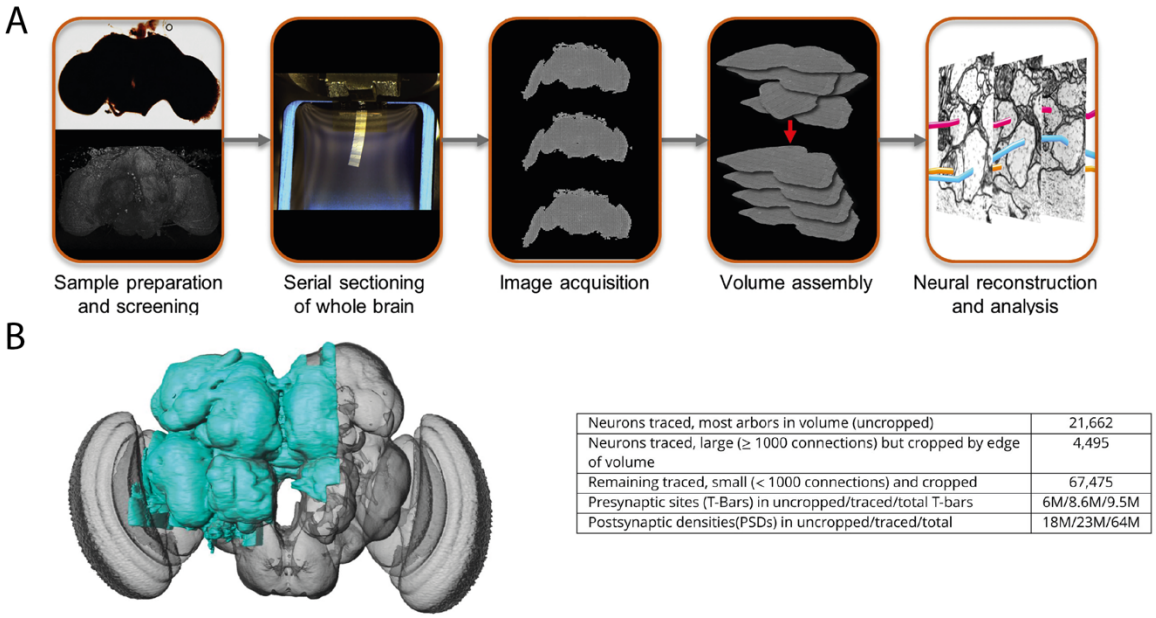

Neurons traced, most arbors in volume (uncropped)	21,662
Neurons traced, large (≥ 1000 connections) but cropped by edge of volume	4,495
Remaining traced, small (< 1000 connections) and cropped	67,475
Presynaptic sites (T-Bars) in uncropped/traced/total T-bars	6M/8.6M/9.5M
Postsynaptic densities(PSDs) in uncropped/traced/total	18M/23M/64M

Figure 5. Generation of whole-brain EM datasets in adult *Drosophila*
A) Work ow for the generation of the FAFB dataset. Blocks of brain tissue are incubated in heavy metals to label cell membranes, embedded in a resin polymer, and screened with X-ray tomography. Blocks were then serially sectioned with a diamond knife. Groups of three serial sections are placed on metal slot grids for imaging in custom high-throughput TEM systems (TEMCA2 or ATPS). The imaged sections were then assembled into an aligned volume with a custom software pipeline. Reconstruction and analyses of neural circuits in the volume were conducted with the CATMAID tracing environment (Saalfeld et al., 2009). For further info, see Zheng et al., 2018. B) The hemibrain and some basic statistics. The highlighted area shows the portion of the central brain that was imaged and

reconstructed, superimposed on a grayscale representation of the entire Drosophila brain. The table on the right shows some statistics related to the dataset. Uncropped neurons have most arbours contained in the volume; otherwise, neurons are categorized as cropped. Image adapted from Scheffer et al., 2020.

1.4 The mushroom bodies

As previously discussed, the insect mushroom body (MB) represents one if not the best candidate system to generate experimental data in support of the pattern separation theory. The MBs are two symmetrical neuropils located in the central region of each hemisphere which importance for memory formation and retrieval was firstly described by Martin Heisenberg in 1985 and later confirmed by other major groups in the field (Aso, Hattori, et al., 2014; de Belle & Heisenberg, 1994; Dubnau et al., 2001; Heisenberg et al., 1985; McGuire et al., 2001). In particular, Heisenberg observed a learning deficit in flies were both mushroom bodies were chemically ablated, thus confirming the necessity of these structures for the formation of associative memory (Heisenberg et al., 1985).

Mushroom bodies of various insects, including flies, honeybees and cockroaches share similar morphology: two mirror-symmetrical stalks (peduncles) extend from dorsocaudal to rostroventral through the midbrain and divide frontally into a medial and a vertical lobe (Heisenberg, 2003). The intrinsic cells of the MB are known as Kenyon cells (KCs). They are around 200,000 in the cockroach, 170,000 in the honeybee and 2,000 in *Drosophila* (Aso, Hattori, et al., 2014; Heisenberg, 2003), with their small cell bodies densely packed above the dorsocaudal cell body rind and their long thin axons forming the peduncle and lobes (Figure 6) (Heisenberg, 2003). In *Drosophila*, the MB receives mainly olfactory input, though optical, temperature and humidity information is also represented (Marin et al. 2020; Frank et al. 2015; J. Li et al. 2020).

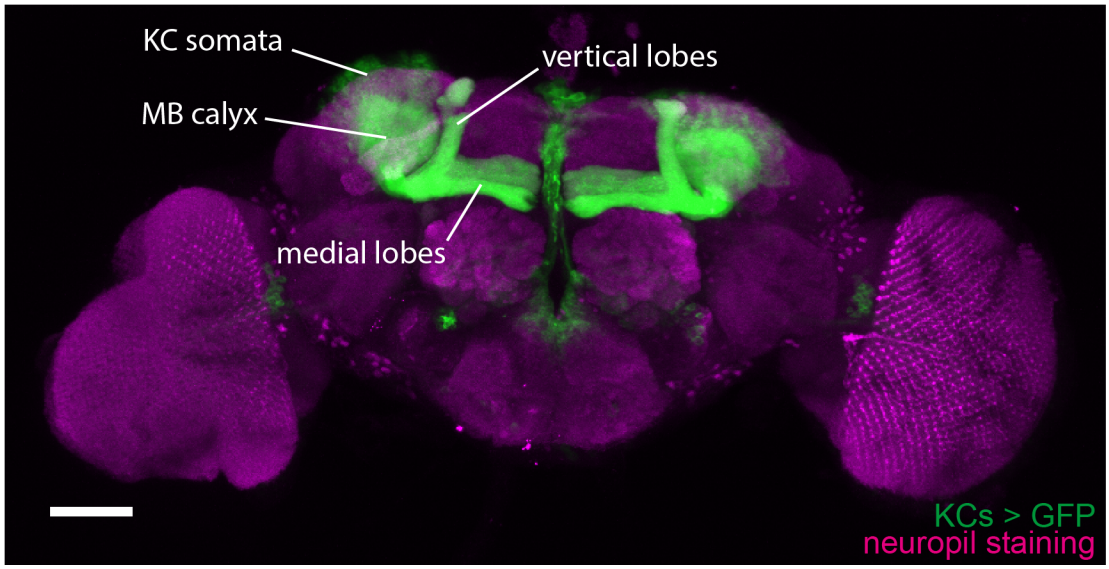

Figure 6. The *Drosophila* MB.
Confocal microscopy image of a whole brain preparation in which a membrane tag GFP is expressed in MB´s intrinsic cells, the KCs. An additional neuropil staining (nc82 antibody, magenta) was performed to make the entire brain visible. Scale bar=50μm.

1.4.1 The fly olfactory system: structure and computation

Odours in the fly brain are detected by a set of ~1300 olfactory receptor neurons (ORNs) expressing chemically-tuned odorant receptors together with the coreceptor Or83b (Clyne et al., 1999; Hallem & Carlson, 2006a; Larsson et al., 2004). In total, there are ~50 ORN types, corresponding roughly to the 50–60 odorant receptors expressed in the adult antennae and maxillary palps (Benton et al., 2009; Bruyne et al., 1999; Couto et al., 2005). ORNs project to the 51 distinct olfactory glomeruli in the adult antennal lobe (AL) in a stereotyped manner, with ORNs expressing the same odorant receptor projecting to the same glomerulus (Figure 7A) (Gao et al., 2000; Grabe et al., 2016; Vosshall et al., 2000). Individual ORN types can be broadly tuned, narrowly tuned or in between (Hallem & Carlson, 2006b), and most individual ligands activate multiple ORN types (Figure 7B) (Bruyne et al., 1999; Hallem & Carlson, 2006b). Of notice, some ligands can act as inhibitory and suppress ORN spike rates below their spontaneous activity level (French et al., 2011; Yao et al., 2005). ORN responses are dynamic; spike rates peak rapidly after binding to ligands and subsequently relax to a tonic level of activity. Firing rates increase with

increasing ligand concentration, and ORNs become more broadly tuned at higher concentrations, resulting in larger ORN responses with increasing gradients (Hallem & Carlson, 2006b). As a result, combinatorial and dynamic ORN responses allow flies as well as other species to represent thousands of odours with a limited number of odour-tuned receptors available (Vosshall et al., 2000).

Within glomeruli, ORNs synapse onto second-order neurons, the ~150 projection neurons (PNs), which in turn deliver odour information to higher brain regions such as the MB and the lateral horn (Stocker et al., 1990). Each PN receives direct ORN input from one glomerulus and lateral inputs from other glomeruli via GABAergic local interneurons (Bargmann, 2006; Olsen & Wilson, 2008; Wilson et al., 2004), constituting the first step of olfactory information processing in the fly brain. The nature of these lateral interactions is mainly inhibitory, as a PN's odor response is disinhibited by silencing input to other glomeruli (Asahina et al., 2009; Olsen & Wilson, 2008). Also, this lateral inhibition scales with the total ORN activity and is thought to act as an input gain control function in glomeruli of the AL by providing divisive normalization of ORN responses (Olsen et al., 2010). The result of this transformation is that PN odour representations are more intensity invariant compared to ORN stimuli representations (Olsen et al., 2010). Of notice, this is in line with the finding that some KCs, postsynaptic partners of the PNs in the MB, respond selectively to a particular odour regardless of its concentration (Stopfer et al., 2003; Y. Wang et al., 2004). Next, within the MB input region, the main calyx, PNs deliver olfactory information to the third neuronal layer, the KCs of the MB.

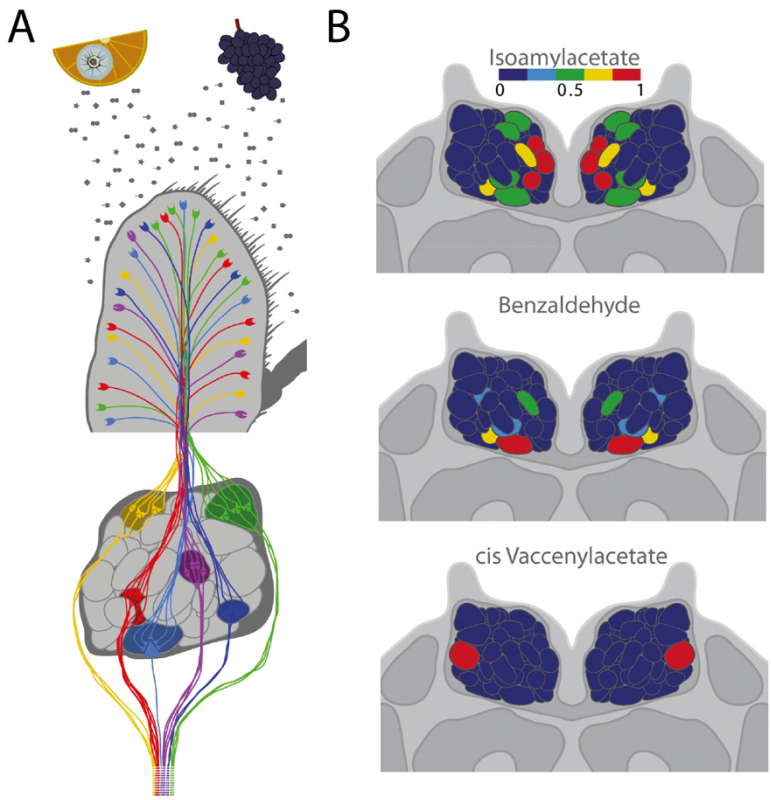

Figure 7. Olfactory perception in the fly
A) Odour molecules originating from different sources are detected by ORNs located in the fly´s sensory organs. ORNs then project to the AL where they segregate into glomeruli in a stereotyped manner, with ORNs expressing the same receptor innervating the same glomerulus. B) Example of broadly, in-between or narrowly tuned odour elicited ORN responses in glomeruli of the AL. Image adapted from Grabe & Sachse, 2018.

In the calyx, PNs synapse onto KCs via complex synaptic structures known as microglomeruli (MGs) (Leiss et al., 2009a; Yasuyama et al., 2002a). At each MG, a single central PN bouton is enwrapped by, on average, 13 claw-like dendritic terminals of as many different KCs (Figure 8A) (Davi D. Bock, personal communication). KCs integrate inputs in a combinatorial manner, with each KC receiving input from 6-8 PNs, on average (Butcher et al., 2012; F. Li et al., 2020b; Turner et al., 2008b; Zheng et al., 2020), of which more than half need to be coactive to elicit spikes (Gruntman and Turner 2013; Inada, Tsuchimoto, and Kazama 2017). As a result, while PN odour-evoked activity is broadly tuned, with odours activating up to 70% of the total population (Figure 8B) (Bhandawat et al., 2007; Perez-Orive et al., 2002), odour representation is sparse and decorrelated at the KCs

layer, where each odour activates only 5-10% of the total KCs (Honegger, Campbell, and Turner 2011; Turner, Bazhenov, and Laurent 2008; Campbell et al. 2013b; Perez-Orive et al. 2002). Such activity patterns are thought to be advantageous for learning and associative memory formation, as they enable neurons to represent a large number of stimuli as unique activity patterns, thus maximizing the representation space generated by a network (Cayco-Gajic et al., 2017; Litwin-Kumar et al., 2017).

Finally, at the MB lobes, KCs are presynaptic to a relatively small number of MB output neurons (MBONs), which project their axons to neuropil outside the MB and guide memory-based actions (Aso, Sitaraman, et al., 2014). As oppose to the AL, where the glomerular connectivity between ORNs and PNs is stereotypic among animals, thus creating a spatial odorant map in the fly brain (Vosshall et al., 2000), the rules of the connectivity between PNs and KCs in the calyx is still under debate. In particular, theoretical studies suggested that pure random connections between input neurons (PNs) and encoding neurons (KCs) would allow the network to achieve the largest possible representation space (Cayco-Gajic & Silver, 2019; Jortner et al., 2007; Litwin-Kumar et al., 2017). However, current experimental evidence, acquired also via recently released adult *Drosophila* whole-brain connectomes, seemed to challenge this view and suggest that the connections between PNs and KCs might be structured to some degree (Gruntman & Turner, 2013; F. Li et al., 2020b; Zheng et al., 2020).

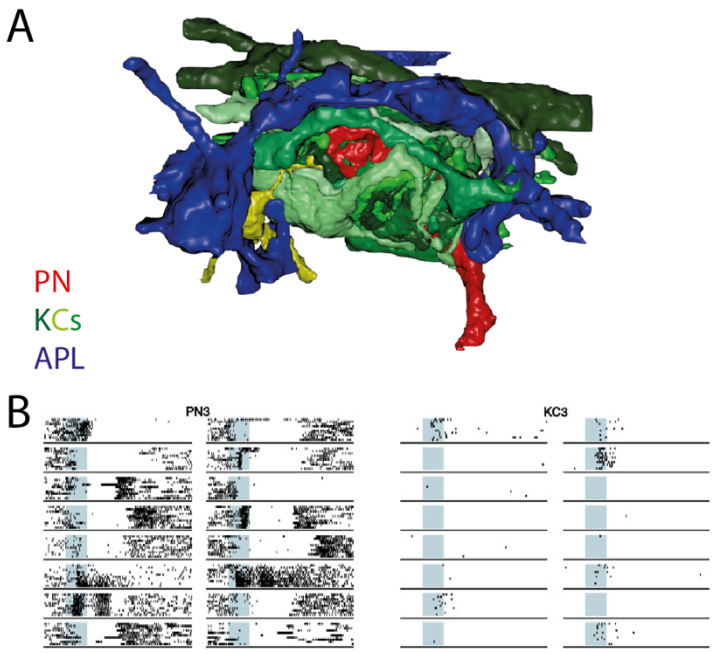

Figure 8. MGs of the MB calyx and their effect on stimuli representations
A) EM reconstruction of an entire MG of the calyx. A central PN bouton (red) is surrounded by several postsynaptic dendritic claws of distinct kenyon cells (greens). Additionally, the APL neuron (blue) also participated to this particular MG described in Baltruschat et al., 2021. B) Example of odour-evoked activity in a PN and a KC of animals exposed to the same combination of 16 odours. While PN odour representations are broadly tuned and overlapping, KC odour-evoked activity is sparse and decorrelated. Image adapted from Perez-Orive et al., 2002

1.4.2 The cerebellar granule layer and the MB calyx: similar circuits, similar functions

There are many similarities between the cerebellar and the MB input regions organization (Figure 9). Like the cerebellar granule layer, the MB calyx circuitry is highly divergent, with PNs delivering information from ~50 distinct AL glomeruli (Bates et al., 2020; Grabe et al., 2016) to the ~2,000 KCs of the MB (Aso et al., 2009), for an expansion ratio of 40 (Litwin-Kumar et al., 2017). Furthermore, the connectivity between input (PNs) and expanded (KCs) populations is sparse. Indeed, each KC receives input from only 6-8 different PNs in MGs of the calyx (Butcher et al., 2012; F. Li et al., 2020b; Turner et al., 2008b; Zheng et al., 2020). Similarly, each granule cell receives input from 4 different mossy fibers in cerebellar glomeruli (Eccles et al., 1966). Finally, inhibition at the MB calyx is provided by a single neuron known as the anterior paired lateral (APL) neuron, which

innervates both the calyx and lobes of the adult MB (Aso, Hattori, et al., 2014; X. Liu & Davis, 2009; Pitman et al., 2011). These similarities with the cerebellar input layer, together with the finding that MBs are responsible for associative memory formation, led to the hypothesis that the MB, and in particular its input synaptic layer, performs pattern separation. This hypothesis was confirmed via experimental data showing, for example, that KC odour evoked responses are more separated that their sensory counterpart at the ORNs (Turner et al., 2008b) and that the ability of a fly to discriminate between odours decreases with increasing overlap among KC odour representations. (Campbell et al., 2013).

Taken together, the cerebellar input layer and the *Drosophila* mushroom body calyx share both structural and functional aspect and satisfy the Marr-Albus criteria for pattern separation. As the fly represent a favourable model to collect experimental data, for several reasons previously discussed, one of the questions explored in this thesis is how the calyx, and in particular the microglomerular microcircuits, support the pattern separation theory and allow for efficient stimuli discrimination in *Drosophila*.

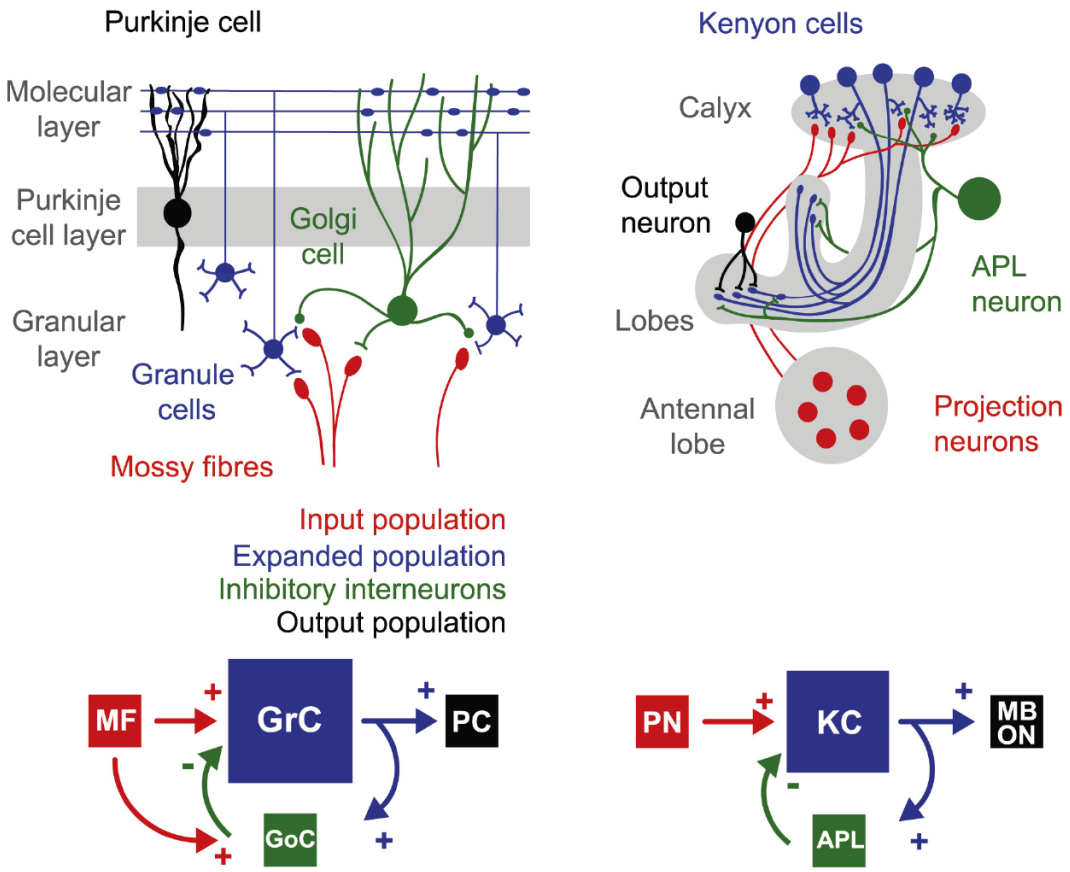

Figure 9. Structural and functional similarities between neuronal networks performing patter separation
Circuit-level (above) and systems-level (below) diagrams of the cerebellar cortex and the mushroom body. Colour key: red, excitatory afferents; dark blue, expanded population; green, inhibitory interneurons; black, output neurons. Size of boxes indicates relative expansion. Adapted from Cayco-Gajic and Angus Silver, 2019.

1.4.3 The anterior paired lateral neuron

At the mushroom bodies, two of the three Marr-Albus network requirements for pattern separation (expansion and sparse coding) are purely related to the size of the PN and KC populations and the way these two layers are connected to each other. Thanks to the advent of *Drosophila* whole brain connectomes (Scheffer et al., 2020a; Zheng et al., 2018), which provide connectivity data at synaptic resolution, experimental data supporting these requirements are accessible via simple searches through datasets (Clements et al., 2020). However, the third requirement, inhibition, requires an additional inhibitory cell type, which in the fly brain is represented by the APL neuron.

The APL neuron is a large GABAergic neuron that innervates the entire MB including calyx, peduncle and lobes (Figure 10A) (Aso, Hattori, et al., 2014; X. Liu & Davis, 2009; Pitman et al., 2011) and has been shown to respond to odours with depolarization and calcium influx (X. Liu & Davis, 2009; Papadopoulou et al., 2011). A link between APL and pattern separation has been already described, as blocking APL output disrupted the KCs sparse odour representations (Figure 10B) and impaired learned discrimination of similar odours in a classical conditioning behavioural assay (A. C. Lin et al. 2014; Lei et al. 2013). APL is currently suggested to regulate KC sparse coding by participating in a closed feedback loop with the KC. In this scenario, APL receives excitation at the KCs output in the MB lobes and inhibits in turn KCs at their dendrites in the calyx, similarly to its homolog giant GABAergic neuron (GGNs) in the locust (Papadopoulou et al. 2011; A. C. Lin et al. 2014). However, this view seems to be challenged by recent evidence. For example, APL was recently described as both pre- and post-synaptic to PNs and KCs in the adult calyx (Baltruschat et al., 2021; Wu et al., 2013; Yasuyama et al., 2002b). Furthermore, APL response to localized stimuli was found to be spatially restricted (Amin et al., 2020), with APL branches at the MB lobes functioning separately from the ones in the calyx, thereby suggesting a possible distinct role of inhibition in these two compartments (Amin et al., 2020).

Hence, although the APL is necessary to maintain odour representations sparse at the MB and allow for efficient stimuli discrimination, a clear mechanism by which APL would modulates this phenomenon is yet to be described. In this thesis, taking advantage of recently release EM datasets and *in vivo* calcium imaging experiments, I tackled this subject and investigated the role of inhibition in the process of stimuli discrimination, with a particular focus to the microglomerular structure in the MB calyx.

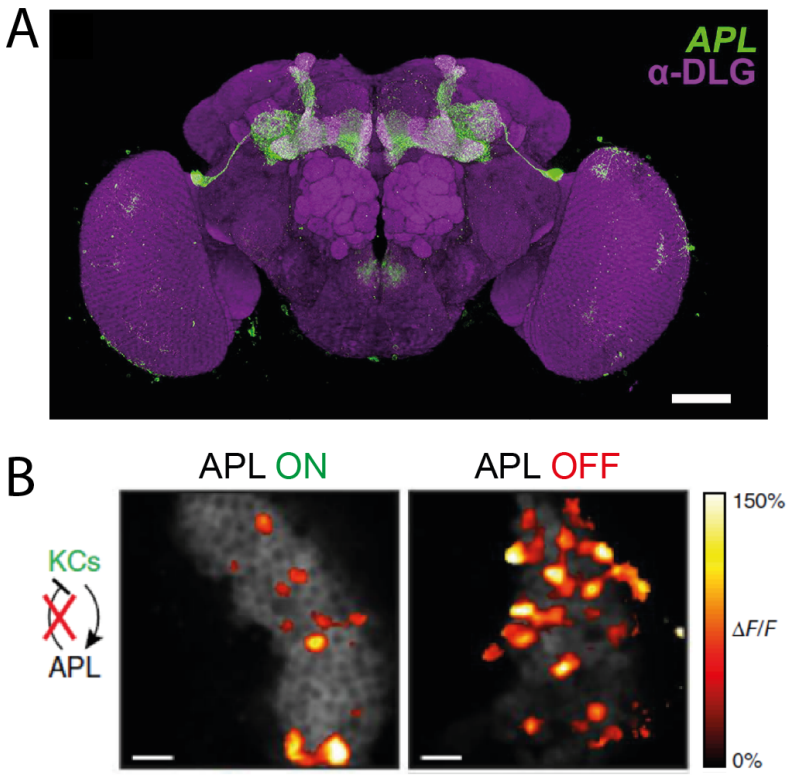

Figure 10. The APL neuron maintains KC odour responses sparse
A) The APL, here labelled via expression of a GFP membrane tag, innervates the entire MB including calyx and lobes. An additional DLG antibody staining (magenta) is performed to allow for visualization of the brain. Scale bar=50μm. Adapted from Wu et al., 2013. B) APL maintains KCs odour responses sparse. Odour evoked activity in KC somata was recorded via expression of the calcium indicator GCaMP3. APL was either expressing a functional (APL ON) or inactive (APL OFF) form of tetanus toxin to silence its output. Adapted from AC Lin et al., 2014.

1.5 Memory formation and learning

As described in the very first paragraph of this thesis, this work is motivated by two fundamental questions: *i*) How is our brain able to detect, represent and recognize a particular stimulus, even when the surroundings change? And *ii*) how are memories related to that particular stimulus formed and maintained in the brain? While the first question has been extensively discussed and introduced in the previous chapters, the aspect of learning and memory formation has been only briefly mentioned thus far.

Learning is defined as the process by which associations among stimuli are formed, whereas memory is the recall of those associations made in the past to predict the outcome of future actions (Okano et al., 2000). The

notion that learning and memory formation has to happen in the brain was already formulated by René Descartes in between the XVI and XVII centuries and was later confirmed and extended by the extraordinary work from several scientists including Cajal, Pavlov, Tanzi and Hebb. Currently, changes in the strength, morphology and number of synapses, the specialized connections between neurons, are assumed to be the mechanism by which memory traces are encoded and stored in the central nervous system. These changes do not interest a single neuron or a single synapse, but are rather widely spread among neuronal ensembles, thus constituting the so-called memory "engram" (Semon and Simon, 1921).

1.5.1 Structural plasticity and memory formation: searching the engram

The first examples of experience-induced structural plasticity date back to the 80s, when alterations in the synaptic structure and number were described after non-associative learning and long-term facilitation in *Aplysia* (Bailey & Chen, 1983; Glanzman et al., 1990) as well as in the mammalian hippocampus in response to injury, stimulation or long-term potentiation induction (Chang & Greenough, 1984; Desmond & Levy, 1983; Lee et al., 1980; van Harreveld & Fifkova, 1975). Following these early findings, many groups joined the search for the memory engram, with a particular focus on specialized postsynaptic structures known as dendritic spines. Spines are characterized by the presence of a post synaptic density (PSD) enriched with receptors, channels and signalling molecules, hence representing the site of inputs integration and transduction in postsynaptic dendrites. Modulation of spines number and shape has been suggested to provide the basis on which learning is made possible (C H Bailey & Kandel, 2003; Esther A. Nimchinsky et al., 2003), a hypothesis backed by experimental data acquired via state-of-the-art technologies. Namely, it has been shown via two-photon microscopy that induction of long-term potentiation led to the formation of new spines in hippocampal slice cultures (Figure 11) (Engert & Bonhoeffer, 1999). Similarly, an increase in spine

density, as well as in the number of synaptic boutons that formed synapses on spines, was found in the mammalian hippocampus 24h after trace eyeblink conditioning (Geinisman et al., 2001; Leuner et al., 2003).

While these examples suggest that the structural plasticity observed at the spines might be the structural correlate of memory, the link between spines and memory formation has always been correlational and not causal, the main reason being the inability to manipulate specific subsets of spines (though some exceptions are present, as in Hayashi-Takagi et al., 2015). Once again, thanks to its genetic toolkit that allows labelling and manipulation os specific subsets of neurons, *Drosophila* represents a valuable model to investigate structural plasticity and its causal link to learning and memory formation.

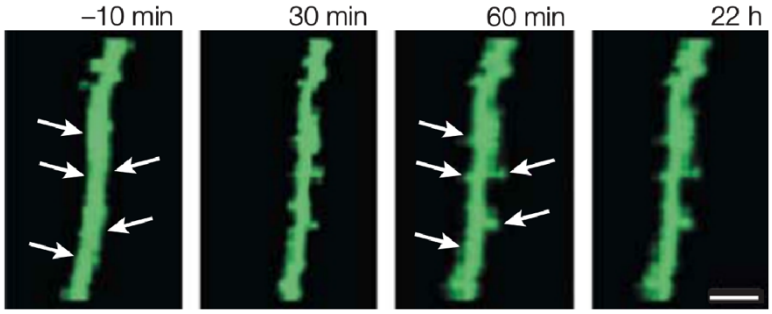

Figure 11. Experience-induced structural plasticity
Visualization of new spine growth (white arrows) after long-term potentiation of postsynaptic neurons using two-photon microscopy. Adapted from Engert & Bonhoeffer, 1999.

1.5.2 Associative learning in the fly MB

In *Drosophila*, the most common behavioural protocol used to study learning and memory formation is the classical olfactory conditioning paradigm, where flies are exposed to two odorants (conditioned stimuli, CS), one coupled with electric shocks (CS+) and one presented alone (CS-). After conditioning, memory is tested in a T-maze, providing arms containing each of the odours, and allowing the flies to distribute between them. Finally, a performance index is calculated as the proportion of flies that choose the CS+ over the CS-. The rationale behind this paradigm is that the simultaneous exposure to the CS+ and the US will make flies link

these two stimuli and thereby create an aversive associative memory towards the CS+ (Quinn et al., 1974; Tully & Quinn, 1985b). Several variations of this original paradigm have been created and tested, and allowed for the dissection of different memory phases in *Drosophila* (STM, MTM, ARM and LTM) together with the genes that regulate each of them (for a detailed description of each phase with its related genes, see Davis, 2011; Keene & Waddell, 2007; Margulies et al., 2005).

From a molecular point of view, the memory trace in the fly brain is considered to be stored in the MB lobes as plasticity in the synapses between KCs and MBONs (Aso, Hattori, et al., 2014; Aso, Sitaraman, et al., 2014). Importantly, MBONs can drive either approach or avoidance behaviour if active, and their activity is balanced in naïve flies so that the net output from the MB is null in untrained animals. However, the simultaneous activation of KCs and Dopaminergic neurons (DANs) conveying information about reward or punishment at the MB lobes (Aso, Hattori, et al., 2014; C. Liu et al., 2012; Masek et al., 2015; Yamagata et al., 2015) induce changes in the strength of the KC-to-MBON synapses, hence destabilising the equilibrium between approach and avoidance (Aso, Hattori, et al., 2014; Hige et al., 2015; Owald et al., 2015). Specifically, DANs induce synaptic depression in the output of the opposite behaviour: when a fly is exposed to an odour paired to electric shock, the punishment DANs will inhibiting the connections between KCs and the approach MBONs, therefore tilting the balance in favour of avoidance (Figure 12).

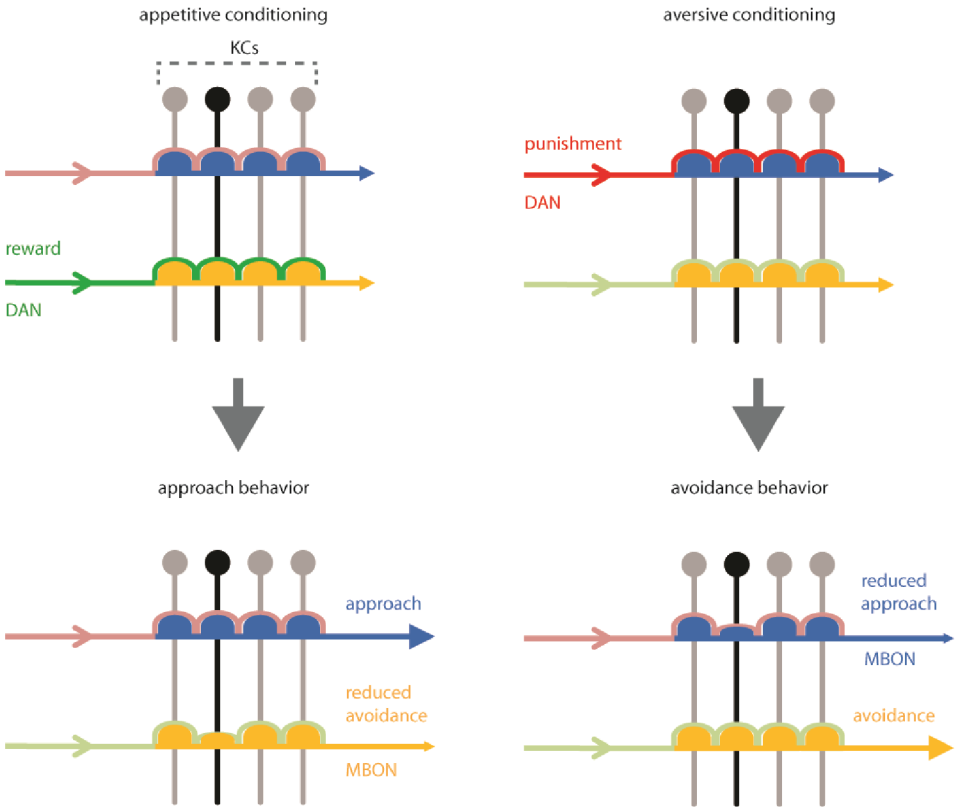

Figure 12. Associative learning in the MB
During classical conditioning (top), a specific set of KCs (black) is activated by the odour and simultaneously the DANs are activated by either a reward (green) or punishment (red). The release of Dopamine induces synaptic plasticity at the KC to MBON (orange and blue) synapses (semicircles). When the odour is presented a second time (below), the balance of the network has shifted (smaller semicircles) due to the Dopamine induced plasticity. In the case of appetitive conditioning, the connection between KCs and the avoidance promoting MBONs is weakened and approached behaviour is induced. During aversive conditioning, the connections between KCs and the approach promoting MBONs is weakened, thus the network drives avoidance behaviour. Adapted from Cognigni, Felsenberg, and Waddell 2018.

1.5.3 Microglomeruli of the MB calyx as targets of structural plasticity

In addition to the KC-to-MBON synapses at the MB lobes, the PN-to-KC connections in MGs of the MB calyx represent another candidate where memories could be stored in the shape of structural modifications. Although these synaptic complexes received less attention from the field over the years, there are several indications on why the MGs could play a much more critical role in memory formation than previously suggested. First of all, the volume of the mushroom body calyx varied depending on rearing

conditions and visual experience in several insects including flies, bees and ants (Durst et al., 1994; Kühn-Bühlmann & Wehner, 2006; Withers et al., 1993). In honey bees, the number and size of calycal MGs increased in animals reared in an enriched environment compared to a hive-trapped group (Groh et al., 2012; Groh & Rössler, 2014). Also, after long-term memory (LTM) formation, the density of MGs was increased in calyces of bees in a protein synthesis-dependent way (Hourcade et al., 2010). Additionally, the MGs density and morphology was modified both in leaf-cutting ants and cockroaches, with those modifications lasting up to 48h and 24h after learning, respectively (Falibene et al., 2015; Lent et al., 2007).

Concerning *Drosophila*, block of presynaptic PN transmission led to an increase in the average microglomerular size (Kremer et al., 2010), and long-term exposure to an odour induced stable presynaptic depression in the boutons involved in that particular odour representation (Pech et al., 2015). Finally, additional MGs were involved in the CS+ representation after short-term gustatory conditioning in the fly. In summary, these data indicate that there is a correlation between experience and structural changes in the calyx. While this correlation is still not casual, as for the mammalians data discussed in the previous paragraphs, *Drosophila* and its related genetical advantages are currently the most valuable system where this causality can be addressed.

For this reason, in this thesis, taking advantage of EM connectomes, behavioural paradigms, transgenic lines and state of-the-art imaging approaches such as *in vivo* two-photon calcium imaging, my colleagues and I gave our contribution to the "search for the engram" by analysing structural plasticity in MGs of the MB calyx upon LTM formation.

1.6 Aim of the thesis

How does our brain represent and discriminate among sensory stimuli? And how are these representations used to create and maintain memories? With these two questions in mind, I will here investigate olfactory sensory representations and experience induced modifications in the input region of a neuropil involved in both processes in *Drosophila*. Focusing on the microglomerular complexes in the MB calyx, I will first look at if, and how, stimuli representations get modified in an input-dependent way in the calyx after long-term associative memory formation. Second, I will take an even closer look at the microglomerular structure, and analyse the possible role of inhibitory synapses provided by the APL neuron in the process of stimuli discrimination.

Taken together, the data presented in this thesis will help understand how sensory information is processed, encoded and possibly modified in higher brain regions involved in learning and memory formation. Most importantly, as these neuronal motifs are shared across multiple species including insects, rodents and humans, the principles described in this work are not only restricted to the fly but can be applied to all organisms displaying a similar network organization.

2 Circuit reorganization in the *Drosophila* mushroom body calyx accompanies memory consolidation

The following chapter represents a paper that was published on March 16th, 2021 in the journal Cell Reports (https://www.cell.com/cell-reports/home).

2.1 Introduction

The search for the memory engram, modifications in the strength and number of synapses through which memories are formed in the brain (Semon and Simon, 1921), begun hundreds of years ago and is still ongoing. Although many studies observed structural changes after learning or environmental shifts (Bailey & Chen, 1983; Chang & Greenough, 1984; Desmond & Levy, 1983; Engert & Bonhoeffer, 1999; Geinisman et al., 2001; Glanzman et al., 1990; Lee et al., 1980; Leuner et al., 2003; van Harreveld & Fifkova, 1975), the link between these two phenomena has been mainly correlative and not causal.

In this work, we aimed at covering this gap by investigating long-term memory induced plasticity in MGs of the *Drosophila* MB calyx. Previous observations in insects including *Drosophila*, honey bees, ants and cock roaches already showed that MGs undergo structural changes upon learning, altered experience and suppression of synaptic inputs (Falibene et al., 2015; Groh & Rössler, 2014; Hourcade et al., 2010; Kremer et al., 2010; Lent et al., 2007; Pech et al., 2015). However, the precise molecular mechanisms as well as the precise neurons involved in this process during a specific task could not be identified. In other words, a specific task-related memory trace has not been described yet. Taking advantage of the genetic tools available in the fly, we here describe the use of a transgenic fly line that labels only selected neurons involved in the representation of a particular odour, the pheromone cis-Vaccenyl Acetate (cVA). After training flies with cVA in a long-term appetitive conditioning paradigm, we show how the representation of the interested odour changes in microglomeruli

of the calyx. In addition, via two-photon *in vivo* calcium imaging experiments, we look at modifications in the functional representation of the conditioned stimulus in KC dendritic ends.

2.2 Statement of contribution

Lothar Blatruschat and Gaia Tavosanis conceived the original project. Lothar Baltruschat, Luigi Prisco and Philipp Ranft constructed fly strains, performed the behavioral experiments, produced and analyzed the anatomical data. J. Scott Lauritzen and Davi. D. Bock established the set of EM data, and Philipp Ranft performed the tracings presented here. Scripts and routines for the analysis were established by Lothar Baltruschat and Luigi Prisco. Functional imaging experiments were designed and performed by Lothar Baltruschat and Luigi Prisco with support from André Fiala. The manuscript was written by Gaia Tavosanis, Lothar Baltruschat, Luigi Prisco and Philipp Ranft.

2.3 Publication

Circuit reorganization
in the *Drosophila* mushroom body calyx
accompanies memory consolidation

Lothar Baltruschat*, Luigi Prisco*, Philipp Ranft*, J. Scott Lauritzen, André Fiala, Davi D. Bock and Gaia Tavosanis

doi: 10.1016/j.celrep.2021.108871

* = Authors contributed equally

Cell Reports

Circuit reorganization in the *Drosophila* mushroom body calyx accompanies memory consolidation

Graphical abstract

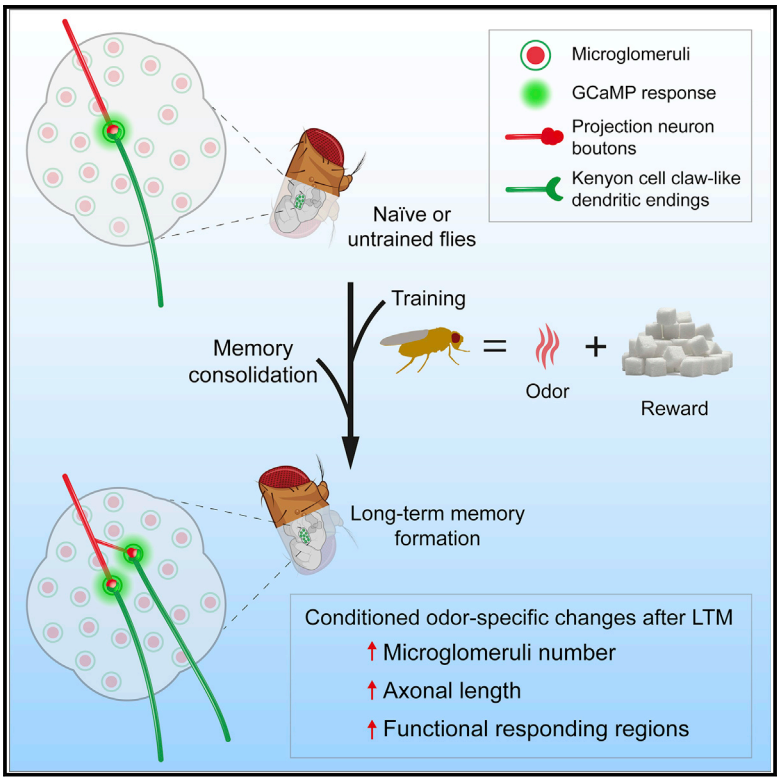

Highlights

- Synaptic microglomeruli linked to a specific odor can be identified in *Drosophila*
- Microglomeruli represent complex microcircuits involving different types of neurons
- Long-term memory results in increased microglomeruli in an input-specific manner
- Newly formed microglomeruli participate in conditioned odor representation

Authors

Lothar Baltruschat, Luigi Prisco, Philipp Ranft, J. Scott Lauritzen, André Fiala, Davi D. Bock, Gaia Tavosanis

Correspondence

gaia.tavosanis@dzne.de

In brief

Baltruschat et al. investigate structural modifications upon memory consolidation in a center essential for olfactory memory in *Drosophila*, in which second- and third-order neurons connect via synaptic microglomeruli. Although short-term memory reveals no evidence of structural plasticity, appetitive long-term memory is associated with increased microglomeruli in an input-specific manner.

Baltruschat et al., 2021, Cell Reports *34*, 108871
March 16, 2021
https://doi.org/10.1016/j.celrep.2021.108871

Cell Reports

CellPress
OPEN ACCESS

Report

Circuit reorganization in the *Drosophila* mushroom body calyx accompanies memory consolidation

Lothar Baltruschat,[1,6] Luigi Prisco,[1,6] Philipp Ranft,[1,6] J. Scott Lauritzen,[2] André Fiala,[3] Davi D. Bock,[2,4] and Gaia Tavosanis[1,5,7,*]

[1]Center for Neurodegenerative Diseases (DZNE), 53175 Bonn, Germany
[2]Janelia Research Campus, Howard Hughes Medical Institute, Ashburn, VA 20147, USA
[3]Molecular Neurobiology of Behaviour, University of Göttingen, 37077 Göttingen, Germany
[4]Department of Neurological Sciences, University of Vermont, Burlington, VT 05405, USA
[5]LIMES Institute, University of Bonn, 53115 Bonn, Germany
[6]These authors contributed equally
[7]Lead contact
*Correspondence: gaia.tavosanis@dzne.de
https://doi.org/10.1016/j.celrep.2021.108871

SUMMARY

The formation and consolidation of memories are complex phenomena involving synaptic plasticity, microcircuit reorganization, and the formation of multiple representations within distinct circuits. To gain insight into the structural aspects of memory consolidation, we focus on the calyx of the *Drosophila* mushroom body. In this essential center, essential for olfactory learning, second- and third-order neurons connect through large synaptic microglomeruli, which we dissect at the electron microscopy level. Focusing on microglomeruli that respond to a specific odor, we reveal that appetitive long-term memory results in increased numbers of precisely those functional microglomeruli responding to the conditioned odor. Hindering memory consolidation by non-coincident presentation of odor and reward, by blocking protein synthesis, or by including memory mutants suppress these structural changes, revealing their tight correlation with the process of memory consolidation. Thus, olfactory long-term memory is associated with input-specific structural modifications in a high-order center of the fly brain.

INTRODUCTION

The capacity to use past experience to guide future action is a fundamental and conserved function of the nervous system. Associative memory formation, initiated by the coincident detection of a conditioned stimulus (CS; e.g., odor) and an unconditioned stimulus (US; e.g., sugar reward), leads to a short-lived memory (STM) trace within distinct circuits (Josselyn and Tonegawa, 2020, Boto et al., 2020, Wang et al., 2008, Liu et al., 2012, Burke et al., 2012). Memories can be consolidated into long-term memories (LTMs) through processes that depend on *de novo* protein synthesis (Tully et al., 1994, Bailey et al., 1996), require structural modifications within the involved neuronal circuits, and might lead to the recruitment of additional ones (Dubnau and Chiang, 2013, Cervantes-Sandoval et al., 2013, Kitamura et al., 2017, Caroni et al., 2012, Holtmaat and Caroni, 2016, Kleim et al., 2002, Hihara et al., 2006, Bassett et al., 2011, Gu et al., 2015, Maviel et al., 2004). Compared with modulation of existing connections, the reorganization of circuits affords the unique possibility of sampling for potential new partners (Chklovskii et al., 2004, Gogolla et al., 2007, Bennett et al., 2018). Nonetheless, only few examples of rewiring associated with learning have been established thus far (Boele et al., 2013, Hihara et al., 2006, Chen et al., 2015, Poort et al., 2015, Grewe et al., 2017).

The formation and retrieval of olfactory-associative memories in *Drosophila* require the mushroom body (MB; de Belle and Heisenberg, 1994). Within the main MB input compartment, the calyx (MBC), second-order projection neurons (PNs), delivers olfactory information through cholinergic synapses to the intrinsic MB neurons, the Kenyon cells (KCs; Figure 1A). In the MBC, large, olfactory PN boutons are enwrapped by the claw-like dendrite termini of ~11 KCs on average (Butcher et al., 2012, Caron et al., 2013), thereby forming characteristic synaptic complexes, the microglomeruli (MGs; Yasuyama et al., 2002), which display functional and structural plasticity in adaptation and upon silencing (Kremer et al., 2010, Pech et al., 2015, Leiss et al., 2009). To start systematically addressing the mechanisms that support memory consolidation, we sought to investigate the properties of identifiable synaptic MGs in the MB of the adult brain of *Drosophila* after the establishment of LTMs.

Combining behavioral experiments with high-resolution microscopy and functional imaging, we demonstrate that the consolidation of appetitive olfactory memories closely correlates with an increase in the number of MGs formed by the PNs that deliver the conditioned stimulus and their postsynaptic KC partners. These structural changes result in additional, functional synaptic connections. Thus, the circuit in the calyx of the fly MB reorganizes accompanying the consolidation of associative memories.

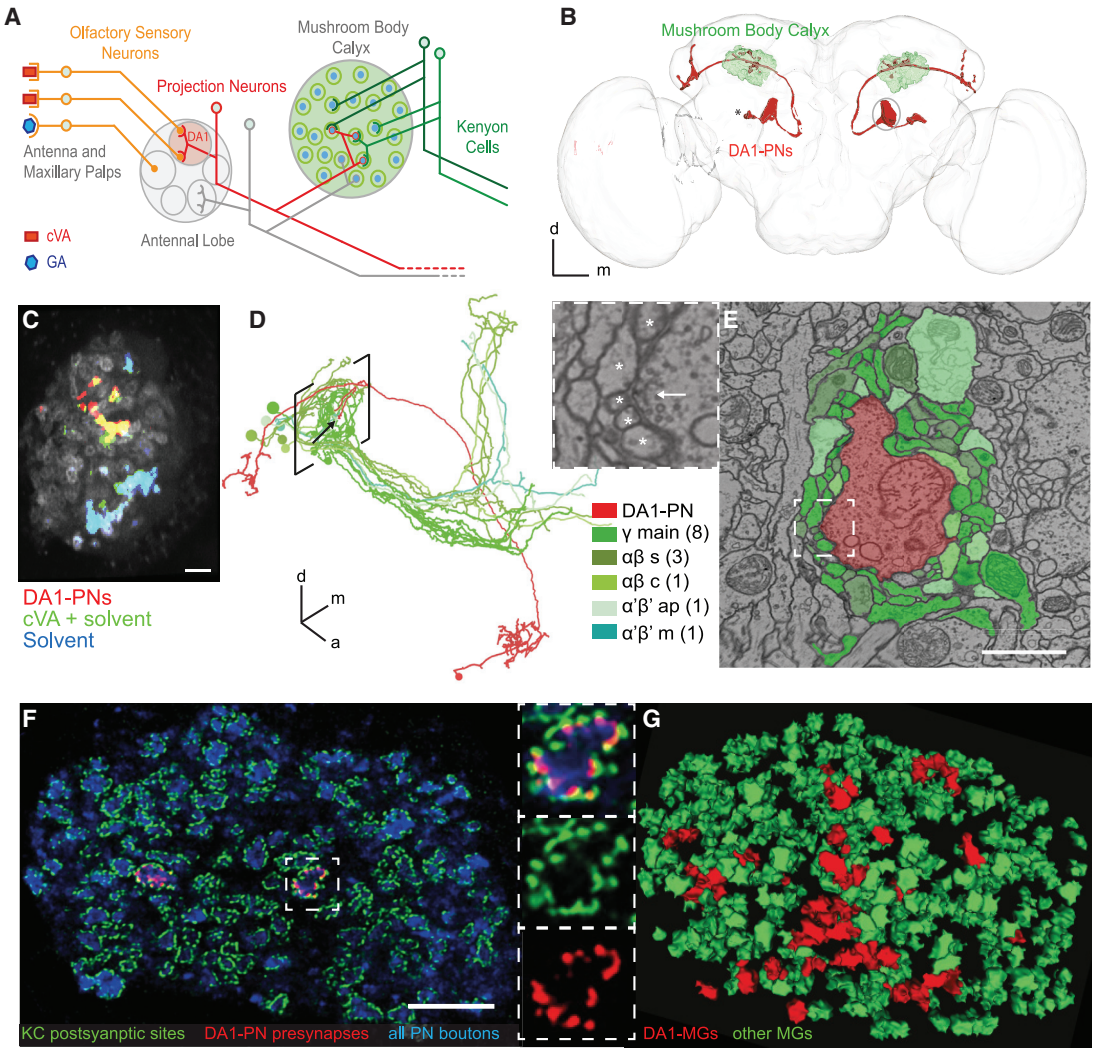

Figure 1. Identification of the synapses in the MBC responding to cVA odor stimulation

(A) Schematic representation of the olfactory circuit starting from the activation of specific olfactory sensory neurons (OSNs) by two exemplary odors, cVA and GA. In the AL, cVA-responsive OSNs converge on the DA1 glomerulus (pale red), where they synapse onto DA1-PNs (red). These deliver the cVA signal to the MBC via axon collaterals that terminate with boutons forming large synaptic complexes, the MGs (circles). Postsynaptic KCs are represented in green.

(B) Reconstruction from a full confocal serial section set of the DA1-PNs (red; *R37H08-Gal4 > UAS GAP43::Venus*); MBC (green; *MB247-Dα7::GFP*); DA1-PN cell bodies (*); brain neuropil (light gray; α-synapsin antibody).

(C) Volumetric calcium imaging of the calyx of flies carrying *MB247-Homer::GCaMP3* (gray) and in which DA1-PNs are genetically labeled (red; *R37H08-Gal4 > UAS tdTomato*). cVA-elicited postsynaptic responses (green; cVA 1:400 dissolved in 5% EtOH) are specific to DA1-PNs as revealed by the overlap between the two channels (red + green = yellow). Generic response to the solvent (cyan = overlap of the responses to cVA 1:400 dissolved in 5% EtOH, green; and to 5% EtOH only, blue). Scale bar, 10 μm.

(D) Single DA1-PN (red) and the 14 KCs (green) postsynaptic to the DA1-PN bouton indicated by the arrow. Tracings performed on the EM FAFB dataset (Zheng et al., 2018). Square brackets indicate the location of MBC. Different green shades represent different KC subtypes, as in (E). Numbers in brackets in the legend represent the number of cells.

(E) Single EM section through the MG, arrow in (D). Scale bar, 1 μm. White square is magnified in the left top panel with the arrow pointing to a T-bar of the AZ, and the asterisk (*) labels the fine dendritic postsynaptic profiles of KCs.

(F) Single plane confocal image of the MBC displaying PN boutons (blue; α-synapsin antibodies); the PSDs of KCs (green; *MB247-Dα7::GFP*) and the AZs of DA1-PN boutons only (red; *R37H08-Gal4 > UAS-brp-short^{cherry}*) identifying the cVA-responsive MGs. Scale bar, 10 μm. The MG in the white square is magnified in the right panels.

(G) Automated 3D reconstruction of a confocal stack, including the image shown in (F). The reconstruction of MGs is based on Dα7-GFP (green) (see also Figure S1), and MGs receiving presynaptic input from DA1-PNs are marked by Brp–short^{cherry} (red). All other MGs are in green.

Full genotypes used and statistics for Figures 1, 2, 3, and 4 are included in Table S2.

RESULTS

Identifiable synaptic microglomeruli in the calyx respond to cVA

To reveal potential changes in synapse organization linked to memory consolidation, we first developed a setup allowing us to identify the individual synapses of olfactory PNs that deliver a conditioned odor to the MB. The pheromone and odorant 11-*cis*-vaccenylacetate (cVA) specifically activates PNs that project their dendrites to the DA1 glomerulus in the antennal lobe (AL) (Datta et al., 2008, Kurtovic et al., 2007, Schlief and Wilson, 2007). The DA1 glomerulus is mostly excluded from complex processing of sensory information in the AL (Lebreton et al., 2014, Lebreton et al., 2015), suggesting that, by genetically marking the DA1 PNs, we could identify the individual boutons in the MBC that deliver the olfactory response to cVA. We tested this by recording, with volumetric calcium imaging, the response to odor stimulation in the MBC of animals expressing a genetically encoded calcium indicator tethered at the KC postsynapses (Pech et al., 2015) in combination with a presynaptic fluorescent tag (*UAS-tdTomato*) expressed in DA1 PNs only (Figure 1C). Regions of interest (ROIs) containing fluorescently labeled DA1-MGs showed a postsynaptic response specifically tuned to cVA stimulation (84% ± 8% of the fluorescently labeled DA1-MGs responded to cVA and not to the solvent alone, 9% ± 7% did not respond to cVA or the solvent, and 7% ± 5% responded to both. Data are expressed as means ± SD; n = 7; Figure 1C).

Therefore, by selecting the combination of the cVA odorant and the DA1 subset of PNs, we established a system in which we can track a fly's neuronal response toward a specific odor on the level of individual synaptic complexes in the MBC (Figures 1A–1C).

To gain insight into the complexity of the MG microcircuit formed by a single DA1-PN bouton, we took advantage of the availability of an adult whole-brain electron microscopy (EM) volume (Zheng et al., 2018). With this dataset, we reconstructed a complete MG connectome by tracing neurites from every pre- and postsynaptic contact of a DA1-PN bouton until the corresponding neuron's identity was anatomically determinable (Figures 1D and 1E; Table S1). This particular DA1-PN bouton made 33 excitatory cholinergic contacts, all polyadic and identifiable by the presence of a T-bar and a synaptic cleft (Figure 1E, inset), apposed to 277 postsynaptic profiles. Most profiles (248) postsynaptic to the bouton originated from 14 KCs of five different subtypes: γmain (8), αβs (3), αβc (1), α′β′ap (1), and α′β′m (1) (Aso et al., 2014). γMain profiles were the most abundant in this particular bouton, although DA1-PN boutons are located within a region of the MBC predominantly occupied by αβs KCs (Lin et al., 2007). Each KC contacted the bouton with a single claw receiving eight to 25 presynaptic inputs from the PN bouton, in line with previous estimates (Butcher et al., 2012, Leiss et al., 2009). Within the MG, the bouton received presynaptic input from four cells: two additional γmain KCs forming divergent triads that included a KC, the PN bouton, and the anterior paired lateral neuron (Liu and Davis, 2009); APL itself, and one of the two MB calyx 1 neurons (MB-C1) (Table S1). Taken together, a single MG represents a highly complex microcircuit, involving many neurons (19 in this example) of different types (here, eight).

Structural changes in calycal MGs upon memory consolidation

To investigate whether such a complex structure undergoes plastic changes, we designed a setup to observe and measure the properties of identifiable MGs after olfactory conditioning.

In confocal images, we highlighted cVA-responsive MGs in the MBC by expressing the presynaptic active zone (AZ) marker Brp-short^{cherry} in DA1-PNs only (Schmid et al., 2008, Kremer et al., 2010). The postsynaptic densities (PSDs) of KC dendrites were decorated by cell-type-specific expression of the GFP-tagged Dα7 subunit of the acetylcholine receptor (Kremer et al., 2010). We developed a software-based automated three-dimensional (3D)-reconstruction tool to identify the MGs exploiting the *MB247-Dα7::GFP* signal and classified them as DA1-PN-positive if they additionally displayed Brp-short^{cherry} co-labeling (DA1-MG; Figures 1G and S1). Further, we established a standard appetitive-associative conditioning paradigm using cVA or geranyl acetate (GA) as CS in STM or LTM paradigms (Figures 2A and S2A–S2C; see STAR Methods) and applied it to flies expressing the reporters described above (Figures 2B, 2F, and 2J). Alternatively, we mock-trained the flies by presenting odors and sugar reward separately to avoid the formation of appetitive association (Figures 2A, 2B, 2F, and 2J; Tempel et al., 1983). GA was chosen because it activates a separate and non-overlapping set of PNs in comparison to cVA (Bhandawat et al., 2007), and 5% EtOH was added to both odors to provide a food-related context to the starved flies (Lebreton et al., 2015, Pohl et al., 2012), which was essential to elicit STM (Figure S2B). To assess whether MGs formed by DA1-PN boutons (DA1-MGs) underwent morphological modifications after learning, we prepared for confocal imaging female fly brains dissected at 1 min (STM) or at 24 h (LTM) after training. After STM establishment (Figure 2B), the total number, MG volume, and lumen volume of DA1-MGs was unchanged in cVA-conditioned (cVA CS$^+$) flies compared with the GA-conditioned (GA CS$^+$) or mock control groups (average MG numbers: mock 28.91; GA CS$^+$ 30.40; cVA CS$^+$ 28.76; n = 10–17; Figures 2C–2E). However, in the LTM paradigm (Figure 2F), the DA1-MGs total volume and lumen volume were decreased in cVA CS$^+$ flies compared with GA CS$^+$ or mock-control flies (Figures 2G and 2H). In addition, the total number of DA1-MGs was increased (average MG numbers: mock 27.31; GA CS$^+$ 27.47; cVA CS$^+$ 32.06; n = 18-32; Figure 2I). Thus, LTM, but not STM, was accompanied by an input-specific structural reorganization of the MBC circuit, including an increase in MG number. These changes were specific to the conditioned odor because they did not appear in the DA1-MGs when the conditioned odor was GA. These data suggest that the neurons delivering the CS form new boutons, which are smaller and are enveloped by KC claws.

Olfactory associative learning relies on the function of the Ca^{2+}/CaM-dependent adenylyl cyclase Rutabaga (Tempel et al., 1983, Levin et al., 1992, Thum et al., 2007), and a defining trait of LTM is its dependence on protein synthesis (Lagasse et al., 2009, Tully et al., 1994, Davis, 2011). Indeed, a mutation in the *rutabaga* gene (*rut^{2080}*(Han et al., 1992) or feeding flies with the protein synthesis inhibitor cycloheximide (CHX) immediately after training abolished LTM (Figures 2J and S2D). Importantly, loss of *rut* function or CHX feeding also suppressed the

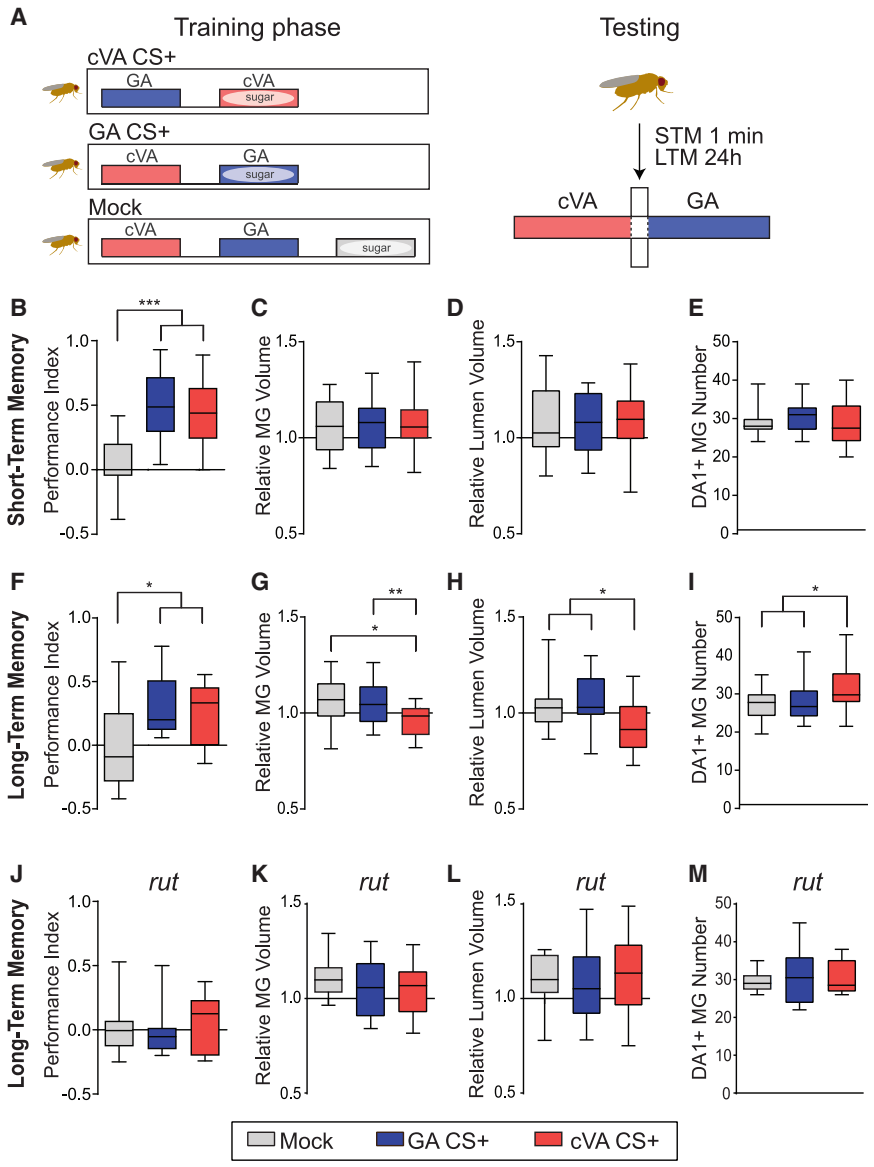

Figure 2. Microglomeruli undergo structural changes upon appetitive long-term memory formation

(A) Schematic illustration of the appetitive-conditioning paradigm. For training, the conditioned odor cVA (red box) or GA (blue box) is paired with sugar. In STM experiments, flies are trained for 2 min with a 2 min interval between CS^+ and CS^- presentation and tested 1 min after training. In LTM experiments, flies are trained for 5 min + 5 min with a 2-min stimulus interval and are tested 24 h after training. In the mock control, the two odors and the sugar reward are presented in a temporally spaced sequence with a 2-min inter-stimulus pause.

(B, F, and J) Performance indices of flies *R37H08-Gal4/MB247-DαGFP, UAS-brp-short^{cherry}* in the STM (B), ***$p < 0.001$, n = 19–25; or in the LTM paradigm (F), *$p < 0.05$, n = 14–19; and the performance index of *rut* mutant flies in LTM (J), $p > 0.05$, n = 17–18. Performance index values of the mock control group (gray) were compared with groups trained with GA CS^+ (blue) or cVA CS^+ (red). Multiple comparisons are tested throughout this study with one-way ANOVA with Bonferroni correction. Significance level is set at $p < 0.05$. *$p < 0.05$, ****$p < 0.0001$.

(C, G, and K) The MG volume comprises the volume contained within a ring of *MB247-Dα7::GFP* PSDs and the volume of the *MB247-Dα7::GFP* PSDs .

(D, H, and L) The MG lumen is the volume contained within a ring of *MB247-Dα7::GFP* PSDs (see Figure S1D). In STM, the relative volume (ratio of the average DA1-MG/non-DA1-MG per animal) of DA1- MGs (C) and of their lumen (D) is not different between groups ($p > 0.05$, n = 15–20). In LTM, the relative MG volume (G) and lumen volume (H) of DA1-MGs in flies trained with cVA CS^+ are smaller than in flies from the mock control group or in flies trained with GA CS^+ (*$p < 0.05$, **$p < 0.01$, n = 19–25).

(E, I, and M) Number of DA1-PN-positive MGs is unaffected in STM (E) ($p > 0.05$, n = 18–24). In LTM, number of DA1-PN-positive MGs in cVA CS^+ trained flies is greater compared with flies of the mock control or GA CS^+ group (I) (*$p < 0.05$, n = 18–24). The structural modifications of DA1- MGs in cVA CS^+ trained flies after the appetitive LTM protocol, were suppressed in *rut* mutants (K)–(M) ($p > 0.05$, n = 13–21). In all boxplots, the edges of the boxes are the first and third quartiles, thick lines mark the medians, and whiskers represent data range.

structural changes in the DA1-MGs, supporting the correlation between LTM formation and structural changes in the circuit (Figures 2K–2M and S2E–S2G).

The increase in DA1-PN-positive MG number after LTM formation with cVA CS^+ suggests that new boutons might be formed during consolidation. To gain insight into the cellular fundamentals of these modifications, we expressed the membrane-tagged fluorescent protein *UAS-GAP43::Venus* in DA1-PN axons, together with *UAS-brp-short^{cherry}*, and highlighted the postsynaptic densities on KC dendrites using *MB247-Dα7::GFP* (Figures 3A–3D). Serial optical sections of the MBCs of these flies trained with cVA CS^+, with GA CS^+, or in the mock paradigm (Figure S2H) were used to generate 3D reconstructions that were then aligned to a reference brain (JFRC2; Jenett et al., 2012). The DA1-PN axons were then traced in the aligned high-resolution scans of the MBC (Figure 3E). The DA1-PN boutons were highly clustered in the dorsal-posterior part of the calyx (Clark and Evans, 1954), supporting the view that the localization of DA1-PN boutons within the MBC is not entirely random (Figure 3F; Jefferis et al., 2007). The total length of DA1-PN collaterals measured from the point at which they leave the inner antennocerebral tract (iACT) was increased in flies that had formed LTMs after cVA CS^+ training compared with mock-control flies (Figure 3G). In addition, the total volume within the MBC containing DA1-PN-positive boutons was increased in flies that had formed cVA CS^+ LTMs (Figure 3H). These observations suggest that during

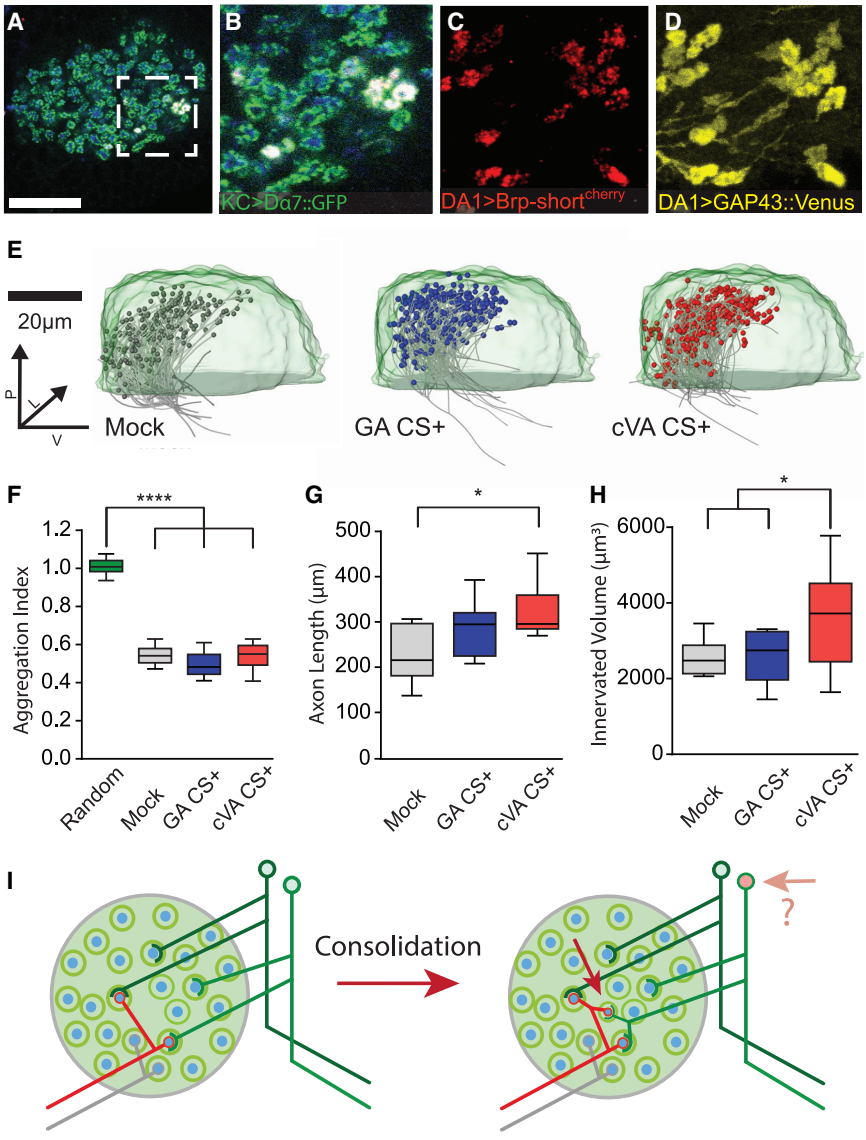

Figure 3. Modifications of axon collaterals and wiring properties of projection neurons within the mushroom body calyx after long-term memory formation

(A) Single optical section of the MBC of flies expressing Dα7GFP (green) in the KCs and Brp-short^{cherry} (red) plus GAP43-Venus (yellow) in DA1-PNs (*R37H08-Gal4*); PN boutons (blue; anti-Synapsin antibodies). Scale bar, 20 µm.

(B–D) Magnification of the white square in (A) displaying its merge (B) or a maximum-intensity projection of Brp-short^{cherry} (C) or of GAP43-Venus (D) signals.

(E) Medial view of registered PN axons (gray) with traced boutons (gray, blue, red spheres) within a standard calyx (light green). The registered PN traces are of mock (gray), GA CS$^+$ (blue) or cVA CS$^+$ (red) trained groups. n = 10 for each group.

(F) Boutons are highly clustered, independent of the treatment (Clark and Evans aggregation index compared with a hypothetical random distribution; ****$p < 0.0001$, n = 10).

(G) Total collateral axons length of mock control, GA CS$^+$ or cVA CS$^+$ flies. (*$p < 0.05$, n = 10).

(H) The convex hull volume containing all DA1-boutons in the MBC per condition is increased in cVA CS$^+$ flies compared with the mock control and GA CS$^+$ group (*$p < 0.05$, n = 10).

(I) We suggest that the increased number of MGs after consolidation is due to the formation of additional boutons responding to cVA. The additional boutons form full MGs, as postsynaptic profiles of KCs surround them. It is unclear whether this reorganization might lead to the recruitment of additional responding KCs (see Discussion). In all boxplots, the edges of the boxes are the first and third quartiles, thick lines mark the medians, and whiskers represent data range.

consolidation, additional boutons are created by local growth at existing DA1-PN collaterals (Figure 3I).

Altered functional response in calycal microglomeruli upon memory consolidation

To address whether the observed structural changes within the MGs after LTM effect on the functional representation of the CS in the MBC, we analyzed calcium dynamics in KC dendrites. For that, we used flies carrying *MB247-homer::GCaMP3* (Pech et al., 2015), in combination with volumetric calcium imaging (Figure 4A). We used this simple genotype to guarantee that flies performed well in LTM experiments (Figure S2I). We measured calcium response in the entire MBC volume during a single odor application (5 s odor stimulation) of either cVA (1:400 in 5% EtOH) or EtOH alone (5%). To identify areas with increased calcium dynamics during odor stimulation, we overlaid a grid consisting of 5 × 5-µm^2 ROIs over each optical section of the volumetric time series. Based on the grid segmentation, we then calculated the average ΔF/F% for each ROI in the MBC. ROIs were classified as odor responsive if the measured calcium response exceeded a set threshold (ΔF/F% > 3 × SD; see STAR Methods) during the first 2 s of stimulation (Figures 4B, 4C, S3A, and S3B). The response pattern elicited specifically by cVA was defined after subtraction of the EtOH response (Figures 4C, S3C, and S3D; see also Figure 1C and STAR Methods). After appetitive LTM formation, the percentage of cVA-responsive ROIs was increased in cVA CS$^+$ flies compared with the mock control (Figure 4D; n = 7, $p < 0.05$), suggesting that the additional DA1-PN boutons are functionally connected to their postsynaptic KC counterparts and are capable of initiating a response in the postsynaptic KCs. Linear regression analysis of the fluorescence change over time during odor stimulation showed a steeper drop of the linear fit in cVA CS$^+$ flies (R^2 = 0.6429) toward baseline compared with flies of the mock control group (R^2 = 0.1124) (Figures 4E and 4F). In addition, the response toward the odor was more variable in mock-trained flies compared with the cVA CS$^+$ flies (Figure S3F). Initially (0–4 s after

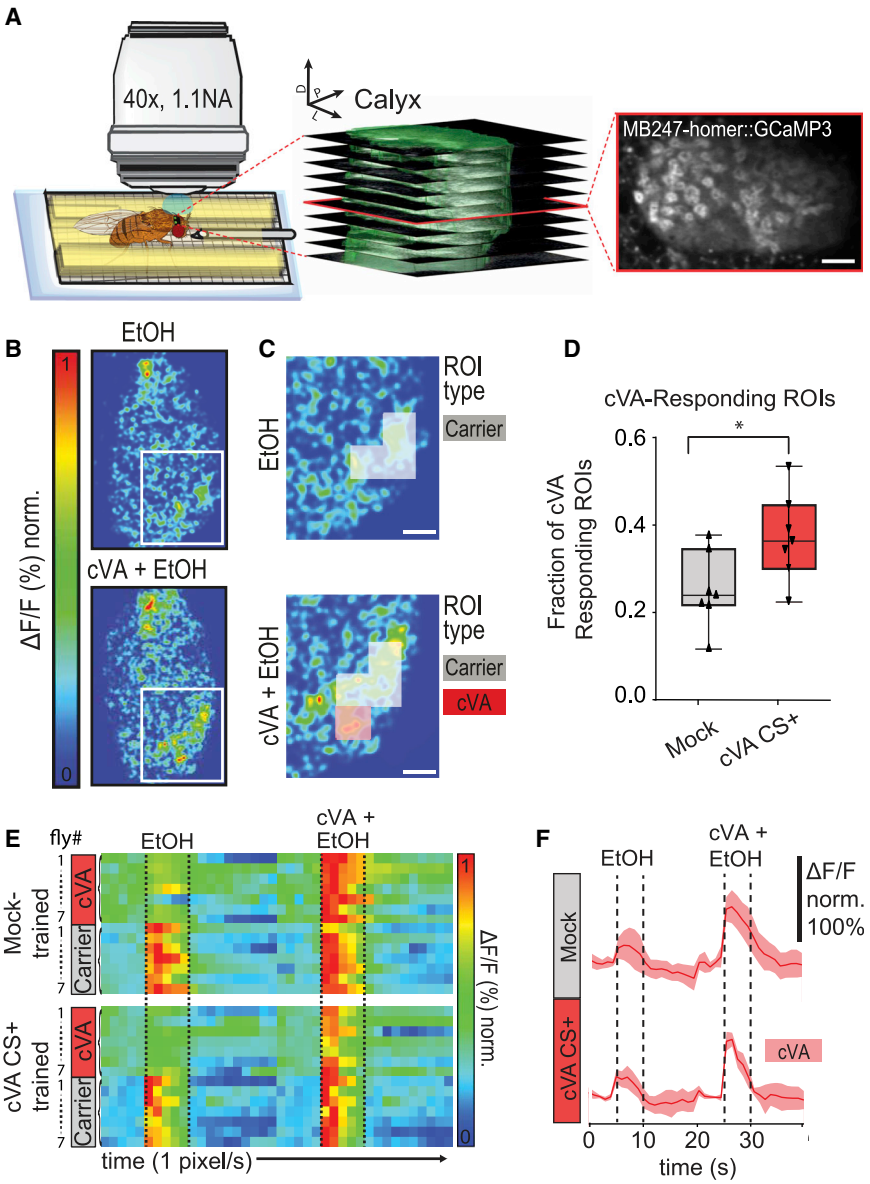

Figure 4. Functional plasticity in the mushroom body calyx associated with long-term memory

(A) Two-photon *in vivo* imaging setup. Schematic of a fly placed on a custom-made holder under a two-photon microscope equipped with a ×40 1.1 NA water-immersion objective. The odor was delivered for 5 s with a moisturized, constant air stream through a 1.2-mm cannula. (Center) z series of the entire MBC volume of flies expressing post-synapse-tagged Homer-GCaMP3 imaged during odor application at 1 Hz (10 optical sections per volume, 4-μm step size). (Right) A single slice of the image stack shown in the middle panel. Scale bar, 10 μm.

(B) Representative optical section from a volumetric time series showing false-colored response of KC dendrites to 5-s exposure to EtOH (top) or cVA + EtOH (bottom).

(C) Magnification of the white square area in (B). 5 × 5-μm^2 ROIs were classified as cVA-responsive (red) if they were only active during cVA + EtOH application but did not respond to EtOH alone. ROIs that responded to both conditions were classified as carriers. Scale bar, 5 μm.

(D) The fraction of cVA responsive ROIs increased after LTM acquisition compared with that of the mock control (boxplot represents first and third quartiles, thick lines mark the medians, and whiskers represent data range. *$p < 0.05$, $n = 7$).

(E) Dynamics of ΔF/F% changes over time in KCs of *MB247-homer::GCaMP3* flies after mock training (top) or LTM acquisition (bottom). Each row of the heatmap represents average responses per animal of all cVA-responsive ROIs (red) or of all carrier EtOH-responsive ROIs (gray) within one MBC over time. Each column represents 1 s. Flies are first exposed to the EtOH (5 s) and then to cVA + EtOH (5 s), as indicated by the dashed lines.

(F) Plot of average calcium dynamics over time of cVA-responsive ROIs during 5-s stimulation with EtOH or with cVA in EtOH (dashed lines) in mock-trained (top) or cVA CS^+ (bottom) flies ($n = 7$). Data are represented as means ± SD.

start of stimulation), the total response toward cVA stimulation was indistinguishable between mock control and cVA CS^+ group. However, at subsequent time points (4–7 s after start of stimulation) responses were significantly lower in KC dendrites of the cVA CS^+ group compared with the mock control, showing a faster calcium decay toward the trained odor in CS^+ flies ($n = 7$, $p < 0.05$) (Figure S3G). Together, these data indicate a temporal sharpening of the odor response.

DISCUSSION

We report input-specific reorganization of the adult MBC circuit associated with the formation of long-term, appetitive memory. By visualizing presynaptic markers in PNs and the KC postsynaptic densities, we uncover an increase in the number of PN boutons and, at the same time, reveal that these boutons are enveloped by KC postsynaptic profiles, suggesting that new MGs are formed during memory consolidation. These findings are particularly remarkable, given the high degree of complexity of the MG microcircuits revealed by our EM reconstruction and including the dendrite claws of multiple KCs of distinct subtypes. The cellular mechanisms leading to the increased number of odor-specific complex MGs remain to be clarified, but they will require a tight coordination between pre- and postsynaptic partners. In this context, mutations in synaptic proteins or in proteins mediating cell-cell interactions, which specifically block LTM, will be of great interest (Silva et al., 2020, Gouzi et al., 2018). We suggest that remodeling could be driven by intrinsic reactivation of KCs during the consolidation phase (Ichinose et al., 2015, Cognigni et al., 2018) or by modulatory inputs into the calyx (Mao and

Davis, 2009, Chen et al., 2012, Aso et al., 2014, Busch et al., 2009, Boto et al., 2019). In either case, we expect a complex pattern of activation, which might be difficult to reproduce in artificial settings (Kremer et al., 2010, Warth Pérez Arias et al., 2020). Although our present observations are limited for technical reasons to the specific case of cVA, the overall density of PN boutons in the MBC increases after appetitive long-term conditioning in honeybees, as well as in leaf-cutting ants after avoidance learning (Hourcade et al., 2010, Falibene et al., 2015). Based on that and given that the olfactory pathway of cVA is not distinguishable from that of other odors, we thus suggest that our findings might be generalizable. In comparison with those systems, however, we use genetic and functional identification of PN subsets to reveal that the structural modifications are specific and limited to the PNs conveying the conditioned odor. Importantly, our *in vivo* functional imaging data support the view that the circuit reorganization leads to additional functional MGs responding to the conditioned odor. In addition, they demonstrate a specific change in functional response in the KC dendrites toward the trained odor because the calcium levels drop faster toward baseline after appetitive associative conditioning. The faster decay kinetics and more skewed response toward the onset of the stimulus could contribute to a more-efficient temporal summation of responses or refine the KC response and might be related to inhibitory modifications (Gupta and Stopfer, 2014, Haenicke et al., 2018). An important open question is the effect of the increased number of responding MGs on the pattern of KC activation. KCs respond sparsely to odor input and require the coincident activation of multiples of their claws to produce an action potential (Gruntman and Turner, 2013). Our data might underlie the addition of connections between the active PNs and a set of already-responding KCs, leading to facilitated response to the conditioned odor without changing the set of responding KCs. A recent publication, however, suggests an exciting alternative view. After aversive LTM establishment, the number of KCs responding to the conditioned odor is increased (Delestro et al., 2020). If we hypothesize that appetitive conditioning leads to a similar outcome, our data could provide anatomical and functional support to these findings. The pattern of KC response could, thus, be modulated by experience in adulthood and might represent a rich signifier of sensory stimulus and context. Reconstruction of an MG from EM serial sections derived from FAFB dataset (Zheng et al., 2018). Video S1 shows a DA1-PN bouton (red) and all profiles that are directly pre- or postsynaptic to it. The DA1-PN bouton is surrounded by the claws of 14 KCs of five subtypes (different green shades according to Figures 1D and 1E). Three additional neurons contribute to this MG: APL (blue), which is pre- and postsynaptic to the PN bouton, and both MB-C1 neurons (yellow). Finally, two γmain KCs (dark green) form presynaptic connections with the bouton. See also Table S1. All genotypes and statistical tests (including p values) used throughout the document, are ordered by appearance.

STAR★METHODS

Detailed methods are provided in the online version of this paper and include the following:

SUPPLEMENTAL INFORMATION

Supplemental information can be found online at https://doi.org/10.1016/j.celrep.2021.108871.

ACKNOWLEDGMENTS

We thank LMF and IDAF sections at DZNE and A. Mueller, R. Kerpen, and J. C. Vijayakumar for technical assistance. We are grateful to C.B. Fisher, S.A. Calle-Schuler, N. Sharifi, B. Gorko, L. Kmecova, I.J. Ali, N. Masoodpanah, J. Hsu, and F. Li in the D.D.B. laboratory for their support in tracing evaluation. We thank Y. Aso, HHMI Janelia, the Kyoto Drosophila Genetic Resource Center, and the Bloomington Stock Center for fly lines and FlyBase. We are grateful for their assistance to the DZNE IDAF in the establishment of the cluster analysis, S. Dipt with initial calcium imaging experiments, and R. Court for providing the brain aligner and support. We thank S. Sachse, D. Isbrandt, T. Hige, S. Remy, M. Nawrot, O. Barnstedt, the members of the Tavosanis lab for discussion and/or critical reading of the manuscript, and B. Schaffran for help with video editing. L.B. acknowledges support by the Bonn International Graduate School of Neuroscience. This work was supported by the DFG FOR 2705 to G.T.

AUTHOR CONTRIBUTIONS

L.B. and G.T. conceived the project and designed the experiments. L.B., P.R., and L.P. constructed fly strains, performed the behavioral experiments, and produced and analyzed the anatomical data. J.S.L. and D.D.B. established the set of EM data, and P.R. performed the tracings presented here. Scripts and routines for the analysis were established by L.B. and L.P. Functional imaging experiments were designed and performed by L.B and L.P. with support from A.F. The manuscript was written by G.T., L.B., P.R., and L.P.

DECLARATION OF INTERESTS

The authors declare no competing interests.

Received: August 26, 2020
Revised: January 7, 2021
Accepted: February 24, 2021
Published: March 16, 2021

REFERENCES

Aso, Y., Hattori, D., Yu, Y., Johnston, R.M., Iyer, N.A., Ngo, T.T., Dionne, H., Abbott, L.F., Axel, R., Tanimoto, H., and Rubin, G.M. (2014). The neuronal

architecture of the mushroom body provides a logic for associative learning. eLife *3*, e04577.

Bailey, C.H., Bartsch, D., and Kandel, E.R. (1996). Toward a molecular definition of long-term memory storage. Proc. Natl. Acad. Sci. USA *93*, 13445–13452.

Bassett, D.S., Wymbs, N.F., Porter, M.A., Mucha, P.J., Carlson, J.M., and Grafton, S.T. (2011). Dynamic reconfiguration of human brain networks during learning. Proc. Natl. Acad. Sci. USA *108*, 7641–7646.

Bennett, S.H., Kirby, A.J., and Finnerty, G.T. (2018). Rewiring the connectome: evidence and effects. Neurosci. Biobehav. Rev. *88*, 51–62.

Bhandawat, V., Olsen, S.R., Gouwens, N.W., Schlief, M.L., and Wilson, R.I. (2007). Sensory processing in the Drosophila antennal lobe increases reliability and separability of ensemble odor representations. Nat. Neurosci. *10*, 1474–1482.

Boele, H.J., Koekkoek, S.K., De Zeeuw, C.I., and Ruigrok, T.J. (2013). Axonal sprouting and formation of terminals in the adult cerebellum during associative motor learning. J. Neurosci. *33*, 17897–17907.

Boto, T., Stahl, A., Zhang, X., Louis, T., and Tomchik, S.M. (2019). Independent contributions of discrete dopaminergic circuits to cellular plasticity, memory strength, and valence in *Drosophila*. Cell Rep. *27*, 2014–2021.e2.

Boto, T., Stahl, A., and Tomchik, S.M. (2020). Cellular and circuit mechanisms of olfactory associative learning in *Drosophila*. J. Neurogenet. *34*, 36–46.

Burke, C.J., Huetteroth, W., Owald, D., Perisse, E., Krashes, M.J., Das, G., Gohl, D., Silies, M., Certel, S., and Waddell, S. (2012). Layered reward signalling through octopamine and dopamine in *Drosophila*. Nature *492*, 433–437.

Busch, S., Selcho, M., Ito, K., and Tanimoto, H. (2009). A map of octopaminergic neurons in the *Drosophila* brain. J. Comp. Neurol. *513*, 643–667.

Butcher, N.J., Friedrich, A.B., Lu, Z., Tanimoto, H., and Meinertzhagen, I.A. (2012). Different classes of input and output neurons reveal new features in microglomeruli of the adult *Drosophila* mushroom body calyx. J. Comp. Neurol. *520*, 2185–2201.

Cardona, A., Saalfeld, S., Schindelin, J., Arganda-Carreras, I., Preibisch, S., Longair, M., Tomancak, P., Hartenstein, V., and Douglas, R.J. (2012). TrakEM2 software for neural circuit reconstruction. PLoS ONE *7*, e38011.

Caron, S.J., Ruta, V., Abbott, L.F., and Axel, R. (2013). Random convergence of olfactory inputs in the *Drosophila* mushroom body. Nature *497*, 113–117.

Caroni, P., Donato, F., and Muller, D. (2012). Structural plasticity upon learning: regulation and functions. Nat. Rev. Neurosci. *13*, 478–490.

Cervantes-Sandoval, I., Martin-Peña, A., Berry, J.A., and Davis, R.L. (2013). System-like consolidation of olfactory memories in *Drosophila*. J. Neurosci. *33*, 9846–9854.

Chen, C.C., Wu, J.K., Lin, H.W., Pai, T.P., Fu, T.F., Wu, C.L., Tully, T., and Chiang, A.S. (2012). Visualizing long-term memory formation in two neurons of the *Drosophila* brain. Science *335*, 678–685.

Chen, J.L., Margolis, D.J., Stankov, A., Sumanovski, L.T., Schneider, B.L., and Helmchen, F. (2015). Pathway-specific reorganization of projection neurons in somatosensory cortex during learning. Nat. Neurosci. *18*, 1101–1108.

Chklovskii, D.B., Mel, B.W., and Svoboda, K. (2004). Cortical rewiring and information storage. Nature *431*, 782–788.

Clark, P.J., and Evans, F.C. (1954). Distance to nearest neighbour as a measure of spatial relationships in populations. Ecology *35*, 445–453.

Cognigni, P., Felsenberg, J., and Waddell, S. (2018). Do the right thing: neural network mechanisms of memory formation, expression and update in *Drosophila*. Curr. Opin. Neurobiol. *49*, 51–58.

Costa, M., Manton, J.D., Ostrovsky, A.D., Prohaska, S., and Jefferis, G.S. (2016). NBLAST: rapid, sensitive comparison of neuronal structure and construction of neuron family databases. Neuron *91*, 293–311.

Cuntz, H., Forstner, F., Borst, A., and Häusser, M. (2010). One rule to grow them all: a general theory of neuronal branching and its practical application. PLoS Comput. Biol. *6*, e1000877.

Datta, S.R., Vasconcelos, M.L., Ruta, V., Luo, S., Wong, A., Demir, E., Flores, J., Balonze, K., Dickson, B.J., and Axel, R. (2008). The *Drosophila* pheromone cVA activates a sexually dimorphic neural circuit. Nature *452*, 473–477.

Davis, R.L. (2011). Traces of *Drosophila* memory. Neuron *70*, 8–19.

de Belle, J.S., and Heisenberg, M. (1994). Associative odor learning in *Drosophila* abolished by chemical ablation of mushroom bodies. Science *263*, 692–695.

Delestro, F., Scheunemann, L., Pedrazzani, M., Tchenio, P., Preat, T., and Genovesio, A. (2020). In vivo large-scale analysis of *Drosophila* neuronal calcium traces by automated tracking of single somata. Sci. Rep. *10*, 7153.

Dubnau, J., and Chiang, A.S. (2013). Systems memory consolidation in *Drosophila*. Curr. Opin. Neurobiol. *23*, 84–91.

Falibene, A., Roces, F., and Rössler, W. (2015). Long-term avoidance memory formation is associated with a transient increase in mushroom body synaptic complexes in leaf-cutting ants. Front. Behav. Neurosci. *9*, 84.

Gogolla, N., Galimberti, I., and Caroni, P. (2007). Structural plasticity of axon terminals in the adult. Curr. Opin. Neurobiol. *17*, 516–524.

Gouzi, J.Y., Bouraimi, M., Roussou, I.G., Moressis, A., and Skoulakis, E.M.C. (2018). The *Drosophila* receptor tyrosine kinase Alk constrains long-term memory formation. J. Neurosci. *38*, 7701–7712.

Grabe, V., Strutz, A., Baschwitz, A., Hansson, B.S., and Sachse, S. (2015). Digital in vivo 3D atlas of the antennal lobe of *Drosophila* melanogaster. J. Comp. Neurol. *523*, 530–544.

Grewe, B.F., Gründemann, J., Kitch, L.J., Lecoq, J.A., Parker, J.G., Marshall, J.D., Larkin, M.C., Jercog, P.E., Grenier, F., Li, J.Z., et al. (2017). Neural ensemble dynamics underlying a long-term associative memory. Nature *543*, 670–675.

Gruntman, E., and Turner, G.C. (2013). Integration of the olfactory code across dendritic claws of single mushroom body neurons. Nat. Neurosci. *16*, 1821–1829.

Gu, S., Pasqualetti, F., Cieslak, M., Telesford, Q.K., Yu, A.B., Kahn, A.E., Medaglia, J.D., Vettel, J.M., Miller, M.B., Grafton, S.T., and Bassett, D.S. (2015). Controllability of structural brain networks. Nat. Commun. *6*, 8414.

Gupta, N., and Stopfer, M. (2014). A temporal channel for information in sparse sensory coding. Curr. Biol. *24*, 2247–2256.

Haenicke, J., Yamagata, N., Zwaka, H., Nawrot, M., and Menzel, R. (2018). Neural correlates of odor learning in the presynaptic microglomerular circuitry in the honeybee mushroom body calyx. eNeuro *5*, eneuro.0128-18.2018.

Han, P.L., Levin, L.R., Reed, R.R., and Davis, R.L. (1992). Preferential expression of the *Drosophila* rutabaga gene in mushroom bodies, neural centers for learning in insects. Neuron *9*, 619–627.

Hihara, S., Notoya, T., Tanaka, M., Ichinose, S., Ojima, H., Obayashi, S., Fujii, N., and Iriki, A. (2006). Extension of corticocortical afferents into the anterior bank of the intraparietal sulcus by tool-use training in adult monkeys. Neuropsychologia *44*, 2636–2646.

Holtmaat, A., and Caroni, P. (2016). Functional and structural underpinnings of neuronal assembly formation in learning. Nat. Neurosci. *19*, 1553–1562.

Hourcade, B., Muenz, T.S., Sandoz, J.C., Rössler, W., and Devaud, J.M. (2010). Long-term memory leads to synaptic reorganization in the mushroom bodies: a memory trace in the insect brain? J. Neurosci. *30*, 6461–6465.

Ichinose, T., Aso, Y., Yamagata, N., Abe, A., Rubin, G.M., and Tanimoto, H. (2015). Reward signal in a recurrent circuit drives appetitive long-term memory formation. eLife *4*, e10719.

Jefferis, G.S., Potter, C.J., Chan, A.M., Marin, E.C., Rohlfing, T., Maurer, C.R., Jr., and Luo, L. (2007). Comprehensive maps of *Drosophila* higher olfactory centers: spatially segregated fruit and pheromone representation. Cell *128*, 1187–1203.

Jenett, A., Rubin, G.M., Ngo, T.T., Shepherd, D., Murphy, C., Dionne, H., Pfeiffer, B.D., Cavallaro, A., Hall, D., Jeter, J., et al. (2012). A GAL4-driver line resource for *Drosophila* neurobiology. Cell Rep. *2*, 991–1001.

Josselyn, S.A., and Tonegawa, S. (2020). Memory engrams: Recalling the past and imagining the future. Science *367*, eaaw4325.

Kitamura, T., Ogawa, S.K., Roy, D.S., Okuyama, T., Morrissey, M.D., Smith, L.M., Redondo, R.L., and Tonegawa, S. (2017). Engrams and circuits crucial for systems consolidation of a memory. Science *356*, 73–78.

Kleim, J.A., Freeman, J.H., Jr., Bruneau, R., Nolan, B.C., Cooper, N.R., Zook, A., and Walters, D. (2002). Synapse formation is associated with memory storage in the cerebellum. Proc. Natl. Acad. Sci. USA *99*, 13228–13231.

Kremer, M.C., Christiansen, F., Leiss, F., Paehler, M., Knapek, S., Andlauer, T.F., Förstner, F., Kloppenburg, P., Sigrist, S.J., and Tavosanis, G. (2010). Structural long-term changes at mushroom body input synapses. Curr. Biol. *20*, 1938–1944.

Kurtovic, A., Widmer, A., and Dickson, B.J. (2007). A single class of olfactory neurons mediates behavioural responses to a *Drosophila* sex pheromone. Nature *446*, 542–546.

Lagasse, F., Devaud, J.M., and Mery, F. (2009). A switch from cycloheximide-resistant consolidated memory to cycloheximide-sensitive reconsolidation and extinction in *Drosophila*. J. Neurosci. *29*, 2225–2230.

Lebreton, S., Grabe, V., Omondi, A.B., Ignell, R., Becher, P.G., Hansson, B.S., Sachse, S., and Witzgall, P. (2014). Love makes smell blind: mating suppresses pheromone attraction in *Drosophila* females via Or65a olfactory neurons. Sci. Rep. *4*, 7119.

Lebreton, S., Trona, F., Borrero-Echeverry, F., Bilz, F., Grabe, V., Becher, P.G., Carlsson, M.A., Nässel, D.R., Hansson, B.S., Sachse, S., and Witzgall, P. (2015). Feeding regulates sex pheromone attraction and courtship in *Drosophila* females. Sci. Rep. *5*, 13132.

Leiss, F., Groh, C., Butcher, N.J., Meinertzhagen, I.A., and Tavosanis, G. (2009). Synaptic organization in the adult *Drosophila* mushroom body calyx. J. Comp. Neurol. *517*, 808–824.

Levin, L.R., Han, P.L., Hwang, P.M., Feinstein, P.G., Davis, R.L., and Reed, R.R. (1992). The *Drosophila* learning and memory gene rutabaga encodes a $Ca2^{+}$/calmodulin-responsive adenylyl cyclase. Cell *68*, 479–489.

Lin, H.H., Lai, J.S., Chin, A.L., Chen, Y.C., and Chiang, A.S. (2007). A map of olfactory representation in the *Drosophila* mushroom body. Cell *128*, 1205–1217.

Liu, X., and Davis, R.L. (2009). The GABAergic anterior paired lateral neuron suppresses and is suppressed by olfactory learning. Nat. Neurosci. *12*, 53–59.

Liu, C., Plaçais, P.Y., Yamagata, N., Pfeiffer, B.D., Aso, Y., Friedrich, A.B., Siwanowicz, I., Rubin, G.M., Preat, T., and Tanimoto, H. (2012). A subset of dopamine neurons signals reward for odour memory in *Drosophila*. Nature *488*, 512–516.

Louis, T., Stahl, A., Boto, T., and Tomchik, S.M. (2018). Cyclic AMP-dependent plasticity underlies rapid changes in odor coding associated with reward learning. Proc. Natl. Acad. Sci. USA *115*, E448–E457.

Mao, Z., and Davis, R.L. (2009). Eight different types of dopaminergic neurons innervate the *Drosophila* mushroom body neuropil: anatomical and physiological heterogeneity. Front. Neural Circuits *3*, 5.

Maviel, T., Durkin, T.P., Menzaghi, F., and Bontempi, B. (2004). Sites of neocortical reorganization critical for remote spatial memory. Science *305*, 96–99.

Pech, U., Revelo, N.H., Seitz, K.J., Rizzoli, S.O., and Fiala, A. (2015). Optical dissection of experience-dependent pre- and postsynaptic plasticity in the *Drosophila* brain. Cell Rep. *10*, 2083–2095.

Pohl, J.B., Baldwin, B.A., Dinh, B.L., Rahman, P., Smerek, D., Prado, F.J., 3rd, Sherazee, N., and Atkinson, N.S. (2012). Ethanol preference in *Drosophila* melanogaster is driven by its caloric value. Alcohol. Clin. Exp. Res. *36*, 1903–1912.

Poort, J., Khan, A.G., Pachitariu, M., Nemri, A., Orsolic, I., Krupic, J., Bauza, M., Sahani, M., Keller, G.B., Mrsic-Flogel, T.D., and Hofer, S.B. (2015). Learning enhances sensory and multiple non-sensory representations in primary visual cortex. Neuron *86*, 1478–1490.

Prokop, A., and Meinertzhagen, I.A. (2006). Development and structure of synaptic contacts in *Drosophila*. Semin. Cell Dev. Biol. *17*, 20–30.

Saalfeld, S., Cardona, A., Hartenstein, V., and Tomancak, P. (2009). CATMAID: collaborative annotation toolkit for massive amounts of image data. Bioinformatics *25*, 1984–1986.

Schindelin, J., Arganda-Carreras, I., Frise, E., Kaynig, V., Longair, M., Pietzsch, T., Preibisch, S., Rueden, C., Saalfeld, S., Schmid, B., et al. (2012). Fiji: an open-source platform for biological-image analysis. Nat. Methods *9*, 676–682.

Schlief, M.L., and Wilson, R.I. (2007). Olfactory processing and behavior downstream from highly selective receptor neurons. Nat. Neurosci. *10*, 623–630.

Schmid, A., Hallermann, S., Kittel, R.J., Khorramshahi, O., Frölich, A.M., Quentin, C., Rasse, T.M., Mertel, S., Heckmann, M., and Sigrist, S.J. (2008). Activity-dependent site-specific changes of glutamate receptor composition *in vivo*. Nat. Neurosci. *11*, 659–666.

Silva, B., Niehage, C., Maglione, M., Hoflack, B., Sigrist, S.J., Wassmer, T., Pavlowsky, A., and Preat, T. (2020). Interactions between amyloid precursor protein-like (APPL) and MAGUK scaffolding proteins contribute to appetitive long-term memory in *Drosophila melanogaster*. J. Neurogenet. *34*, 92–105.

Tanaka, N.K., Tanimoto, H., and Ito, K. (2008). Neuronal assemblies of the *Drosophila* mushroom body. J. Comp. Neurol. *508*, 711–755.

Tempel, B.L., Bonini, N., Dawson, D.R., and Quinn, W.G. (1983). Reward learning in normal and mutant *Drosophila*. Proc. Natl. Acad. Sci. USA *80*, 1482–1486.

Thévenaz, P., Ruttimann, U.E., and Unser, M. (1998). A pyramid approach to subpixel registration based on intensity. IEEE Trans. Image Process. *7*, 27–41.

Thum, A.S., Jenett, A., Ito, K., Heisenberg, M., and Tanimoto, H. (2007). Multiple memory traces for olfactory reward learning in *Drosophila*. J. Neurosci. *27*, 11132–11138.

Tully, T., Preat, T., Boynton, S.C., and Del Vecchio, M. (1994). Genetic dissection of consolidated memory in *Drosophila*. Cell *79*, 35–47.

Wang, Y., Mamiya, A., Chiang, A.-S., and Zhong, Y. (2008). Imaging of an early memory trace in the *Drosophila* mushroom body. J. Neurosci. *28*, 4368–4376.

Warth Pérez Arias, C.C., Frosch, P., Fiala, A., and Riemensperger, T.D. (2020). Stochastic and arbitrarily generated input patterns to the mushroom bodies can serve as conditioned stimuli in *Drosophila*. Front. Physiol. *11*, 53.

Yasuyama, K., Meinertzhagen, I.A., and Schürmann, F.W. (2002). Synaptic organization of the mushroom body calyx in *Drosophila melanogaster*. J. Comp. Neurol. *445*, 211–226.

Zheng, Z., Lauritzen, J.S., Perlman, E., Robinson, C.G., Nichols, M., Milkie, D., Torrens, O., Price, J., Fisher, C.B., Sharifi, N., et al. (2018). A complete electron microscopy volume of the brain of adult *Drosophila melanogaster*. Cell *174*, 730–743.e22.

STAR★METHODS

KEY RESOURCES TABLE

REAGENT or RESOURCE	SOURCE	IDENTIFIER
Antibodies		
Mouse monoclonal anti-synapsin	DSHB	Cat#3C11; RRID:AB_528479
Rabbit polyclonal anti-RFP	Rockland	Cat#600-401-379; RRID:AB_2209751
Rabbit monoclonal anti-GFP	Invitrogen	Cat#G10362; RRID:AB_2536526
Mouse monoclonal anti-β-Galactosidase	Abcam	Cat#ab116; RRID:AB_298194
Alexa Fluor568-conjugated goat anti-mouse	Life Technologies	Cat#A11004; RRID:AB_2534072
Alexa Fluor488-conjugated goat anti-rabbit	Life Technologies	Cat#ab150077; RRID:AB_2630356
Alexa Fluor568-conjugated goat anti-rabbit	Life Technologies	Cat#A-11011; RRID:AB_143157
Alexa Fluor633-conjugated goat anti-mouse	Life Technologies	Cat#A21050; RRID:AB_141431
Chemicals, peptides, and recombinant proteins		
11-cis vaccenyl acetate (cVA)	Cayman Chemicals	Cat#10010101; CAS:6186-98-7
Geranyl acetate (GA)	Sigma-Aldrich	Cat#W250910-100G-K; CAS:105-87-3
Cycloheximide (CHX)	Sigma-Aldrich	Cat#C4859; CAS: 66-81-9
Carmine	Sigma-Aldrich	Cat#1159330025CAS: 1390-65-4
Experimental models: organisms/strains		
D. melanogaster: MB247-Dα7::GFP,UAS-brp-short^{cherry}	Kremer et al., 2010	N/A
D. melanogaster: R37H08-Gal4	Bloomington Drosophila Stock center	BDSC 49970; FlyBase: FBti0135337
D. melanogaster: P{w[+mC] = UASp-Venus.GAP43}10	Bloomington Drosophila Stock center	BDSC 30896; FlyBase: FBti0129930
D. melanogaster: P{ry[+t7.2] = IArB}rut [2080];P{w[+mC] = UAS-rut.Z}2	Bloomington Drosophila Stock center	BDSC 9405 FlyBase: FBti0038655 FBti0003267
D. melanogaster: P{UAS-GCaMP3.homer}	Pech et al., 2015	FlyBase: FBtp0180847
D. melanogaster: P{UAS-tdTomato.S}2	Bloomington Drosophila Stock center	BDSC 36327; FlyBase: FBti0145103
D. melanogaster: MB247-Dα7::GFP	Kremer et al., 2010;	FlyBase: FBtp0069947
D. melanogaster: UAS-brp-short^{cherry}	Kremer et al., 2010	FlyBase: FBal0286209
Software and algorithms		
Prism7.01	GraphPad	https://www.graphpad.com/scientific-software/prism/
Definiens Developer XD^{TM}	Definiens Inc.	https://www.astrazeneca.com/sustainability.html
TREES toolbox	Cuntz et al., 2010	https://www.treestoolbox.org/
Amira	Zuse Institute Berlin, Thermo Fischer Scientific	https://www.thermofisher.com/us/en/home/industrial/electron-microscopy/electron-microscopy-instruments-workflow-solutions/3d-visualization-analysis-software/amira-life-sciences-biomedical.html
Fiji/ImageJ	Schindelin et al., 2012	https://imagej.net/Fiji

RESOURCE AVAILABILITY

Lead contact

Further information and requests for resources and reagents should be directed to and will be fulfilled by the lead contact, Gaia Tavosanis (gaia.tavosanis@dzne.de)

Materials availability

All stable reagents generated in this study are available from the lead contact upon request.

DATA AND CODE AVAILABILITY

The electron microscopy dataset analyzed in this study was generated in Zheng et al. (2018).

The Definiens™ script used in this study for microglomeruli detection and analysis is available from the Lead Contact on request.

EXPERIMENTAL MODEL AND SUBJECT DETAILS

Flies were raised at 25°C, 60% relative humidity in a 12h/12h light-dark cycle on a standard cornmeal-based diet and collected 0-4d after eclosion for experiments. Behavioral experiments were performed on mixed populations of female and male adult flies. Brains of adult females were dissected for immunohistochemistry and calcium imaging experiments. The fly stocks used in this work were *R37H08-Gal4* (Kind gift of Y. Aso, HHMI, Janelia), *P{UASp-Venus.GAP43}10* (Bloomington *Drosophila* Stock center), *P{UAS-tdTom.S}2* (Bloomington *Drosophila* Stock center), *P{ry[+t7.2] = IArB}rut[2080]* (Han et al., 1992), *P{UAS-GCaMP3.homer}* (Pech et al., 2015), *MB247-Dα7::GFP* (Kremer et al., 2010) and *UAS-brp-short^{cherry}* (Kremer et al., 2010).

METHOD DETAILS

Behavior

All experimental steps were performed at 23°C, 60% relative humidity using mixed populations of *Drosophila* males and females maintained in a 12h/12h light/dark cycle. Flies were collected 0-4d after eclosion, starved for 24 hours on wet paper tissue (Kimberly-Clark Worldwide Inc.) allowing for water uptake and then trained. In appetitive memory experiments ~80 flies were first exposed to an odor (CS-) alone (2min in short- and 5 minutes in long-term memory experiments). After a 2min inter-stimulus pause flies were trained by receiving dry sucrose on filter paper (3M Chr, Whatman) paired with a second odor (CS+) (2min in short- and 5 minutes in long-term memory experiments). 5 minutes of sugar availability improved the survival of flies undergoing the LTM paradigm. In mock controls, all stimuli used in the associative conditioning experiment were presented separately. Flies were tested after 1min retention time for short- or after 24h retention time for long-term memory. During the 24h retention flies were deprived of food and maintained in tubes containing moist paper tissue. During the test flies were allowed to choose between CS+ and CS- odors in a T-maze for 2min. Odors used for conditioning were 11-*cis* vaccenyl acetate (Cayman Chemicals) 1:400 in 5% EtOH in PBS, geranyl acetate (Sigma Aldrich) 1:100 in 5% EtOH in PBS or 5% EtOH in PBS. EtOH was necessary to provide a food-related context to the starved flies (Figure S2B).

De-novo protein synthesis inhibition

Immediately after training, flies were fed 35 mM cycloheximide (Sigma-Aldrich) (Tully et al., 1994) dissolved in 125mM sucrose and 0.01% carmine solution for 30min. The red dye carmine allowed confirming rapid drug uptake. A control group fed with 125mM sucrose and 0.01% carmine (Sigma-Aldrich) solution showed no learning defects.

Immunohistochemistry

2-5 flies were randomly picked from conditioning experiments right before testing. Brains of females were dissected in cold phosphate-buffered saline (PBS) with 0.05% Triton and subsequently fixed in PBS containing 4% formaldehyde at RT for 50 min. After fixation brains were washed in PBS with 0.3% Triton before incubation overnight at 4°C with the following primary antibodies all diluted in PBS with 0.3% Triton: rabbit anti-RFP (1:2000; Rockland), rabbit anti-GFP (1:200; Life Technologies), mouse monoclonal anti-synapsin (3C11, 1:100; DSHB), mouse monoclonal anti-β-Galactosidase (1:200 Abcam). After washing, the brains were incubated with secondary antibodies in PBS containing 0.3% Triton for 4h at RT.

The secondary antibodies were Alexa Fluor568-conjugated goat anti-rabbit, Alexa Fluor488-conjugated goat anti-rabbit, Alexa Fluor568-conjugated goat anti-mouse, Alexa Fluor633-conjugated goat anti-mouse (all used 1:200 and from Life Technologies). Brains were mounted in Vectashield (Vector) and imaged with a laser scanning confocal microscope (LSM 780, Zeiss). For high resolution scans we used a C Plan-Apochromat 63x/1,4 Oil objective (Zeiss; https://www.micro-shop.zeiss.com/?s=1087224394abbdd&l=en&p=us&f=o&a=v&m=s&id=421782-9900-000) with a voxel size of 0.09x0.09x0.25μm^3 for quantitative analysis. Overviews of entire brains were taken with an LCI Plan-Apochromat 25x/0.8 objective (Zeiss) at a voxel size of 0.55x0.55x1μm^3.

To analyze axon and bouton distribution in the calyx, membrane-tagged Venus was expressed in addition to the previously used markers under the control of a DA1-PN Gal4-driver line (*R37H08-GAL4, UAS-Gap43::Venus / MB247-Dα7::GFP, UAS-brp-short^{cherry}*). Brains of 10 female flies per condition were immunolabelled with anti-synapsin antibodies (as above) and imaged. For PN axon reconstruction a high-resolution scan (0.09x0.09x0.25μm^3, 63x NA1.4 oil immersion) of the right brain hemisphere of female flies was acquired with a confocal microscope. In addition, an overview scan used for registration was taken with a low magnification objective (25x; NA 0.8 multi-immersion).

Two-photon *in vivo* calcium imaging

A mixed population of up to 4d old *MB247-homer::GCaMP3* flies were starved for 18h at 22°C before appetitive conditioning with cVA (1:400, 5% EtOH in PBS), GA (1:100, 5% EtOH in PBS) was used as CS-. Starved untrained flies displayed no bias toward either of these odors at 24 hours. Flies used for imaging were randomly picked from the trained group right before testing. They were used for imaging only if the remaining flies from the same group had learned. For imaging, flies were briefly anesthetized on a Peltier element at 4°C, placed into a custom-built imaging chamber (Figure 4A) and fixed using adhesive tape. The head capsule was opened under Ringerś solution (5 mM HEPES, pH 7.4, 130 mM NaCl, 5 mM KCl, 2 mM $CaCl_2$, 2 mM $MgCl_2$). To minimize movement brains were stabilized with 1,5% low melting agarose (Thermo Scientific) in Ringerś solution. Flies were imaged with a two-photon laser-scanning microscope (LaVision BioTec, TriM Scope II) equipped with an ultra-fast z-motor (PIFOC® Objective Scanner Systems 100μm range) and a Zeiss C-Apochromat 40x, 1.1 NA water –immersion objective. Two-photon images were analyzed using Fiji/ImageJ (Schindelin et al., 2012). GCaMP fluorescence was excited at 920 nm using a Ti:sapphire laser (Coherent Chameleon). A stack consisting of ~10 optical sections was taken at 1Hz in approximately 0,26x0,26μm xy- and at 4μm z- resolution. Odors were applied with a constant humidified air stream (10ml/s) using a commercial device (Stimulus Controller CS 55, Ockenfels SYNTECH GbmH) triggered 5 s after acquisition of the 1st frame by a multifunction I/O module (NI USB-6008), which was controlled by MATLAB (Data Acquisition Toolbox). To record DA1 neurons specific responses, *UAS-tdTomato; R37H08-GAL4, MB247-Homer::GCaMP3* flies were anesthetized on ice, positioned in a polycarbonate imaging chamber (Louis et al., 2018), and immobilized using Myristic Acid (Sigma-Aldrich). To allow optical access to the Calyx, a small window was opened through the head capsule under Ringerś solution. Two-photon microscopy was conducted as described above.

QUANTIFICATION AND STATISTICAL ANALYSIS

EM reconstruction and identification

Neuron skeletons were reconstructed in a serial section transmission electron microscope (ssTEM) volume of a complete female adult *Drosophila melanogaster* brain (Zheng et al., 2018) and manually traced using CATMAID (Saalfeld et al., 2009). Thus, traced neuron skeletons represent the branching of neurons and the location of their cell bodies and synapses. Chemical synapses were manually annotated and identified consistently with the criteria of other CATMAID-based *Drosophila* connectomic studies (Zheng et al., 2018): 1) an active zone (AZ) surrounded by vesicles, 2) a presynaptic specialization (e.g., T-bar), 3) synaptic cleft and 4) a post synaptic density zone (PSD), which however can be absent. If the PSD is absent, we annotated all cells along the synaptic cleft as postsynaptic (Zheng et al., 2018, Prokop and Meinertzhagen, 2006). Neuron identity is based on previously described morphologies in light microscopy (KC subtypes, APL, MB-C1, PN), such as dendritic branching, axonal projection and location in the neuropil (Aso et al., 2014, Tanaka et al., 2008, Liu and Davis, 2009, Grabe et al., 2015, Jefferis et al., 2007). Additionally, we performed a neuron search against a light microscopy dataset in NBLAST (Costa et al., 2016), as described in Zheng et al. (2018) for PN subtype identification. 3D reconstructions of the PN bouton and KC claws from ssTEM sections were created manually with the ImageJ plugin TrakEM2 (Cardona et al., 2012).

Behavior

A performance index (PI) was calculated as the ratio of the difference between the number of flies that chose the CS+ and those that chose the CS- odor and the total number of flies: $PI = \frac{(CS+)-(CS-)}{(CS+)+(CS-)}$.

Axon reconstruction

PN axon reconstruction was performed on the high-resolution scan of Venus signal in the trees toolbox available for MATLAB (Cuntz et al., 2010). In a second step, tracings and high-resolution images were aligned to the registered calyx. For generation of a standard calyx with a volume of 37583 μm^3 (Figure 3E, light green) the Dα7 signal of three registered calyces was averaged and reconstructed in Amira using the segmentation editor. Next, tracings were aligned to the registered overview scan in two steps. First, the iACT of the high-resolution image and of the registered brain in the Venus channel were aligned. Next, the calyx volume of the high-resolution calyx and the standard calyx went through a rigid registration performed in Amira. The alignment parameters were then applied to the axon reconstructions. Boutons were traced on the now registered high-resolution images with the landmark function in Amira. Bouton distribution inside the MBC was evaluated within a 3D grid of 10 μm^3 cubes.

Two-photon image data processing

The time series was processed with a custom Fiji/ ImageJ macro and corrected for small x/y shifts with the StackReg plug-in (Thévenaz et al., 1998). A grid (ROIs, side length 5 μm) was assigned for each optical slide of a stack covering the entire calyx. Intensity tables of each square of the grid were exported to Microsoft Excel and the ΔF/F was calculated. The baseline (F_0) was set by averaging the intensities within each ROI of the 5 frames prior to odor stimulation. ROIs were regarded as responsive, if their normalized ΔF/F% throughout the first 2 s of odor application exceeded 3x the standard deviation of the F_0 of the same ROI in the 5 s (= 5 images) before odor stimulation. The 3x standard deviation threshold was chosen as it provided the suitable sensitivity for the evaluation of odor-elicited responses without introducing excessive noise. ROIs below that threshold were assigned into the category

"unresponsive." ROIs calcium responses higher than the threshold were further subdivided into three categories. The first category was "Carrier" (responsive to both, 5% EtOH and 1:400 cVA, 5% EtOH). The second category was "cVA" (responsive only to 1:400 cVA, 5% EtOH and not to 5% EtOH) or "EtOH" (response only to 5% EtOH application and not to 1:400 cVA, 5% EtOH). To analyze DA1 boutons responses to 5% EtOH and 1:400 cVA+ 5% EtOH were recorded from naive *UAS-tdTomato; R37H08-GAL4, MB247-Homer::GCaMP3* flies, exported to Fiji/ ImageJ and ROIs were manually drawn around DA1 boutons based on the tdTomato fluorescence. Intensity values of each ROI were transferred to Microsoft Excel and ΔF/F values were calculated using the average of the first 5 frames prior to odor stimulation as baseline (F_0). Responsive ROIs were defined as above. These results were age, gender and sequence independent as presenting the odors in a different order did not change the results of the analysis. Calcium traces were generated in Prism 7 (GraphPad Software).

Statistics

Statistical analyses were performed with Prism7.01 software (GraphPad). All data were tested for normality (D'Agostino & Pearson omnibus normality test) and homogeneity of variances (F-test). Comparisons of normally distributed data were tested by a one-sample t test, a two-sample t test or one-way analysis of variance (ANOVA) followed by planned, pairwise multiple-comparison tests with adjusted p values (Bonferroni). Definition of statistical significance was set to < 0.05. Asterisks denote * $p < 0.05$; ** $p < 0.01$; ***$p < 0.001$; **** $p < 0.0001$; n.s. not significant. All experimental tests performed and their relative p values are reported in Table S2.

Cell Reports, Volume *34*

Supplemental information

Circuit reorganization in the *Drosophila* mushroom body calyx accompanies memory consolidation

Lothar Baltruschat, Luigi Prisco, Philipp Ranft, J. Scott Lauritzen, André Fiala, Davi D. Bock, and Gaia Tavosanis

Supplementary Figures

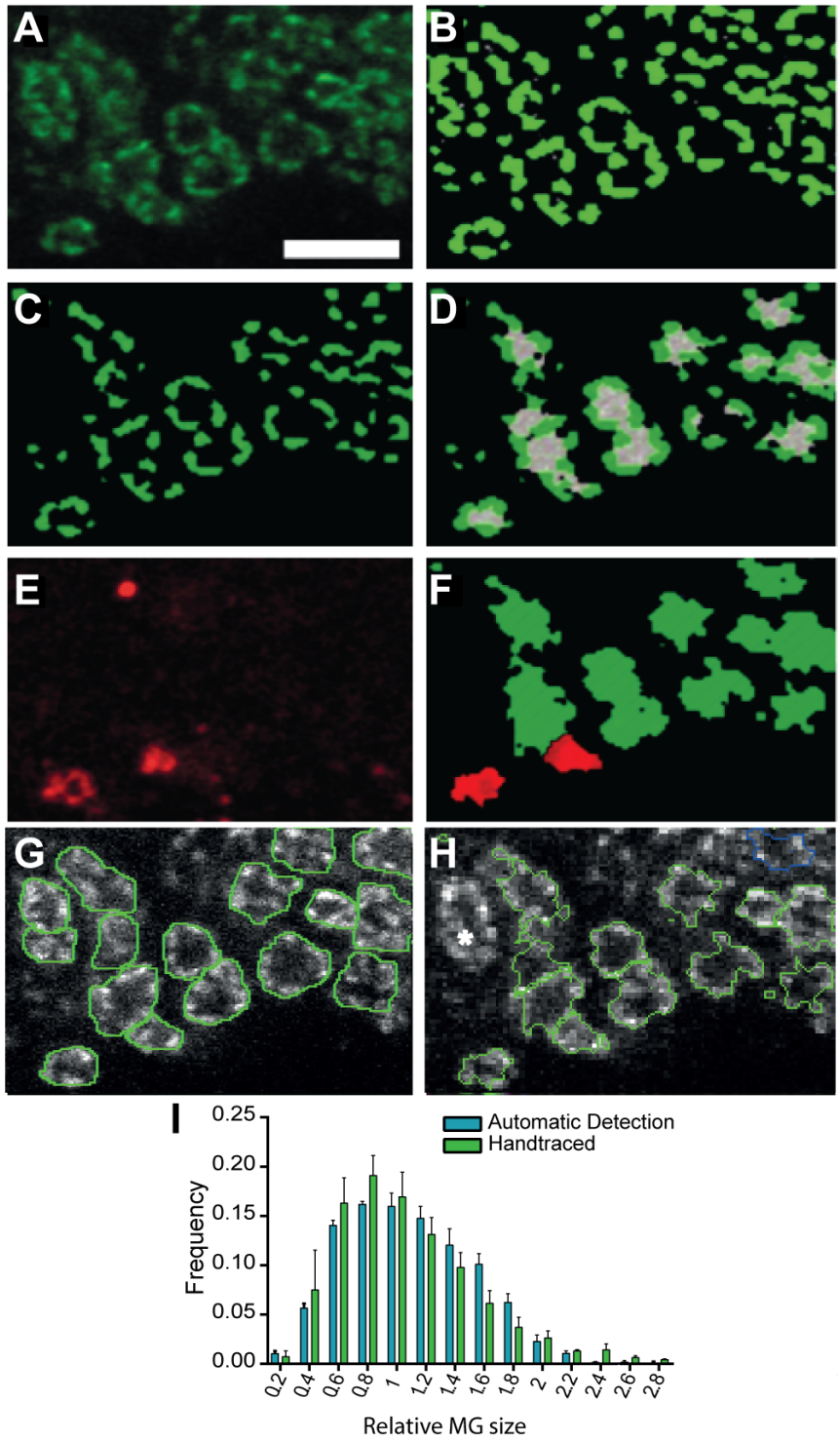

Figure S1| Automated identification and reconstruction of microglomeruli (Related to Figure 1)

(A) Example of a small area from a typical optical section used for the automated detection. Only the green channel containing the Dα7 signal was used for identification of MGs. An anisotropic filter was applied to the original image and contrast was enhanced. Scale bar = 5 µm. **(B)** Initial segmentation of the entire image was performed by grouping pixels with similar grey values into individual objects (green). **(C)** A membership function assigned by applying a histogram shape-based threshold on the brightest objects of this contrast map as candidate objects for MG rings (dark green). **(D)** A second threshold was set to assign seed points for MG lumen within darkest areas surrounded by MG ring candidates. These seed lumen candidate objects grew in a watershed analysis 1 pixel for 5 cycles in 3D into dark areas or until a MG ring candidate object was reached. Lumen candidate objects were classified as "real lumen" (grey) by a fuzzy classification approach depending on lumen candidate volume, their elliptic fit (or roundness) and their relative border with ring candidate objects. Final MG rings (light green) were finally detected in 3D by watersheding into bright areas using the lumens as seed points. **(E)** The red channel containing the Brp-short^{cherry} signal was applied to create objects representing labelled active zones. **(F)** MGs identified in the green channel image that colocalized with the independently generated objects in the red channel image were classified as R37H08-positive (DA1- MGs; red). MGs that did not colocalize with Brp-short^{cherry} signal were displayed in green. **(G)** To evaluate the performance of the routine, all MGs within 4 MBCs were traced manually (green rings) and were overlaid in a custom Matlab script with automatic reconstruction. **(H)** Result of the comparison of the automated and the manual reconstruction shown in (G). MGs detected in the manual reconstruction and in the automated reconstruction are displayed in green ("*correct*"). These were 59% of all manual-counted MG. MGs only detected in the automated reconstruction ("*false-positive*") are displayed in blue and represented ~3.7% of the detected MGs. Additional possible errors of the reconstruction were "*undersegmented*", if multiple MG were fused in the automated reconstruction compared to the manual reconstructions (~2.4% of the detected MGs) and "*false-negative*", if a MG was detected only in the manual reconstruction. **(I)** Comparison of the size distribution of MG detected manually (green) or by the software (blue) in the same optical sections. Comparison of the relative size distribution frequencies with Kolmogorov-Smirnov test revealed no significant difference between manual and automated MG identification ($p>0.5$, $n=4$).

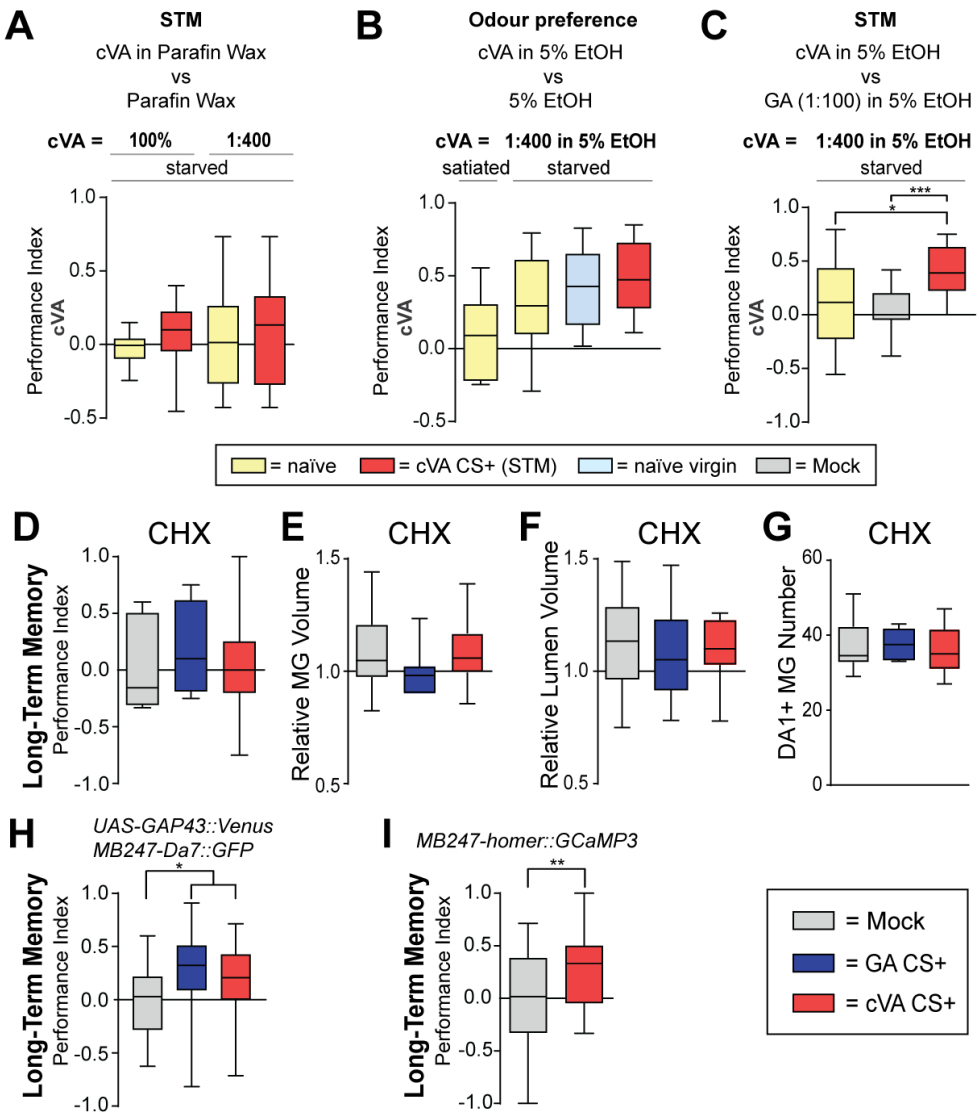

Figure S2| Establishment of appetitive conditioning with cVA, suppression of anatomical modifications after pharmacological blocking of long-term memory (Related to Figure 2) and learning scores of individual genotypes (Related to Figures 3, 4)

(A) Appetitive STM conditioning using pure cVA or cVA diluted 1:400 in paraffin wax induced performance scores towards cVA that were similar to those of naïve flies ($p > 0.05$, n = 8-16). **(B)** The pheromone cVA was attractive for naïve flies when applied in a food context (choice: 1:400 cVA + 5% EtOH versus 5% EtOH). Attraction was stronger if flies were starved, if virgin females were tested or after appetitive conditioning using cVA (1:400 in 5% EtOH) as CS+ and the carrier (5% EtOH) as CS- ($p > 0.05$, n = 9-19). **(C)** Comparison of performance scores towards cVA of flies that were confronted with the choice between cVA (1:400 in 5% EtOH) and GA (1:100 in 5% EtOH). Flies that had been trained in an appetitive STM paradigm with cVA (1:400 in 5% EtOH) as CS+ and GA (1:100 in 5% EtOH) as CS-

displayed higher performance scores towards cVA in comparison to mock-trained flies or starved naïve flies, indicating that flies can learn to associate cVA with a reward in these conditions (*p < 0.05, ***p < 0.001, n = 12-19). **(D)** Pharmacological suppression of LTM by feeding *R37H08-GAL4/ UAS-brp-short^{cherry}, MB247-Dα7::GFP* flies 50 mM cycloheximide (CHX) in 125mM sucrose solution for 30 min after training. Subsequently flies were re-starved for 24h before testing (p > 0.05, n = 8–11). **(E-G)** Suppression of the structural modifications in DA1- MGs in cVA CS+ flies after LTM block by CHX application. (p > 0.05, n = 7-17). Compare to Figure 2G-I. **(H)** Appetitive LTM scores of *R37H08-Gal4, UAS-GAP43::Venus /MB247-Dα7::GFP, UAS-brp-short^{cherry}* flies (*p < 0.5, n= 23-32), used in Figure 3A-H. **(I)** Appetitive LTM scores of *MB247-homer::GCaMP3* flies (**p < 0.01, n = 32-34), used in Figure 4A-F and in Figure S3. In all box plots, the edges of the boxes are the first and third quartiles, thick lines mark the medians, and whiskers represent data range.

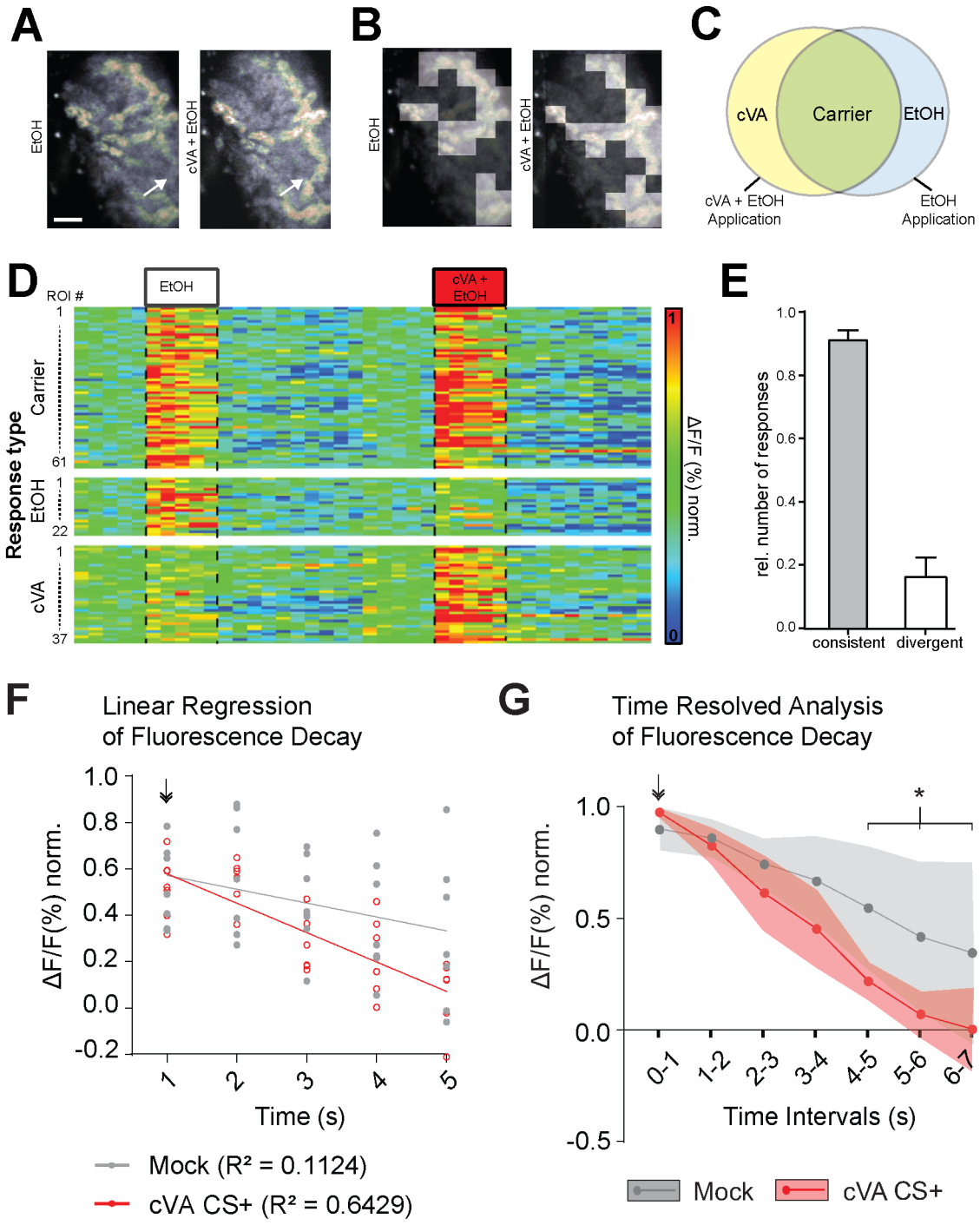

Figure S3| Classification of calcium responses in the MBC (Related to Figure 4)

(A) Representative optical section of a time z-stack series consisting of 30 cycles with 10 sections per stack at a frame rate of 1 Hz. The odour was applied for 5s after 5 cycles. With a typical calycal diameter along the dorsal/ventral axis of 35µm and an average MG diameter of 5µm this imaging settings reliably captured calcium dynamics of the entire MBC. The grey scale image was created by averaging images from one optical plane over the last 15 acquisition cycles after odour application. False color-coded images were created by subtracting the background (generated by averaging 5 images preceding the odour

application) from the first two averaged images during odour application. White arrows point to areas only responsive to cVA. Scale bar = 10 µm **(B)** Single optical planes were overlaid with a grid of 5x5 μm^2 meshes (ROIs). White squares represent ROIs, which were classified as responsive to odour stimulation. For classification the mean response as ΔF/F% during the first 2s of odour application was calculated for each ROI. ROIs were classified as odour responsive, if the mean ΔF/F% during the first 2s of odour application was greater than 3x the standard deviation of the ΔF/F% during the 5s preceding odour stimulation. **(C)** Schematic of ROI classification strategy. ROIs were classified as responsive to "cVA" if they displayed an above-threshold response to cVA (1:400, 5% EtOH), but not to EtOH only (5% EtOH). "Carrier" ROIs responded to both stimuli and "EtOH" only to EtOH (5% EtOH), but not to cVA (1:400, 5% EtOH). **(D)** Temporal dynamics of fluorescence changes to odour stimulation within a single MBC. Each lane of the matrix represents a single ROI identified as responsive towards the carrier (top matrix), EtOH only (mid matrix) or cVA (bottom matrix) as in (C). Each column of the matrix represents 1s. White and red boxes and dashed lines represent 5s of odour stimulation with 5% EtOH or cVA (1:400, 5% EtOH), respectively. Out of 120 responsive ROIs in one MBC, 61 ROIs were classified as responsive to the carrier, 22 to EtOH and 37 were specific to cVA. **(E)** Number of consistent responses (ROI present in trial 1 that are also detected in trial 2) in the MBC after repetitive odour stimulation with 5% EtOH. After two consecutive odour stimulations ~90% of the responsive areas kept consistent compared to a previous stimulation (n = 6). The fraction of ROIs only responsive during 2nd odour stimulation, and classified as divergent, was ~16%. **(F)** Comparison of calcium signal decay in KC dendrites by linear regression analysis. From its peak after the start (arrow) of five seconds stimulation with cVA, calcium response decays more rapidly in cVA CS+ trained flies than in mock trained flies. A linear fit described the decrease of GCaMP fluorescence well in cVA CS+ trained flies, whereas decay was less homogenous in flies from the mock trained group. ($p < 0.05$, n = 7). **(G)** Time resolved analysis of fluorescence decay of GCaMP after the initial peak. During the initial two seconds of cVA stimulation (arrow) average responses in KC dendrites reached their peak in each condition. The calcium response was undistinguishable between the two groups until 3-4 s of stimulation, but it decayed more rapidly from 4-5 s on in the cVA CS+ flies (*$p < 0.05$, n = 7). Data represented as mean ± std.

Connection to DA1-PN bouton	Cell type	Number of cells	Number of synaptic connections
Postsynaptic to the DA1-PN bouton	KC αβp	0	0
	KC αβc	1	12
	KC αβs	3	11-21
	KC α'β'ap	1	25
	KC α'β'm	1	8
	KC γmain	8	12-24
	KC γd	0	0
	APL	1	2
	MB-C1	2	1-3
Presynaptic to the DA1-PN bouton	KC γmain	2	1
	APL	1	3
	MB-C1	1	1

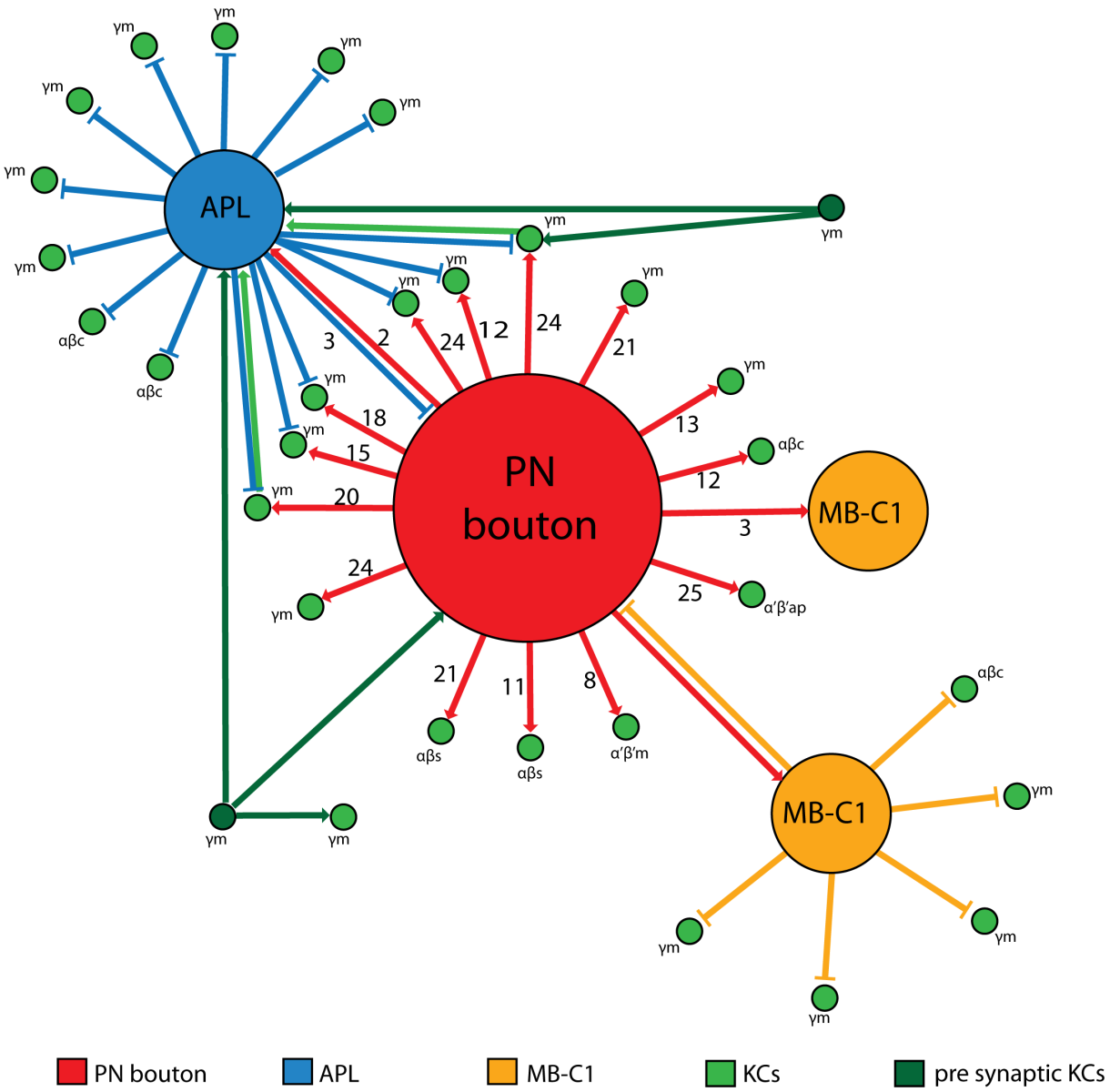

Supplementary Table1| Neurons contributing to a DA1-PN microglomerulus and their synaptic connections (Related to Figure 1)

Top: Table representing the identified direct synaptic contacts between the DA1-PN bouton (see Figure 1) and other neurons, revealed from reconstructions in the FAFB EM dataset. Bottom: Scheme of the MG network of the DA1-PN bouton (see Figure 1) reconstructed in the FAFB EM dataset. If synaptic connections are more than one, their number is indicated along the arrows. The network consists of a DA1-PN bouton (red), surrounded by the APL neuron (blue), two MB-C1 neurons (orange), 14 postsynaptic KC claws and two additional KCs (dark green), which are presynaptic to the PN bouton and to APL. APL and MB-C1 form polyadic synapses with the PN bouton including KCs. Some of these are not postsynaptic to the PN bouton and are therefore placed in the scheme around the respective APL or MB-C1 neuron.

2.4 Summary

The aim of this work was to identify mechanisms supporting long-term memory formation in synaptic MGs of the fly MB calyx. In order to detect potential changes in synapse organization linked to memory consolidation, we first developed a setup that allowed us to identify individual synapses of olfactory PNs delivering a conditioned odour to the MB. The cVA odourant/DA1-PNs proved to be the best candidate to track a fly's neuronal response towards a specific odour in MGs of the calyx. Additionally, we reconstructed with EM resolution a full DA1-MG, which revealed the high degree of complexity of the microglomerular structure. Next, combining behavioural experiments with high-resolution microscopy, we showed that the formation of long-term appetitive memories correlates with an increase in the number of MGs formed by the DA1-PNs involved in the cVA odour representation and the KCs postsynaptic to them. Such changes could not be observed in naïve flies that were exposed to the cVA and the reward separately, as well as in *rutabaga* null mutants lacking a type I calcium/calmodulin-activated adenylate cyclase (AC) required for olfaction (Han et al., 1992; Tempel et al., 1983; Tully & Quinn, 1985a). Additionally, *in vivo* calcium imaging experiments showed that these new MGs actively participate in the cVA representation at the calyx.

Hence, in this publication we report input-specific reorganization of the adult MB calyx associated with the formation of long-term appetitive memory. Notably, as the olfactory pathway of cVA is not distinguishable from that of other odours, we speculate that these findings can be generalized to all stimuli representations. Finally, a recent publication showed that the number of KCs responding to the conditioned odour was increased after aversive long-term memory formation (Delestro et al., 2020). If we assume that appetitive conditioning would induce a similar outcome, our data could provide anatomical and functional support to these findings. Thus, odour-evoked representations in KCs could be modulated by experience in adult flies.

3 The anterior paired lateral neuron normalizes odour-evoked activity at the mushroom body calyx

The following chapter represents a paper that was published as a preprint on September 22th, 2021 on BiorXiv (https://www.biorxiv.org/) and submitted to the Journal eLife (https://elifesciences.org/).

3.1 Introduction

Pattern separation is defined as a process by which highly overlapping stimuli are transformed into distinguishable ones (Santoro, 2013). Its main function is to supports stimuli discrimination., and it is often found in neuronal layer involved in associative memory formation such as the cerebellar cortex, the dentate gyrus and the fly MB.

In *Drosophila*, pattern separation is achieved via sparse representations by around 2,000 KCs of the MB, a neuropil responsible for associative memory formation in the insects' brain (Aso, Hattori, et al., 2014; de Belle & Heisenberg, 1994; Turner et al., 2008b). Extensive theoretical work investigated how sparse stimuli representations are achieved in the MB. In particular, the combination of expansion in neuronal populations (at the MB, around 150 PNs synapse to 2,000 KCs ca; Aso, Hattori, et al., 2014), sparse connectivity (each KC receives input from 6-8 PNs only; F. Li et al., 2020b; Zheng et al., 2020) and inhibition were described as the main requirements for efficient pattern separation (revised in Cayco-Gajic & Silver, 2019). However, experimental data supporting these findings are lacking due to technical limitations.

In this work, we investigate the role of the inhibitory anterior paired lateral neuron (APL) in microcircuits at the input region of the MB, the calyx. The APL was already shown to maintain KC odour responses sparse (Lei et al., 2013; Lin et al., 2014); however, the mechanisms by which this is obtained are currently under debate (Amin et al., 2020). Here, we exploit recently released whole brain connectomes (Scheffer et al., 2020a; Zheng et al., 2018) and analyse the interactions between APL and MGs of the MB calyx.

Furthermore, to understand how these inhibitory synapses assists the formation of a sparse code, we perform two-photon *in vivo* calcium imaging experiments targeting the APL as well as the other two cellular specializations known to participate in the microglomerular microcircuit: PN boutons and KC claws (Leiss et al., 2009b).

3.2 Statement of contribution

Luigi Prisco and Gaia Tavosanis conceived the original project. Luigi Prisco, Stephan H. Deimel and Hanna Yeliseyeva constructed fly strains, designed, performed and analysed *in vivo* calcium imaging experiments, with support from André Fiala. Scripts, plugins and python codes to analyse calcium imaging experiments were established by Luigi Prisco and Stephan H. Deimel. Python codes to analyse publicly available EM datasets were established by Luigi Prisco and Hanna Yeliseyeva. The manuscript was written by Luigi Prisco and Gaia Tavosanis.

3.3 Publication

The anterior paired lateral neuron normalizes odour-evoked activity at the mushroom body calyx

Luigi Prisco, Stephan Hubertus Deimel, Hanna Yeliseyeva, André Fiala, Gaia Tavosanis

doi: https://doi.org/10.1101/2021.09.20.461071

The anterior paired lateral neuron normalizes odour-evoked activity at the mushroom body calyx

Luigi Prisco[1], Stephan Hubertus Deimel[2], Hanna Yeliseyeva[1], André Fiala[2], Gaia Tavosanis [1, 3,*]

[1]Dynamics of neuronal circuits, German Center for Neurodegenerative Diseases (DZNE), Bonn, DE

[2]Department of Molecular Neurobiology of Behavior, University of Göttingen, Göttingen, DE

[3]LIMES, Rheinische Friedrich Wilhelms Universität Bonn, Bonn, DE

[*]to whom correspondence should be addressed: gaia.tavosanis@dzne.de

Abstract

To identify and memorize discrete but similar environmental inputs, the brain needs to distinguish between subtle differences of activity patterns in defined neuronal populations. The Kenyon cells of the *Drosophila* adult mushroom body (MB) respond sparsely to complex olfactory input, a property that is thought to support stimuli discrimination in the MB. To understand how this property emerges, we investigated the role of the inhibitory anterior paired lateral neuron (APL) in the input circuit of the MB, the calyx. Within the calyx, presynaptic boutons of projection neurons (PNs) form large synaptic microglomeruli (MGs) with dendrites of postsynaptic Kenyon cells (KCs). Combining EM data analysis and *in vivo* calcium imaging, we show that APL, via inhibitory and reciprocal synapses targeting both PN boutons and KC dendrites, normalizes odour-evoked representations in MGs of the calyx. APL response scales with the PN input strength and is regionalized around PN input distribution. Our data indicate that the formation of a sparse code by the Kenyon cells requires APL-driven normalization of their MG postsynaptic responses. This work provides experimental insights on how inhibition shapes sensory information representation in a higher brain centre, thereby supporting stimuli discrimination and allowing for efficient associative memory formation.

1 Introduction

Every day we are challenged to navigate through a complex and variable environment, often characterized by similar stimuli combined in different ways. Yet, our brain excels in assessing if, and how, the current experience is

different or similar to a previously encountered one. The ability to discriminate across stimuli is achieved by minimizing the overlap between patterns of neuronal activity through a process defined as "pattern separation" (Santoro 2013). This conserved property is intrinsic to diverse circuits such as the mammalian cerebellum, the dentate gyrus and the *Drosophila* mushroom body (MB) (Cayco-Gajic and Silver 2019). In the current models, all the aforementioned circuits support pattern separation by utilizing different degree of inhibitory mechanisms. (Tyrrell and Willshaw 1992; Schweighofer, Doya, and Lay 2001; Sahay, Wilson, and Hen 2011; Cayco-Gajic, Clopath, and Silver 2017; Litwin-Kumar et al. 2017). Experimental evidence in support of these inhibitory circuits has been described over the years (Vos, Volny-Luraghi, and de Schutter 1999; Duguid et al. 2015; Inada, Tsuchimoto, and Kazama 2017; Parnas et al. 2013; Olsen, Bhandawat, and Wilson 2010; A. C. Lin et al. 2014), however, the mechanism by which inhibition contributes to pattern separation is not yet fully understood, often due to technical limitations.

With an extended genetic toolkit and a brain of only ~100,000 neurons (Raji and Potter 2021; Alivisatos et al. 2012) largely reconstructed at the EM Level (Zheng et al. 2018; F. Li et al. 2020a), *Drosophila* represents an attractive system to provide experimental evidence on the mechanisms behind pattern separation. The fly MB receives mainly olfactory input, though optical, temperature and humidity information is also represented (Marin et al. 2020; Frank et al. 2015; J. Li et al. 2020). The MB is required for memory formation and retrieval (Heisenberg et al. 1985; de Belle and Heisenberg 1994; Dubnau et al. 2001; S. E. McGuire, Le, and Davis 2001; Aso et al. 2014). Within the MB input region, in the main calyx, olfactory projection neurons (PNs) deliver

sensory information from 51 distinct olfactory glomeruli (Grabe et al. 2016; Bates et al. 2020) to ~2,000 Kenyon cells (KCs) of the MB (Aso et al. 2009), for an expansion ratio of 40 (Litwin-Kumar et al. 2017). In the calyx, PNs synapse onto KCs via complex synaptic structures known as microglomeruli (MGs) (Yasuyama, Meinertzhagen, and Schürmann 2002a; Leiss et al. 2009a). At each MG, a single central PN bouton is enwrapped by, on average, 13 claw-like dendritic terminals of as many different KCs (Davi D. Bock, personal communication). KCs integrate inputs in a combinatorial manner, with each KC receiving input from 6-8 PNs, on average (Butcher et al. 2012; Zheng et al. 2020; F. Li et al. 2020b; Turner, Bazhenov, and Laurent 2008), of which more than half need to be coactive to elicit spikes (Gruntman and Turner 2013; Inada, Tsuchimoto, and Kazama 2017). As a result, while PN odour-evoked activity is broadly tuned (Perez-Orive et al. 2002; Bhandawat et al. 2007), odour representation is sparse and decorrelated at the KCs layer (Honegger, Campbell, and Turner 2011; Turner, Bazhenov, and Laurent 2008; Campbell et al. 2013b; Perez-Orive et al. 2002), therefore reducing overlap between stimuli representation and allowing for better discriminability (Kanerva 1988; Cayco-Gajic, Clopath, and Silver 2017; Olshausen and Field 2004). In addition to sparse PN:KC connectivity and KCs high input threshold, inhibition is required to reduce the overlap among odour representations in the *Drosophila* MB (A. C. Lin et al. 2014; Lei et al. 2013). At the MB, inhibition is provided by the GABAergic anterior paired lateral (APL) neuron, which innervates both the calyx and the lobes of the MB (Liu and Davis 2009; Pitman et al. 2011; Aso et al. 2014). APL responds to odours with depolarization and calcium influx (Liu and Davis 2009; Papadopoulou et al. 2011). Importantly, blocking APL output

disrupts the KCs sparse odour representation and impairs learned discrimination of similar odours, pointing to its critical role in the process (A. C. Lin et al. 2014; Lei et al. 2013). APL is suggested to regulate sparse coding by participating in a closed feedback loop with the MB, similarly to its homolog giant GABAergic neuron (GGN) in the locust (Papadopoulou et al. 2011; A. C. Lin et al. 2014; Litwin-Kumar et al. 2017). However, APL is both pre- and post-synaptic to PNs and KCs in the adult calyx (Yasuyama, Meinertzhagen, and Schürmann 2002b; Wu et al. 2013; Baltruschat et al. 2021). Additionally, APL response to localized stimuli is spatially restricted (Amin et al. 2020). In particular, APL branches at the MB lobes and the ones in the calyx appear to represent two separate compartments (Amin et al. 2020), suggesting a possible distinct role of APL inhibition in these two different compartments. Hence, the mechanisms by which APL modulates sparse coding and its involvement in the process of pattern separation are still unclear. In the present work, we challenge the concept of a broad feedback inhibition to the MB calyx by APL with primary experimental data. In particular, we focused on the APL processes within the MB calyx and set out to identify the role of GABAergic inhibition at the PN:KC synaptic layer. Taking advantage of recently released EM datasets (Scheffer et al. 2020; Zheng et al. 2018), we report the complex synaptic interaction of APL with PNs and KCs within the MGs of the MB calyx. Next, via *in vivo* calcium imaging in the calyx, we explored the role of APL inhibition onto MGs by recording the odour-evoked activity of APL, PN boutons and KC dendritic claws. Our results indicate that APL acts as a normalizer of postsynaptic responses to olfactory inputs in the MGs of the mushroom body calyx, an idea that we confirmed by blocking the output of

APL. Additionally, via volumetric calcium imaging, we addressed the locality of APL activation in the calyx and found that it is odour-specific. We suggest that the normalization of postsynaptic MG responses by APL is essential to determine the key property of KCs to respond only to the coincident input of PNs to multiple claws, allowing for an elevated stimulus discriminability.

2 Results

2.1 APL is an integral part of the microcircuit within microglomeruli in the MB calyx

To better understand the role of GABAergic inhibition at the MB calyx, we investigated APL involvement into the calycal microcircuits with the highest resolution available. The APL of adult *Drosophila* innervates extensively all compartments of the mushroom body, including calyx, lobes and pedunculus (Liu and Davis 2009). Moreover, the neuron appears to be non-polarized in the adult, with strong expression of both pre- and post-synaptic markers in all compartments (Wu et al. 2013). However, little is known regarding the detailed connectivity between APL and the cell types constituting the mushroom body. Taking advantage of emerging electron microscopy (EM) datasets covering a full adult fly brain (FAFB, (Zheng et al. 2018)) or a large fraction of it (Hemibrain, (Scheffer et al. 2020)), we examined the distribution of synaptic contacts between APL, PNs and KCs, the major cell types constituting the MGs of the mushroom body calyx (Leiss et al. 2009b; Yasuyama, Meinertzhagen, and Schürmann 2002a; Baltruschat et al. 2021) (Fig 1A). We recently reconstructed an entire MG in the FAFB dataset, starting from a PN-bouton of

the DA1 glomerulus and tracing all its pre- and post-synaptic partners (Baltruschat et al. 2021). Here, we focused on the synaptic connections involving APL. We found APL to be highly involved in the MG structure, with pre- and post- synaptic contacts with both KC dendrites and PN boutons (Fig S1A) (Baltruschat et al. 2021). Many of those synapses were polyadic, displaying typical configurations within that specific MG (described in Fig S1B). To verify whether such features were specific to the DA1 MG reconstructed in Baltruschat et al. (2021) or common, we exploited the Hemibrain EM dataset (Scheffer et al. 2020) and extracted all calycal connections from and to APL with either KCs or PNs. Out of the 136 PNs reported innervating the main calyx (F. Li et al. 2020b), 126 made and received synapses with APL (full list of PNs and APL interactions available at: Mendeley data link will be available upon publication). To reveal the localization of these synapses, we rendered 3D graphs of single PNs derived from the Hemibrain dataset (Scheffer et al. 2020) and mapped the synapses that they receive from APL within the MB calyx (see Material and Methods for details). Most of the APL-to-PN connections were localized on PN boutons (84 $\pm$ 2%, mean $\pm$ SEM, of the total synapses received by each PN localised on boutons), demonstrating that the majority of APL-PN interactions happens at MGs (Fig 1B, all images available at: Mendeley data link will be available upon publication). Additionally, we found a positive correlation between the number of synapses made by the APL towards a specific PN and the reciprocal synapses formed by that PN onto APL (Fig 1D). Of notice, most of the PNs not connecting to the APL within the main calyx were already described as non-olfactory PNs (Marin et al. 2020), and they all seemed to extend most of their terminals elsewhere, with little to no branches

in the main calyx (Fig S1D). Similarly, of the 1919 KCs present in the dataset, 1871 displayed interactions with APL. Mapping APL synapses onto single KC meshes (Fig 1C, all images available at: Mendeley data link will be available upon publication) showed a majority of connections on KC claws. However, we noticed inhibitory synapses along KC dendrites as well. The KCs constituting the MB are divided in 3 major classes based on their axonal projections: γ, α/β, α'/β' (Crittenden et al. 1998; Lee, Lee, and Luo 1999). We found a difference in the spatial distribution of APL synapses depending on the KC type, suggesting that APL inhibition might have a different impact on different KC types. In particular, APL synapses onto α/β KCs were significantly less localised on claw-like dendritic terminals and more distributed along KC dendritic branches (Fig S1C, n=210 (70 per KC type, randomly selected), $p<0.0001$, Unpaired ANOVA with multiple comparisons). The KCs not interacting with APL displayed a rather atypical structure, with extensive dendritic arborization just outside of the main calyx rather than within (Fig S1E). As in the case of PNs, the number of KC-to-APL synapses positively correlated with the APL-to-KC synapse number (Fig 1E). In conclusion, EM dataset analysis revealed a large involvement of APL in the calycal circuitry, with reciprocal connections to the vast majority of PNs and KCs. APL involvement in the MG structure as reported in Baltruschat et al (2021) might be thus generalized to potentially all MGs of the main calyx.

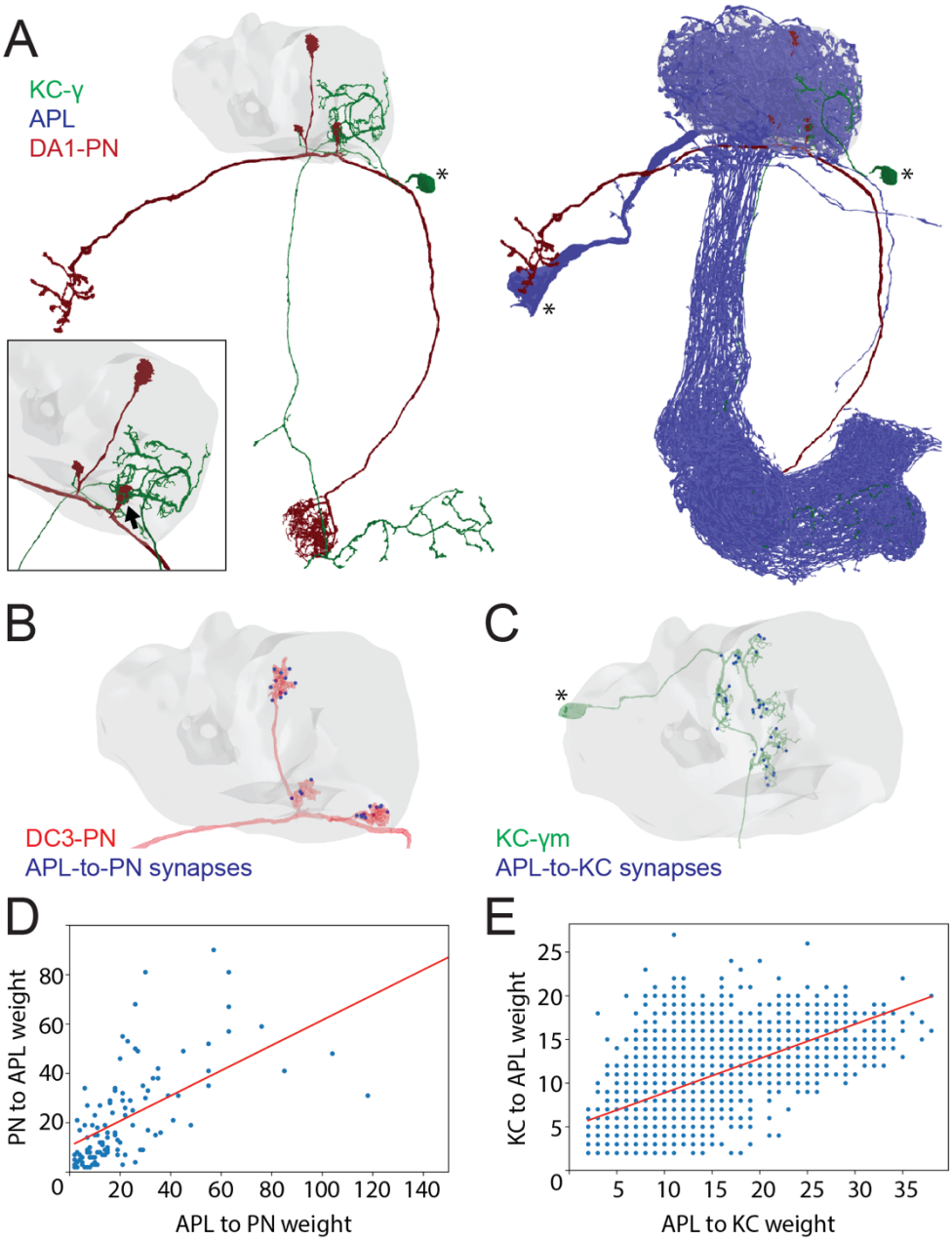

Fig 1. APL participates in the MG microcircuit with reciprocal synapses. **(A)** Left: example of a PN (red) sending collateral boutons into the MB calyx (grey volume), where it connects onto KCs claws via synaptic microglomeruli. For simplicity, only 1 KC is visualised here (green). Bottom-left box: magnification of a PN bouton interacting with a KC claw (black arrow). Right: APL (blue) innervates the entire MB including lobes, peduncle and the calyx. Asterisks indicate cell bodies. **(B)** Visualisation of APL synapses (blue dots) onto a PN 3D mesh within the MB calyx. Most connections are localised on PN boutons. **(C)** Localization of APL synapses (blue) on a KC 3D mesh within the MB calyx. While most are localised on dendritic claws, some connections along dendritic branches could be seen as well (see also S1C). The cell body is

marked by an asterisk. **(D)** Correlation between the number of PN-to-APL reciprocal synapses (r^2=0.63) and KC-to-APL ones **(E)** (r^2=0.60). The correlation was calculated among the entire synaptic weight that individual PNs or KCs had with APL. All 3D plots were created via the Neuprint-python package (see Materials & Methods).

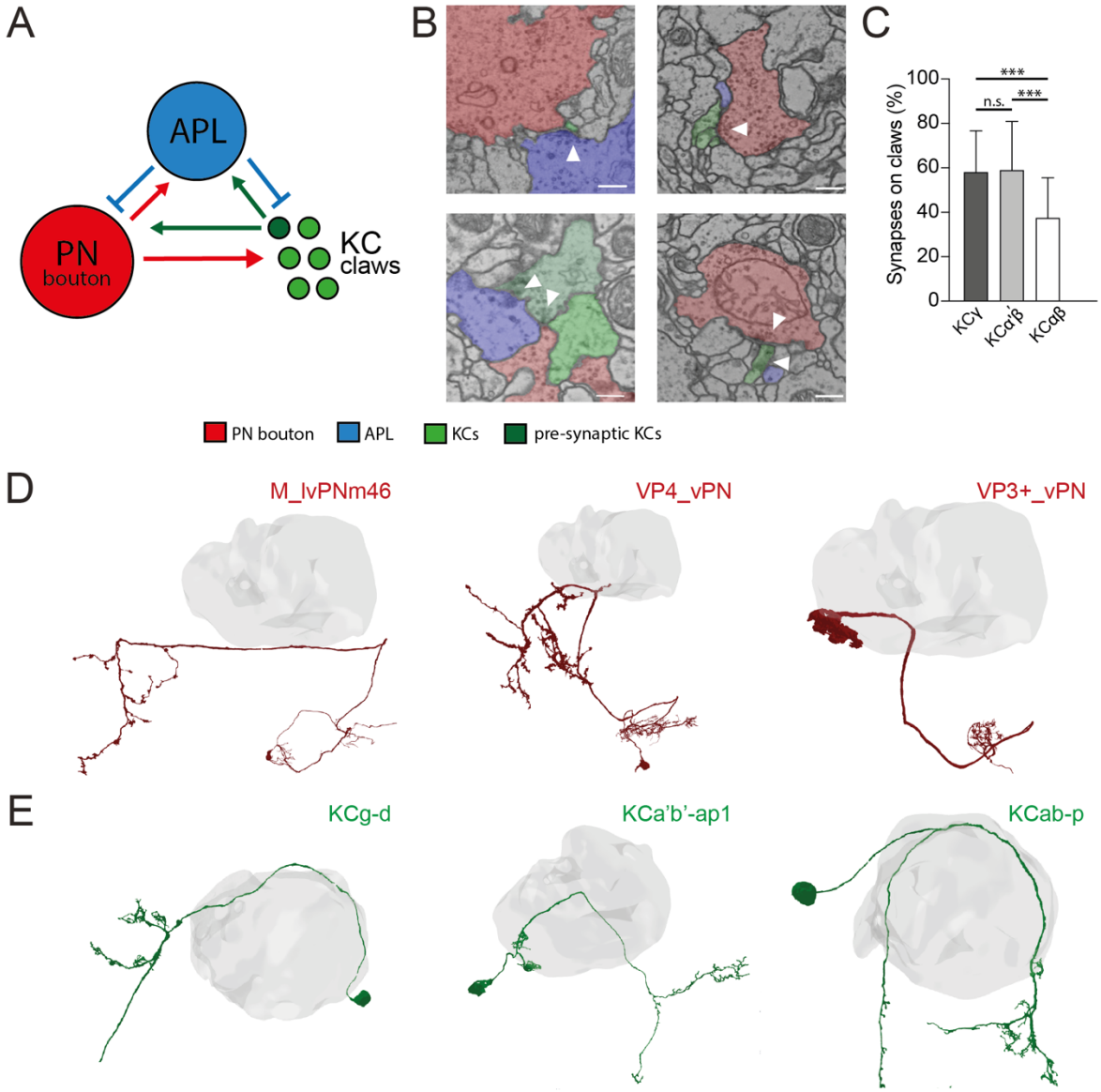

Fig S1 (Related to Fig 1). APL in the microglomerular circuit.

(A) Schematized view of the connectivity patterns found in the DA1-PN MG reconstructed in Baltruschat et al. (2021). Green circles represent KC claws. Dark green circles represent presynaptic KCs. The red circle represents the reconstructed bouton of a DA1-PN. The blue circle represents APL. See Baltruschat et al., (2021) for further explanation, including the full connectome

of this DA1-PN MG. **(B)** Examples of connectivity patterns involving APL in the DA1-PN microglomerulus reconstructed in Baltruschat et al. (2021). Top left: EM image of APL (blue) presynaptic to the PN bouton (red) and the claw of a KC (green). Top right: PN bouton presynaptic to APL and three KC claws. Bottom-left: KC (dark green) presynaptic to PN bouton, APL and another claw. Bottom-right: APL and PN bouton presynaptic to the same KC claw. Scale bar = 250nm. **(C)** Spatial distribution of APL synapses among different KC types. The fraction of APL to KC$\alpha\beta$ synapses localised on KC claws was lower than in other KC types. n=210 (70 per KC type, randomly selected), $p<0.0001$, Unpaired ANOVA with multiple comparisons. Whiskers indicate SD. **(D)** Examples of PNs not interacting with APL at the MB calyx (grey volume). **(E)** Examples of KCs not interacting with APL at the MB calyx (grey volume). 3D neuronal meshes were created via the Neuprint-python package (see Materials & Methods).

2.2 In the calyx, APL displays different response levels to different odours

The analysis of the EM data provided structural evidence for possible feedforward and feedback circuits between APL, PNs and KCs in the MB calyx (Fig S1A-B). To explore the functional role of APL in calycal MGs, we performed *in vivo* functional imaging experiments by expressing the calcium indicator GCaMP6m (Chen et al. 2013b) specifically in APL via the APL intersectional *NP2631-GAL4, GH146-FLP* (APLi) driver (A. C. Lin et al. 2014; Mayseless et al. 2018) and recorded odour-evoked activity in the calyx (Fig 2A, see Materials and Methods). Flies were stimulated with 5 second puffs of odours diluted 1:100 in mineral oil and exposed to sequences of 2 odours starting with 4-methylcyclohexanol (Mch) and 3-octanol (Oct), presented in a randomized fashion. Odour-elicited calcium transients in APL were detectable in the calyx

(Fig 2B,E). Interestingly, we observed a clear difference in the GCaMP fluorescence levels, measured as $\Delta F/F_0$ over the entire calycal region innervated by APL (see also Material and Methods) in response to the two odour stimulations, with Oct eliciting a stronger APL response (Fig 2C-D, n=10, p=0.002, Wilcoxon matched-pairs test). To extend this observation, we exposed flies also to δ-Decalactone (δ-DL), an odour reported to elicit the least overall activity in ORNs (Hallem and Carlson 2006a). Similarly, we measured a difference between the strength of the response to Oct compared to δ-DL (Fig 2F-G, n=10, p<0.0001, paired t test). Moreover, the gap between the δ-DL signal peak and the Oct one was higher compared to the Mch vs Oct group (Δ(Oct-Mch) = 45 ± 27%; Δ(Oct-δ-DL) = 76 ± 30%, n=10, p=0.0234, unpaired t-test with Welch´s correction), suggesting that APL is able to provide a variable, odour-tuned inhibition to MGs of the MB calyx.

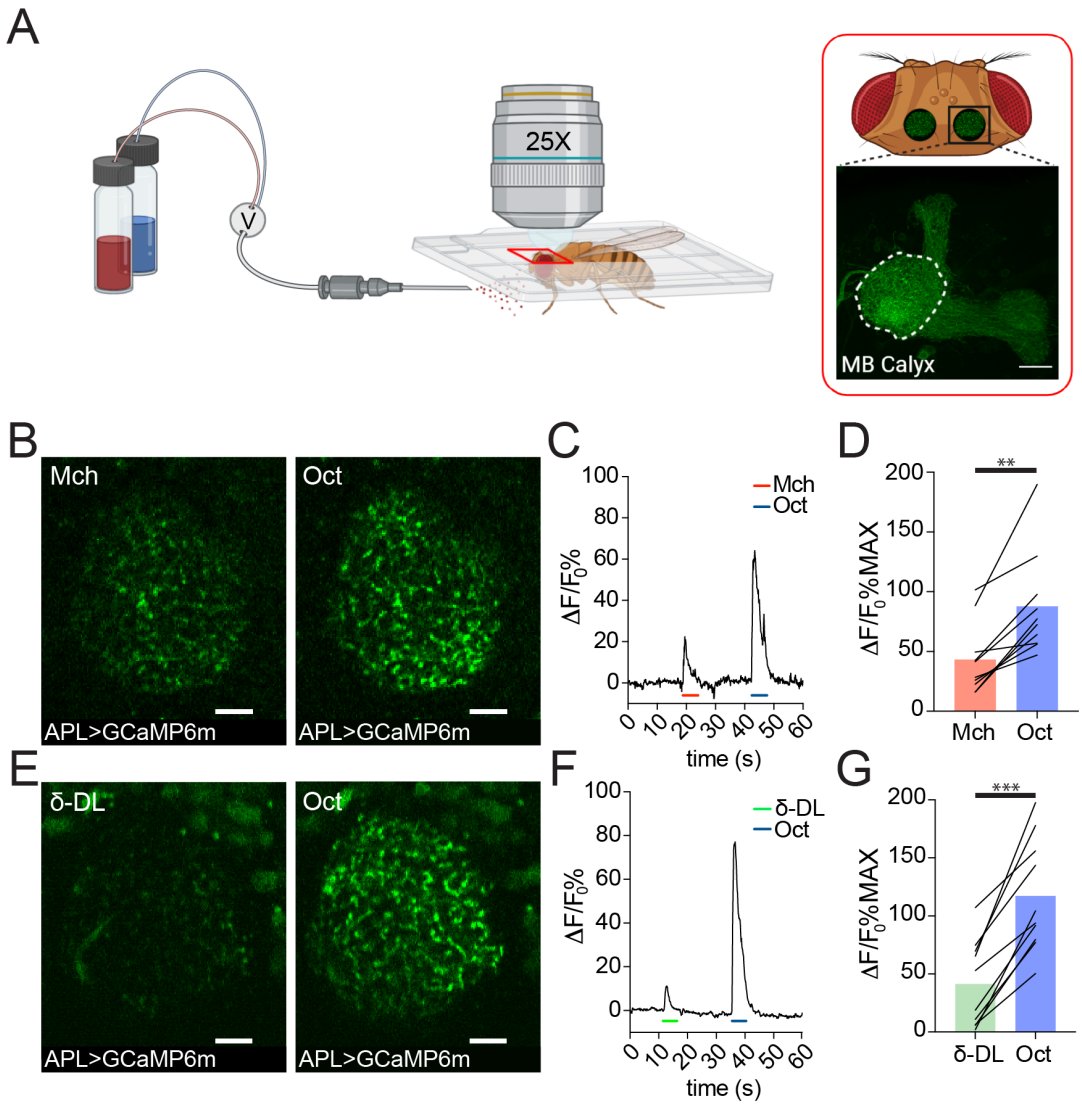

Figure 2. APL responds to odours with variable calcium transients.

(A) Schematic view of the two-photon *in vivo* imaging setup. Scale bar = 20μm. **(B)** Example of APL response to Mch or Oct in the calyx of *APLi-GAL4>UAS-GCaMP6m* flies. Scale bar = 10μm. **(C)** Fluorescence intensity over time for the fly showed in (B). **(D)** APL showed higher intracellular calcium transients in response to Oct compared to Mch. n=10, p=0.002, Wilcoxon matched-pairs test. **(E)** Example of APL GCaMP6m response to δ-DL or Oct. Scale bar = 10μm. **(F)** Fluorescence intensity over time for the fly showed in (E). **(G)** APL peak response comparison for the δ-DL vs Oct odours sequence. n=10, p<0.0001, paired t test. Odours were diluted 1:100, bars indicate means.

2.3 The response to different odours is highly variable in PNs, but more homogeneous in KC dendrites

To investigate the origin and the consequences of the observed difference in APL response at the MB calyx, we performed functional imaging experiments targeting the other two cell types participating in the microglomerular structure: PNs and KCs (Leiss et al. 2009b; Yasuyama, Meinertzhagen, and Schürmann 2002a). Odors are detected by a large set of olfactory receptor neurons (ORNs) expressing chemically-tuned odorant receptors (Clyne et al. 1999; Hallem and Carlson 2006a). ORNs project to the 51 distinct olfactory glomeruli in the adult antennal lobe (AL) in a stereotyped manner, with ORNs expressing the same odorant receptor projecting to the same glomerulus (Q. Gao, Yuan, and Chess 2000; Vosshall, Wong, and Axel 2000; Grabe et al. 2016). Within glomeruli, ORNs synapse onto second-order neurons, the PNs, which deliver odour information to higher brain regions such as the MB and the lateral horn (R. F. Stocker et al. 1990). To investigate whether odour-evoked activity in PNs reflected the differences in strength observed in APL, we expressed GCaMP6m in PNs via the generic PN-Gal4 driver *GH146* (Berdnik et al. 2008), and imaged PN dendrites in the antennal lobe. Flies were exposed to Mch or Oct as described for the APL imaging experiments, and the average peak among the responding glomeruli per brain was used as a general indicator of the total input transmitted by PNs. Imaging was performed on a

single optical section of the antennal lobe, and only the glomeruli that could be unequivocally identified among all tested animals were taken into consideration for the analysis. While the number of responding glomeruli was similar between the two tested odours (Fig S2, also shown on a larger number of AL glomeruli in (Barth et al. 2014)), the overall calcium transient was higher when flies were exposed to Oct (Fig S3A-B, n=10, p=0.002, Wilcoxon matched-pairs test), suggesting that the main source of difference was represented by the degree of PNs activation rather than an additional/decreased number of active neurons. Likewise, a strong difference could be measured when flies were exposed to the δ-DL/Oct odours sequence (Fig S3C-D, n=10, p<0.0001, paired t-test), resembling the differences in APL activation detected at the MB calyx.

To address whether this odour-dependent variability in PN dendrites activity is still detectable within the collateral boutons in the MB calyx, we expressed the presynaptically localized GCaMP3 transgene *UAS-Syp::GCaMP3* (Pech et al. 2015) in PNs and recorded odour-evoked activity in PN boutons of the MB calyx. We exposed flies to Mch or Oct, and calculated per calyx the average peak response among the boutons showing calcium transients. While the number of active boutons did not change between Mch and Oct stimulations (Fig 3D, n=10, p=0.689, paired t-test), the average boutons response was higher when flies were exposed to Oct (Fig 3B, n=10, p=0.0002, paired t-test). Furthermore, plotting the frequency distribution of all boutons activity peaks measured during these experiments showed a clear shift towards higher values of the entire Oct-responding population (Fig 3C, n=10, p<0.0001, Kolmogorov-Smirnov test). Hence, the difference shown in Fig 3B was not just due to a very high response of a few boutons, but rather to an overall increase in PN

boutons activation levels across stimuli . Taken together, these experimental data suggested that the APL neuron activation scales with PN inputs strength. To further extend the correlation between PNs and APL activity in a systematic way, we measured the APL calcium transient levels in response to odours contained in a ORNs response database (Hallem and Carlson 2006b) and plotted it against their PN spikes value obtained via the experimentally supported equation described in Olsen et al. (Olsen, Bhandawat, and Wilson 2010; Parnas et al. 2013). We observed a positive linearity between the two variables (Fig S3E, Pearson r=0.99), hence supporting our experimental data described above. In conclusion, these experiments demonstrated that the overall level of PN activation varies with different odours and correlates with the APL response within the MB calyx.

To clarify the impact of the odour-tuned activation of APL on the response of KCs to odours, we next imaged the functional response of KC claws to odour stimulation. Flies expressing the postsynaptically-tagged calcium indicator homer::GCaMP3 under the KCs promoter *MB247* (Pech et al. 2015) were prepared, stimulated and imaged as described before. Olfactory stimulation caused the activation of different patterns of MGs in an odour-dependent manner (Pech et al. 2015) (Fig 3E, S3F). The number of MGs responding to each odour was not significantly different between Mch and Oct exposure (Fig 3H, n=9, p=0.727, Wilcoxon matched-pairs test), whereas it was lower when flies were stimulated with δ-DL (Fig S3I, n=10, p=0.0059, paired t-test), which elicits the least overall ORN activity (Hallem and Carlson 2006a) and induced a weak and restricted response in PN glomeruli at the AL (Fig S2). Importantly, the average microglomerular postsynaptic response to each odour was not

different when comparing the response to Mch vs Oct stimulation (Fig 3F, n=9, p=0.1648, paired t-test) or δ-DL vs Oct stimulation (Fig S3G, n=10, p=0.767, Wilcoxon matched-pairs test). Additionally, the frequency distributions of the odour-evoked activity peaks were overlapping (Fig 3G, S3H, n=9-10, p=0.0982 and p=0.9554 for Fig 3G and S3H, respectively, Kolmogorov-Smirnov test). Hence, the differences in activation strength described at the input population of MGs (the PN boutons) seemed to be normalized at the next neuronal layer, in the KC claw-like dendritic endings. Thus, the range of postsynaptic responses in MGs appears to be restrained.

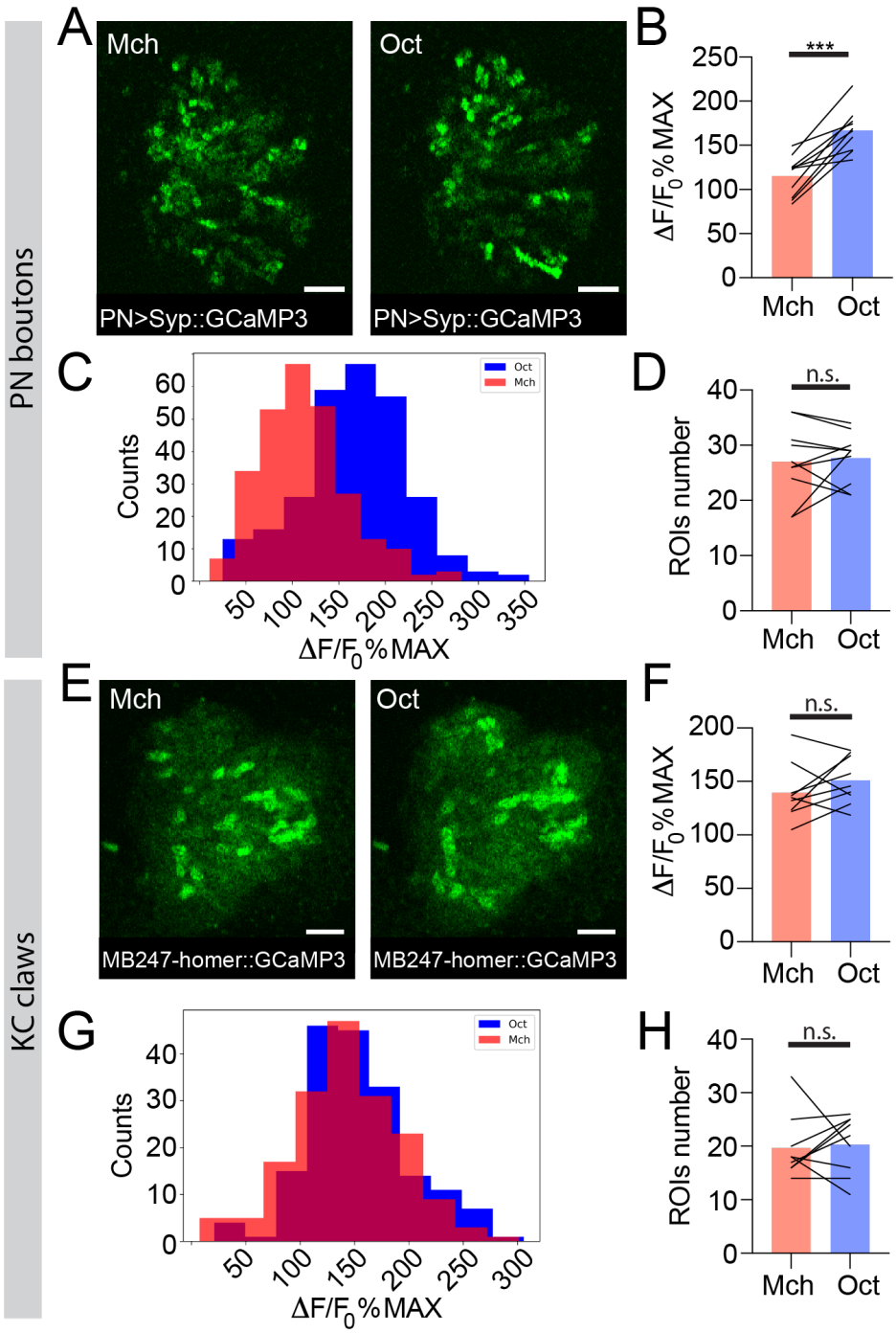

Fig 3. The strength of response to odour stimulation varies in an odour-dependent way in the PN boutons, but is homogenous at the postsynaptic KC claws.

(A) Example of PN boutons fluorescence increase in response to stimulation with Mch or Oct in *NP225-GAL4>UAS-Syp::GCaMP3* flies. Scale bar = 10μm. **(B)** The average activity peak in PN boutons was higher when flies were exposed to Oct compared to Mch. n=10, p=0.0002, paired t-test. **(C)**

Frequency distribution of PN boutons activity peaks in the Mch vs Oct protocol. The Oct population was significantly shifted towards higher $\Delta F/F_0$%MAX values. n=10, p<0.0001, Kolmogorov-Smirnov test. **(D)** The number of ROIs showing odour-evoked activity did not change between the two odour exposures. n=10, p=0.689, paired t-test. **(E)** Example of KC claws fluorescence levels in response to Mch and Oct in *MB247-homer::GCaMP3* flies. Scale bar = 10μm. **(F)** The average activity peak in KC claws was comparable between Mch and Oct exposures. n=9, p=0.1648, paired t-test. **(G)** Frequency distribution of KC claws activity peaks in the Mch vs Oct protocol. The two populations had a similar shape and spread among similar $\Delta F/F_0$%MAX values. n=9, p=0.0982, Kolmogorov-Smirnov test. **(H)** The number of ROIs showing odour-evoked activity did not change between the two odour exposures. n=9, p=0.727, Wilcoxon matched-pairs test. Odours were diluted 1:100, bars indicate means.

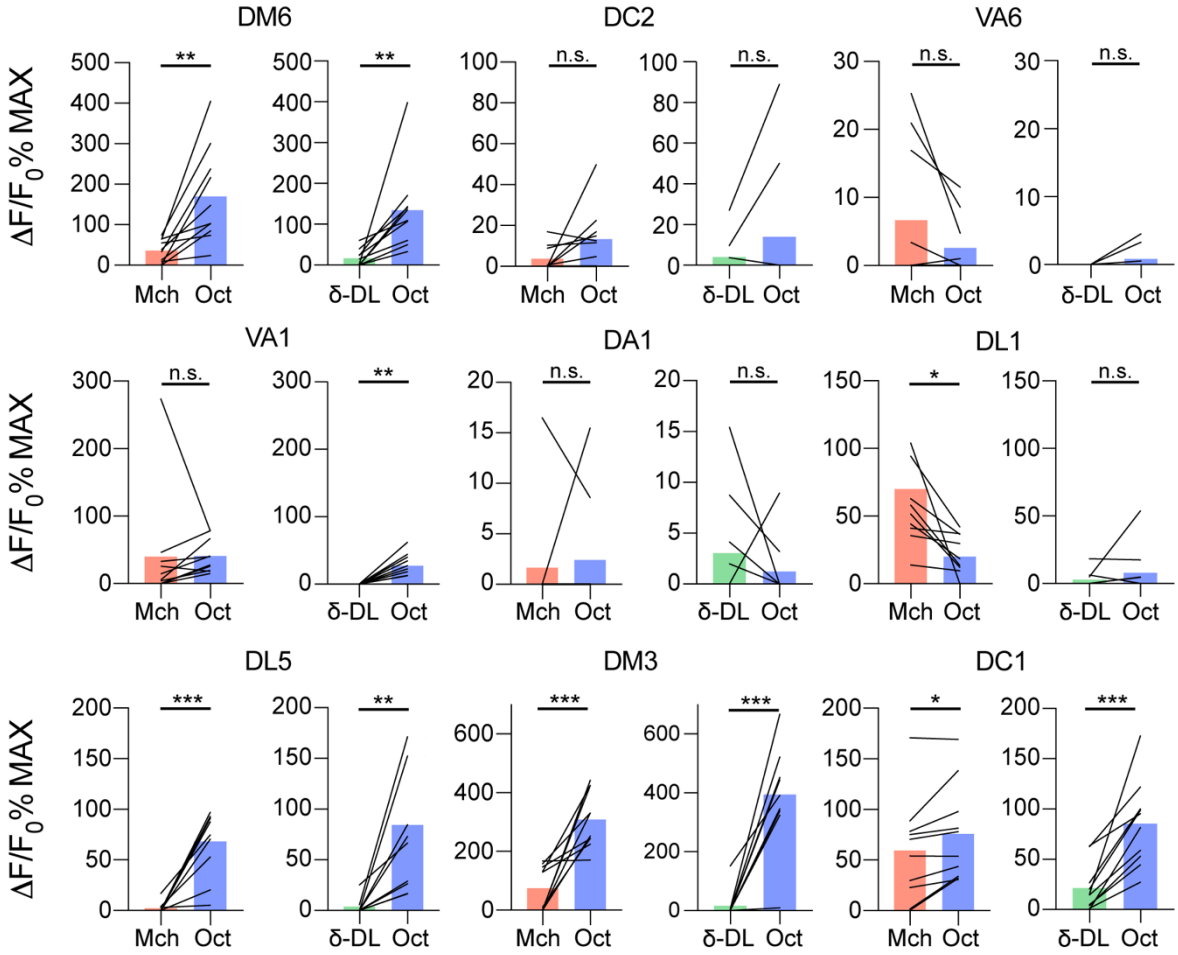

Fig S2 (Related to Fig 3). Single PN glomeruli responses at the AL.

GH146-GAL4>UAS-GCaMP6m flies were stimulated with either Mch vs Oct or δ-DL vs Oct. The activity peak per each glomerulus was extracted and compared. n=10, paired t-test, p value > 0.05 (n.s), ≤ 0,05 (*), ≤ 0,01 (**), ≤ 0,001 (***). Odours were diluted 1:100, bars indicate means.

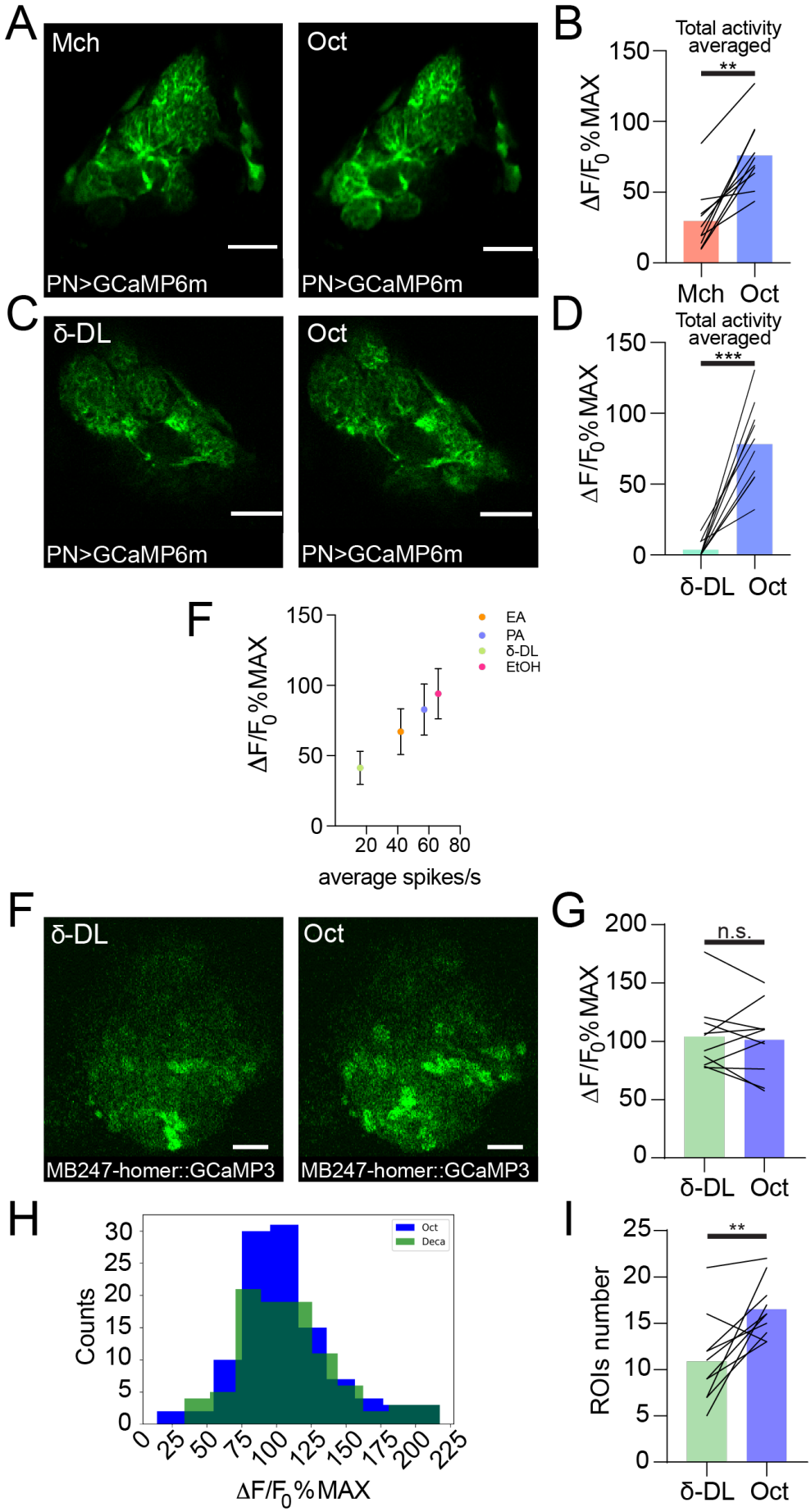

374

Fig S3 (Related to Fig 3). Additional data on PNs and KCs odour evoked activity.

Examples of PN dendritic calcium transients in response to either Mch and Oct **(A)** or δ-DL and Oct **(C)** at the antennal lobe in *GH146-GAL4>UAS-GCaMP6m* flies. Scale bar = 20μm. **(B)** The average activity peak among responding glomeruli was higher when flies were exposed to Oct compared to Mch. n=10, p=0.002, Wilcoxon matched-pairs test. **(D)** The average activity peak among responding glomeruli was higher when flies were exposed to Oct compared to δ-DL. n=10, p<0.0001, paired t-test. **(E)** The APL calcium transient levels in response to 4 chosen odours (ethyl acetate (EA) 1:1000 dilution, pentyl acetate (PA) 1:1000, δ-DL and EtOH 1:100) in *APLi-GAL4>UAS-GCaMP6m* flies linearly correlated with the average PN spiking rate for the respective odour stimulations. The PN spiking rate for 24 AL glomeruli were obtained by feeding ORNs spike values from the Hallem and Carlson 2006 dataset into the ORN-to-PN spike transformation equation described in Olsen et al. 2010 (see also (Parnas et al. 2013)). Pearson r=0.99 **(F)** Example of KC claws fluorescence levels in response to δ-DL and Oct in *MB247-homer::GCaMP3* flies. Scale bar = 10μm. **(F)** The average activity peak in KC claws was comparable between δ-DL and Oct exposures. n=10, p=0.767, Wilcoxon matched-pairs test. **(G)** Frequency distribution of KC claws activity peaks in the δ-DL vs Oct protocol. The two populations had a similar shape and spread among similar $\Delta F/F_0$%MAX values. n=10, p=0.9554, Kolmogorov-Smirnov test. **(H)** The number of ROIs responding to Oct was higher compared to the δ-DL ones. n=10, p=0.0059, paired t-test. Odours were diluted 1:100 unless stated otherwise, bars indicate means.

2.4 APL silencing leads to more variable odour evoked activity at the MGs postsynapses

Taken together, we showed that APL activation varies with different odours and scales with PN boutons activation levels. Together with the higher similarity

among KC claws responses to different odours, this suggests a role of APL as normalizer of olfactory input-elicited response at the KC dendritic claws. If this is correct, blocking APL output would possibly lead to more variable activation of KC claws, mirroring PN bouton activation. We tested this hypothesis by expressing in APL tetanus toxin light chain (TNT), to block vesicle exocytosis and thus silence APL output (Sweeney et al. 1995). To suppress toxin expression during development, we co-expressed the temperature sensitive GAL4 inhibitor *tubP-GAL80^{ts}*. Flies were kept at 18 °C until eclosion, and then transferred at 31 °C for 24h to 48h prior to the experiments. KC responses in APL-silenced flies (APL OFF) were imaged with the postsynaptically-tagged *MB247-homer::GCaMP3* construct. Due to the stochastic nature of *APLi-GAL4* mediated expression (A. C. Lin et al. 2014), flies in which the flippase-dependent expression of TNT in APL did not happen were imaged as control (APL ON). Animals were stimulated with Mch or Oct. As expected, control animals neither show a difference in the average peak response to the two stimuli (Fig 4B, n=10, p=0.949, 2-way ANOVA with Tukey´s multiple comparisons) nor in the number of responding units (Fig 4D, n=10, p=0.995, 2-way ANOVA with Tukey´s multiple comparisons). Furthermore, the frequency distributions of the odour-evoked activity peaks overlapped with each other (Fig 4E, n=10, p=0.0533, Kolmogorov-Smirnov test; see also Fig 3G). In calyces where the APL output was blocked by TNT expression though, we measured a significant difference in the response to the two tested odours, with Oct causing a stronger average odour-evoked activity (Fig 4B, n=10, p=0.0003, 2-way ANOVA with Tukey´s multiple comparisons) as well as a slight increase in the number of responding MGs (Fig 4D, n=10, p=0.047, 2-

way ANOVA with Tukey´s multiple comparisons). Interestingly, small clusters of responding MGs were often found spatially close to each other in the APL OFF scenarios (e.g. compare spatial distribution of Oct responders in 4C vs 4A) suggesting a possible locality of APL-mediated inhibition. Finally, the frequency distribution plot for the APL OFF flies showed two shifted populations, with Oct responses skewed towards higher values (Fig 4F, n=10, $p<0.0001$, Kolmogorov-Smirnov test), resembling the distribution displayed by the PN boutons (Fig 3C). In summary, blocking APL output led to a more variable odour representation at the level of KC claws. This variable odour representation bore a higher similarity to the activity of the input population, hence supporting the hypothesis that APL acts as an input strength normalizer on MGs in the MB calyx.

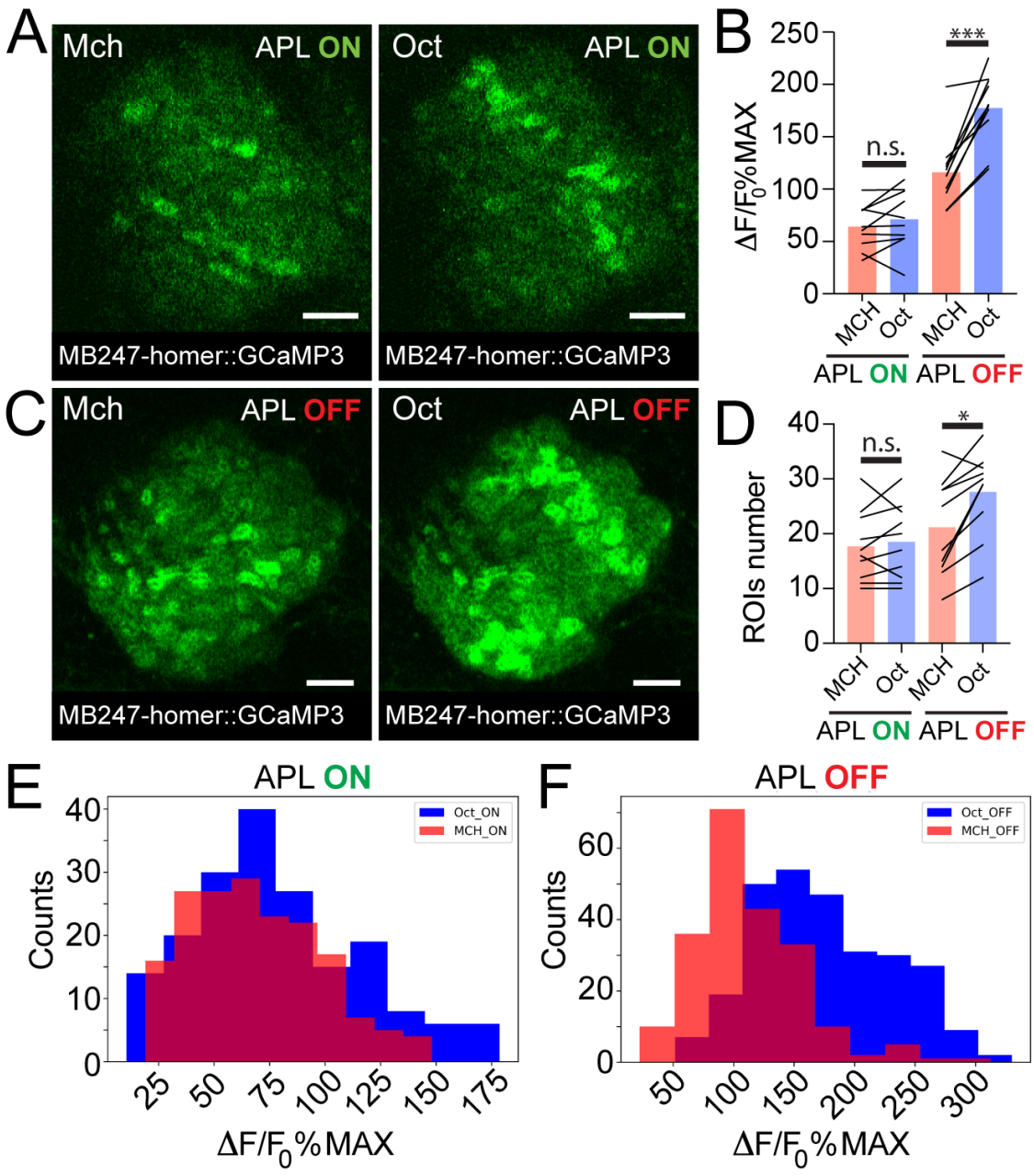

Fig 4. APL silencing leads to more variable odour representations at the MB calyx.

Examples of KC claws fluorescence levels in response to Mch and Oct in control animals **(A**, APL ON**)** or in flies where the output from APL was blocked **(C**, APL OFF**)**. The genotype used is *APLi-GAL4>UAS-TeTx, UAS-mCherry; MB247-homer::GCaMP3*. Scale bar = 10μm. **(B)** The average activity peak in KC claws was similar when APL was active (APL ON, p=0.949), but was highly variable in the absence of APL output (APL OFF, p=0.0003). n=10, 2-way ANOVA with Tukey´s multiple comparisons. **(D)** The number of odour-responding ROIs was

comparable in the presence of active APL (APL ON, p=0.995) and it was slightly increased in the absence of APL output (APL OFF, p=0.047). n=10, p=0.047, 2-way ANOVA with Tukey´s multiple comparisons. **(E)** Frequency distribution of MGs activity peaks in the presence of APL activity. The two populations are highly overlapping, as in Fig 3G. n=10, p=0.0533, Kolmogorov-Smirnov test. **(F)** In the absence of APL inhibition, the distribution of MGs responding to Oct shifted towards higher values, resembling presynaptic PN boutons data shown in Fig 3C. n=10, p<0.0001, Kolmogorov-Smirnov test. Odours were diluted 1:100, bars indicate means.

2.5 APL inhibition onto MGs of the MB calyx is local

Our data indicate that APL contribution to the MG microcircuit yields a normalized postsynaptic response, independently of the variability of olfactory input strength. To understand how this input-tuned inhibition is achieved, we next asked whether the inhibition provided by APL is global and equally delivered to the entire calyx, or whether it might be more locally restricted to the sites of PN activation. Towards this aim, we selected 3 sets of PNs: DM3, VA1d and DC3, that appear to have distinctive bouton distributions in the calyx based on the Hemibrain dataset (F. Li et al. 2020b). We expect the bouton distribution of these PNs to be reproducible among animals (H.-H. Lin et al. 2007; Jefferis et al. 2007). Based on an available database of odorant representations (Münch and Galizia 2016), these PNs are activated by the following odours: Pentyl acetate (PA) activates the glomerulus DM3, whose PNs terminate in the posterior part of the calyx mainly; Methyl Palmitate (MP) activates the glomerulus VA1d, whose PN terminals populate the anterior part of the calyx; Farnesol (FA) activates glomerulus DC3, with PN terminals that populate the anterior part of the calyx, similarly to VA1d (Fig 5A-B). Flies were

exposed to random sequences of the 3 odours, and 3D image stacks were acquired over time to define the localization of the APL response within the entire calycal volume (Fig 5B). Interestingly, we found the ratio of the calcium transients to be highly inconstant throughout the volume of the calyx for the structurally more distant odours PA and MP (see also Material and Methods for details). In particular, the PA/MP fluorescence ratio was higher in the posterior sections of the calyx and reduced in the anterior ones (Fig 5C, black line), reflecting the bouton distribution of the PNs activated by these two odours. By contrast, the fluorescence ratio of FA to MP was more homogeneous across the calyx volume, reflecting the fact that the boutons of the PNs that respond to these odours are located in a similar region of the calyx (Fig 5C, blue line). In other words, not only APL calcium transients were different with different odours, as already shown (Fig 2), but these transients were also differently distributed in the calycal volume depending on the odour, strengthening the link between structural and functional data. Combined with the information about synapse distribution, these data suggest that APL is locally activated in the calyx at the MGs corresponding to activated PNs, and that the tone of APL inhibition in the calyx is a gradient that slowly degrades with increasing distance from the active boutons. Taken together, APL inhibition onto MGs of the MB calyx showed signs of locality. Of notice, a similar spreading mechanism has been observed in APL´s parallel neurites at the MB lobes, where calcium transients failed to propagate over long distances (Amin et al. 2020).

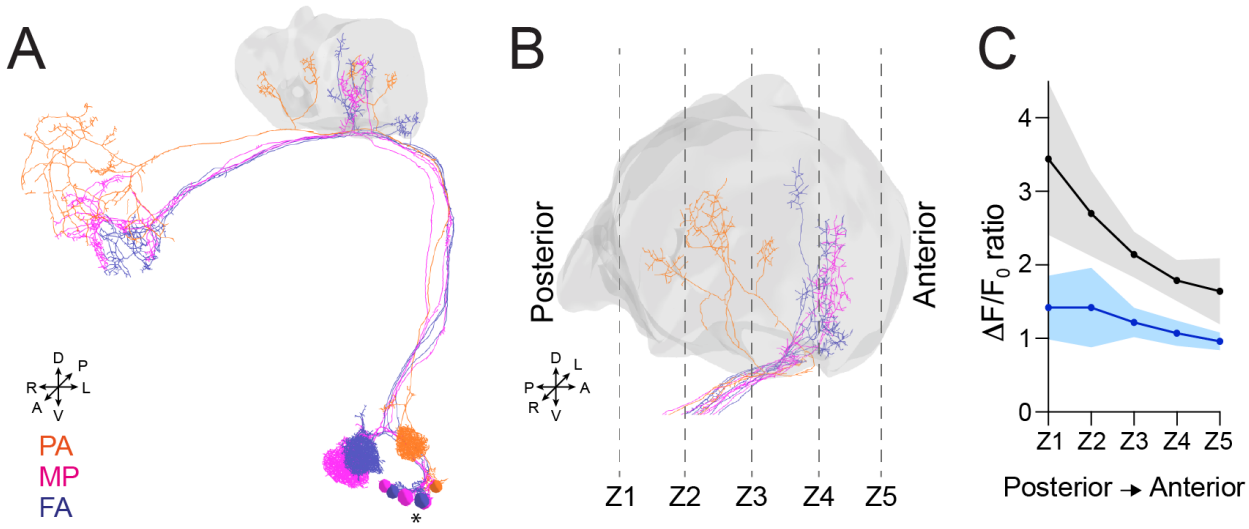

Fig 5. APL inhibition is local within the MB calyx.

(A) 3D skeletons of the PNs activated by the odours used in this experiment: PA (orange), MP (magenta), FA (blue). Asterisk indicate PN cell bodies. **(B)** Side view of the calyx showing the distribution of the PN terminals for the odours used in this experiment. Note the higher spatial segregation between PA and MP PN terminals compared to FA and MP ones. The ticked lines Z1-Z5 show an example of sectioning applied when acquiring image stacks over time. **(C)** The calcium transient ratio of PA to MP (black line) was highly variable throughout different section of the calyx, and was significantly different to the FA to MP one (blue line). n=7, p=0.007 (**), Kolmogorov-Smirnov test. Coloured areas represent SEM.

3 Discussion

While the importance of inhibition in reducing the overlap among stimuli representation has been postulated many decades ago (Marr 1969; Albus 1971; Litwin-Kumar et al. 2017; Cayco-Gajic and Silver 2019) and supported by more recent experimental evidence (Parnas et al. 2013; Olsen, Bhandawat, and Wilson 2010), the complete mechanism by which inhibition supports stimuli discrimination is not fully understood yet. Here, we show that the

519 inhibitory APL neuron, by participating in the structure of MGs of the
520 *Drosophila* MB calyx, provides inhibition scaled to the PNs excitatory inputs to
521 the calyx. As a result, the average strength of postsynaptic responses in KC
522 dendritic claws is homogenous among MGs and different odour
523 representations. We suggest that this normalization of postsynaptic responses
524 operated by APL is at the core of pattern separation in the MB.

525 Pattern separation is obtained in the MB through the formation of a sparse
526 response in the KC layer (Honegger, Campbell, and Turner 2011; Turner,
527 Bazhenov, and Laurent 2008; Campbell et al. 2013a; Perez-Orive et al. 2002).
528 The decoding of a sparse code, in general, increases the storage capacity of
529 associative networks, thereby supporting learning and classification tasks
530 (Olshausen and Field 2004; Kanerva 1988; Tsodyks and Feigel'man 1988;
531 Perez Vicente and Amit 1989; Huerta et al. 2004; García-Sanchez and Huerta
532 2003; Jortner, Farivar, and Laurent 2007). In fact, sparse neuronal
533 representations are described in several organisms including mammals,
534 songbirds, and insects (Rolls and Tovee 1995; Vinje and Gallant 2000;
535 Hahnloser, Kozhevnikov, and Fee 2002; Laurent 2002; Quiroga et al. 2005;
536 GoodSmith et al. 2017; Danielson et al. 2017). APL was reported to play a key
537 role in maintaining KCs responses sparse (A. C. Lin et al. 2014; Lei et al.
538 2013), but the underlying mechanism was far from understood. KCs receive
539 inputs from 6-8 PNs on average (Butcher et al. 2012; Zheng et al. 2020; F. Li
540 et al. 2020b) and, due to KCs high firing threshold (Turner, Bazhenov, and
541 Laurent 2008), require more than half of those inputs to be coactive to spike
542 (Gruntman and Turner 2013). Our data suggest that the APL neuron, by
543 confining KC claws responses within a certain range of activation, ensures that

KCs requirement of multiple coactive claws is respected even in the presence of highly variable input strengths. In other words, APL inhibition makes KC input integration dependent on the combinatorial pattern of inputs rather than on the strength of individual inputs. Of notice, odour discrimination is achieved at multiple levels of the *Drosophila* olfactory pathway by different means of inhibitory mechanisms: from the input gain control normalization executed by GABAergic interneurons in the AL (Olsen and Wilson 2008), to the high-pass filter function performed by inhibitory iPNs at the lateral horn (Parnas et al. 2013).

Interestingly, we found a slight increase in the number of MGs responding to an odour in the absence of APL inhibition (Fig 4D). This could have two possible explanations: i) the postsynaptic response of these additional MGs was so weak in the presence of APL that their activation was below the limit of detection; or ii) the increase in number is the consequence of an expanded number of KC axons spiking action potentials that back-propagate into their dendrites. We tend to exclude the second hypothesis as each MG is constituted, on average, by 13 claw-like dendritic endings from different KCs (Davi D. Bock, personal communication), and each KC connects with its other claws to random PNs (Caron et al. 2013). It seems unlikely that all or a large fraction of randomly assembled claws are all invested by back-propagating action potentials and therefore visible in our recordings.

Our structural and functional data point towards the involvement of APL in a feedforward loop from PN boutons to KC claws, as well as a closed feedback loop with PN boutons. An advantage of using recurrent circuits to provide

568 inhibition is that such a system can deal with a wide range of input strength,
569 as inhibition and excitation strengths are proportional. Indeed, EM analysis
570 revealed both pre- and postsynaptic connection between APL and PN boutons,
571 linearly proportional to each other (Fig 1D), and the differences in the APL
572 calcium influx in response to odours correlated to the variability measured in
573 PNs (Fig 2 and 3). So far, APL has been mainly described as a feedback neuron
574 for KCs (A. C. Lin et al. 2014; Lei et al. 2013; Amin et al. 2020). However,
575 feedforward inhibitory neurons from the input population onto the next layer
576 have been described in other neuronal networks performing pattern separation
577 (Cayco-Gajic and Silver 2019). For example, granule cells receive both
578 feedforward and feedback inhibition from Golgi cells at the cerebellar cortex
579 (Vos, Volny-Luraghi, and de Schutter 1999; Duguid et al. 2015), which are
580 driven by excitatory inputs from the mossy fibers (Kanichay and Silver 2008)
581 and granule cells' axons, respectively (Cesana et al. 2013). Moreover, it has
582 recently been demonstrated that Golgi cells recruitment scales with the mossy
583 fibers input density (Tabuchi et al. 2019), similarly to what we observed in our
584 functional imaging experiments. Additionally, adaptive regulation of KCs
585 sparseness by feedforward inhibition has already been theorized in realistic
586 computational models of insect´s mushroom bodies (Assisi et al. 2007; Luo,
587 Axel, and Abbott 2010). Regarding KCs-to-APL connections, we found a
588 positive linearity among pre- and post-synapses between these two cells (Fig
589 1E), confirming the presence of a local feedback loop within KC dendrites and
590 the APL at the calyx (Amin et al. 2020). Furthermore, we reported that α/β KCs
591 receive more inhibitory synapses along their dendritic trees compared to γ and
592 α'/β', where the majority of synapses received from the APL is localised on KC

593 claws instead (Fig S1C). As the ability of inhibitory synapses to shunt current
594 from excitatory synapses depends on the spatial arrangement of the two inputs
595 (Spruston, Stuart, and Häusser 2016), we speculate that the difference in APL
596 synapses localisation could contribute to some of the electrophysiological
597 differences recorded among distinct KCs type. For example, α/β_c KCs were
598 found to have a higher input resistances and longer membrane time constants
599 compared to α'/β' KCs (Groschner et al. 2018), resulting in a sigmoidal
600 current-spike frequency function rather than a linear one (Groschner et al.
601 2018). Additionally, a difference in synapses distribution can also indicate that
602 two inhibitory mechanisms coexist at the MB calyx, similarly to what has been
603 shown in the cerebellum where Golgi cells are responsible for both tonic
604 inhibition, controlling granule cells spike number (Brickley, Cull-Candy, and
605 Farrant 1996), gain control (Mitchell and Silver 2003), and phasic inhibition,
606 limiting the duration of granule cells responses (D'Angelo and de Zeeuw 2009).

607 Finally, volumetric calcium imaging showed that the APL inhibition is local
608 within the MB calyx. In particular, we found a difference in the APL calcium
609 transients when flies were stimulated with odours that activate PN subsets with
610 segregated bouton distribution in the calyx (Fig 5). These data suggest that
611 APL inhibition onto MGs can be imagined as a gradient that peaks at the MGs
612 active during a given stimulus and attenuates with distance. Non-spiking
613 interneurons in insects are typically large and characterized by complex neurite
614 branching, an ideal structure to support local microcircuits (Roberts, Bush, and
615 Society for Experimental Biology (Great Britain). Neurobiology Group. 1981).
616 As a matter of fact, similar examples of localized APL response as described
617 here have been reported in the *Drosophila* MB (Amin et al. 2020; Wang et al.

2019) as well as in the APL´s homolog GGN in the locust (Ray, Aldworth, and Stopfer 2020; Leitch and Laurent 1996). An advantage of having local microcircuits is that it allows a single neuron to mimic the activity of several inhibitory interneurons, as described in amacrine cells of both mammals (Grimes et al. 2010) and *Drosophila* (Meier and Borst 2019). Additionally, a parallel local-global inhibition is suggested to expand the dynamic range of inputs able to activate KCs (Ray, Aldworth, and Stopfer 2020).

An important open question is whether the APL inhibition onto MGs of the MB calyx is more of a presynaptic phenomenon, therefore acting on PN boutons output, or a postsynaptic one on KCs claws. Our functional data reveal a clear impact of APL on the postsynaptic response in MGs (Fig 3H, S3F), while the PN boutons display a broad range of activity levels (Fig 3A-D, Fig S2, Fig S3A-D). Accordingly, silencing of the $GABA_A$ receptor *Rdl* on KCs increased calcium responses in the MB, including the calyx (Liu, Krause, and Davis 2007), and reduced sparseness of odour representations (Lei et al. 2013). However, due to the presence of presynapses from APL to PN boutons (Fig 1B, 1D), a presynaptic component of APL inhibition is certainly possible.

One possible caveat to our hypothesis is given by the fact that reducing GABA synthesis in APL by RNAi has been found to improve olfactory learning (Liu and Davis 2009). However, this could be explained by a low efficiency of RNAi in this case. Indeed, incomplete silencing might increase KCs´ output without affecting sparseness. As a matter of fact, blockage of APL output via *shibire*^{ts} led to impaired olfactory discrimination (A. C. Lin et al. 2014).

Taken together, our study provides novel insights on how feed-forward inhibition via APL shapes the postsynaptic response to olfactory inputs in the MB calyx and contributes to maintaining odour evoked KC activity sparse. In the future, it will be interesting to investigate the impact of APL on memory consolidation, which has been associated with structural plasticity in the calyx (Baltruschat et al. 2021) and with changes in the KC response (Delestro et al. 2020).

4 Materials and Methods

4.1 Connectomics

Connectomics data were obtained from the Hemibrain EM dataset (Scheffer et al. 2020) via the Neuprint analysis Tool (Clements et al. 2020). In particular, the Neuprint-python package (https://github.com/connectome-neuprint/neuprint-python) was used to filter for annotated synapses made and received by the APL only within the CA(R) ROI. The command *fetch_adjacencies* was used to extract data regarding the connectivity among cell types. To visualize neuron skeletons or filled renders in 3D, the commands *fetch_skeletons* or *fetch_mesh_neuron* were used instead. To visualize APL synapses onto PNs or KCs, the coordinates of those synapses were obtained via *fetch_synapse_connections* and plotted together with the 3D neuronal meshes. The localization of the synapses (e.g., on PN bouton or not) was addressed manually by two separate users in a blind manner, and the average counts were calculated. Detailed tables containing the list of all PNs and KCs

interconnected with the APL within the MB calyx, as well as the weight of those synapses, and 3D images of APL synapses mapped onto PNs and KCs meshes can be found at: Mendeley data link will be available upon publication.

4.2 Fly strains

The following lines were used for experiments: *GH146-Gal4* (Reinhard F. Stocker et al. 1997), *NP225-Gal4* (Hayashi et al. 2002), *NP2631-Gal4* (Hayashi et al. 2002), *GH146-Flp* (Hong et al. 2009), *tubP-GAL80^{ts}* (Sean E. McGuire et al. 2003), *tubP-FRT-GAL80-FRT* (S. Gao et al. 2008; Gordon and Scott 2009), *UAS-GCaMP6m* (Chen et al. 2013a), *MB247-homer::GCaMP3* (Pech et al. 2015), *UAS-Syp::GCaMP3* (Pech et al. 2015), *UAS-TeTx* (Sweeney et al. 1995), *UAS-mCherry::CAAX* (Kakihara et al. 2008). Flies were raised in a 12h/12h light-dark cycle on a standard cornmeal-based diet at 25 °C, 60% relative humidity unless they expressed the temperature-sensitive gene product Gal80^{ts}. Flies carrying *tubP-GAL80^{ts}* were raised at 18°C and placed at 31°C for 24 h-48 h <24 h after eclosion. 1-7 days old flies were used for experiments. All experiments were performed on mixed populations of males and females.

4.3 Two-photon *in vivo* calcium imaging

For *in vivo* imaging in the MB calyx, adult flies were briefly anaesthetized on ice, positioned in a polycarbonate imaging chamber (Louis et al. 2017), and immobilized using Myristic Acid (Sigma-Aldrich). To allow optical access to the Calyx, a small window was opened through the head capsule under Ringer's solution (5 mM HEPES, pH 7.4, 130 mM NaCl, 5 mM KCl, 2 mM $CaCl_2$, 2 mM

687 $MgCl_2$; pH adjusted to 7.2). To minimize movement, fly heads were stabilized
688 with 1,5% low melting agarose (Thermo Scientific) in Ringer's solution,
689 immediately before dissection. Flies were imaged with a two-photon laser-
690 scanning microscope (LaVision BioTec, TriM Scope II) equipped with an ultra-
691 fast z-motor (PIFOC® Objective Scanner Systems 100µm range) and a Nikon
692 25X CFI APO LWD Objective, 1.1 NA water–immersion objective. GCaMP
693 molecules were excited at 920 nm using a Ti:sapphire laser (Coherent
694 Chameleon). Odours were delivered to the *in vivo* preparation via a 220A
695 Olfactometer (Aurora Scientific) in a randomized fashion. Odours were loaded
696 into the respective odour vials with a dilution 10X higher than the desired one,
697 and further diluted 1:10 with clean air during odour stimulation. A constant
698 flow of clean air was provided by a Stimulus Controller CS 55 (Ockenfels
699 SYNTECH GbmH), equipped with two activated carbon inlet filters to avoid air
700 contamination. Animals were stimulated with 2 odour puffs of 5 s each,
701 separated by 20 s clean air intervals. Both clean air and odour flows were kept
702 around 0.5L/min for the entire experimental procedure. For imaging, a region
703 large enough to include an entire z-section of the mushroom body calyx was
704 chosen. The scanning frequency was set around 9 Hz. Single plane videos were
705 acquired unless stated otherwise.

706 For volumetric calcium imaging (Fig 5), flies were mounted and stimulated as
707 described above and 3D stacks of 5 images each were acquired over time for
708 the entire stimulation time. To compensate for the reduced speed caused by
709 the stack acquisition, the frame rate was adjusted to around 16 Hz.

For *in vivo* AL imaging, female adult flies were briefly anaesthetized on ice, positioned in a custom-built fly chamber (Hancock, Bilz, and Fiala 2019), and immobilized using UV-hardening dental glue (Kentoflow, Kent Dental). A small dissection was performed in Ringer's solution (5 mM HEPES, pH 7.4, 130 mM NaCl, 5 mM KCl, 2 mM $CaCl_2$, 2 mM $MgCl_2$; pH adjusted to 7.2). Flies were imaged with a two-photon laser-scanning microscope LSM 7MP (Zeiss) equipped with a 20X/1.0 DIC M27 75mm Plan-Apochromat objective (Zeiss). GCaMP molecules were excited at 920 nm using a Ti:sapphire laser (Coherent Chameleon). Odours were delivered to the *in vivo* preparation via a custom-built olfactometer. Odours were diluted in mineral oil (Sigma-Aldrich) at the required dilution. A constant flow of clean air was provided by a membrane pump "optimal" (SCHEGO). Animals were stimulated with 2 odour puffs of 5 s each, separated by 20 s clean air intervals. Both clean air and odour flows were kept around 1mL/s for the entire experimental procedure. For imaging, a region large enough to include an entire z-section of the mushroom body calyx was chosen. The scanning frequency was set around 5 Hz. Single plane videos were acquired unless stated otherwise.

As the PN Gal4 driver *GH146* used in AL imaging experiments drives expression also in APL (Liu and Davis 2009), the *NP225-Gal4* driver line (Hayashi et al. 2002) was chosen for PN boutons imaging at the calyx, as it targets a similar amount of PNs as *GH146* without including the APL.

4.4 Data Analysis

Two-photon images were analysed using Fiji (Schindelin et al. 2012). Briefly, raw videos were motion corrected via the "Template Matching and Slice Alignment" ImageJ plugin (Tseng et al. 2012). Afterwards, ROIs of the single MGs responding to a given odour were created via the "Cell Tracking by Calcium" ImageJ Macro (designed and written by DZNE IDAF). The generated mask was then applied to the previously registered video in order to extract the average intensity value over time per each of the detected ROIs. Finally, the $\Delta F/F_0\%$ and the $\Delta F/F_0\%MAX$ of each ROI was calculated by using the average intensity of the first 30 frames as F_0. A detailed manual related to the ImageJ Macro, as well as Python notebooks computing the $\Delta F/F_0\%$ and $\Delta F/F_0\%MAX$ given a dataframe of intensity values over time, is available at: Mendeley data link will be available upon publication.

To measure calcium influx among the APL neurites branching in the mushroom body calyx, a manual ROI was drawn around the entire calycal region expressing the GCaMP and the average intensity value over time was extracted. $F/F_0\%$ and $\Delta F/F_0\%MAX$ were calculated as described above.

For the odours response ratio calculated in the APL volumetric calcium imaging experiment (Fig 5), the $\Delta F/F_0\%MAX$ per each odour was calculated as described above. The $\Delta F/F_0\%MAX$ values per each of the 5 frames contained in an image-stack were obtained and averaged among all animals tested. Next, a $\Delta F/F_0\%MAX$ ratio between the odour pairs being compared was calculated and analysed per each of the sections included in an image stack.

4.5 Confocal imaging

To address the presence or not of the *APLi.GAL4* driven *UAS-TNT* and *UAS-mCherry* products, whole flies were fixed on Formaldehyde (FA) 4% in PBS with 0.1% Triton X-100 (PBT 0.1%) immediately after *in vivo* imaging. Once all animals sustained the *in vivo* imaging protocol, brains were dissected using a pair of forceps in a small petri dish covered with a layer of silicon, fixed for further 20 min on FA 4% in PBT 0.1%, washed 3 times for 5 min ca in PBT 0.1% and mounted with Vectashield® Plus Antifade Mounting Medium (Vectorlabs) on 76 x 26 mm Microscope slides (Thermo scientific) with 1# coverslips (Carl Roth). Brains were oriented with the dorsal part facing upwards. Imaging was performed on a LSM 780 confocal microscope (Zeiss) equipped with a Plan-Apochromat 63x/1.4 Oil DIC M27 objective (Zeiss). 512x512 pixels images were acquired, covering a region of the brain big enough to include the APL soma and branches around the MB calyx and MB lobes. Brains and their related *in vivo* imaging data were assigned to the classes “APL OFF” or “APL ON” based on the presence or not of the TNT-co-expressed mCherry fluorescence, respectively.

4.6 Statistics

Statistics were carried out in Prism 8 (GraphPad). Parametric (t-test, ANOVA) or non-parametric tests (Wilcoxon, Mann-Whitney, Kruskal-Wallis, Kolmogorov-Smirnov) were used depending on whether data passed the D’Agostino-Pearson normality test. Statistical power analysis was conducted in G*Power (Faul et al. 2007).

5 Acknowledgements

We thank LMF and IDAF sections at DZNE, Seth Tomchick, Sanjeev Kaushalya and Kevin Kuepper for support in technical development. Rita Kerpen, Phuong Tran and Olga Sharma for technical assistance. We thank the Bloomington Stock Center, Andrew Lin and Oren Schuldiner for fly lines. We thank Andrew Lin, Martin Nawrot, Peter Kloppenburg for discussions. We thank Moshe Parnas, David Owald, Barbara Schaffran and the members of the Tavosanis lab for critical reading of the manuscript. This work was supported by the DFG FOR 2705 to G.T.

6 Financial interests or conflicts of interest

The authors declare no competing interests.

References

Albus, James S. 1971. "A Theory of Cerebellar Function." *Mathematical Biosciences* 10 (1–2): 25–61. https://doi.org/10.1016/0025-5564(71)90051-4.

Alivisatos, A. Paul, Miyoung Chun, George M. Church, Ralph J. Greenspan, Michael L. Roukes, and Rafael Yuste. 2012. "The Brain Activity Map Project and the Challenge of Functional Connectomics." *Neuron*. Cell Press. https://doi.org/10.1016/j.neuron.2012.06.006.

798 Amin, Hoger, Anthi A Apostolopoulou, Raquel Suárez-Grimalt, Eleftheria
799 Vrontou, and Andrew C Lin. 2020. "Localized Inhibition in the Drosophila
800 Mushroom Body." *ELife* 9: 1–31. https://doi.org/10.7554/elife.56954.
801 Aso, Yoshinori, Kornelia Grübel, Sebastian Busch, Anja B. Friedrich, Igor
802 Siwanowicz, and Hiromu Tanimoto. 2009. "The Mushroom Body of Adult
803 *Drosophila* Characterized by GAL4 Drivers." *Journal of Neurogenetics* 23
804 (1–2): 156–72. https://doi.org/10.1080/01677060802471718.
805 Aso, Yoshinori, Daisuke Hattori, Yang Yu, Rebecca M. Johnston, Nirmala A. Iyer,
806 Teri T.B. Ngo, Heather Dionne, et al. 2014. "The Neuronal Architecture of
807 the Mushroom Body Provides a Logic for Associative Learning." *ELife* 3:
808 e04577. https://doi.org/10.7554/eLife.04577.
809 Assisi, Collins, Mark Stopfer, Gilles Laurent, and Maxim Bazhenov. 2007.
810 "Adaptive Regulation of Sparseness by Feedforward Inhibition." *Nature*
811 *Neuroscience* 10 (9): 1176–84. https://doi.org/10.1038/nn1947.
812 Baltruschat, Lothar, Luigi Prisco, Philipp Ranft, J. Scott Lauritzen, André Fiala,
813 Davi D. Bock, and Gaia Tavosanis. 2021. "Circuit Reorganization in the
814 Drosophila Mushroom Body Calyx Accompanies Memory Consolidation."
815 *Cell Reports* 34 (11): 108871.
816 https://doi.org/10.1016/j.celrep.2021.108871.
817 Barth, Jonas, Shubham Dipt, Ulrike Pech, Moritz Hermann, Thomas
818 Riemensperger, and André Fiala. 2014. "Differential Associative Training
819 Enhances Olfactory Acuity in Drosophila Melanogaster." *Journal of*
820 *Neuroscience* 34 (5): 1819–37. https://doi.org/10.1523/JNEUROSCI.2598-
821 13.2014.

822 Bates, Alexander S., Philipp Schlegel, Ruairi J.V. Roberts, Nikolas Drummond,
823 Imaan F.M. Tamimi, Robert Turnbull, Xincheng Zhao, et al. 2020.
824 "Complete Connectomic Reconstruction of Olfactory Projection Neurons in
825 the Fly Brain." *Current Biology* 30 (16): 3183-3199.e6.
826 https://doi.org/10.1016/j.cub.2020.06.042.
827 Belle, J. Steven de, and Martin Heisenberg. 1994. "Associative Odor Learning in
828 Drosophila Abolished by Chemical Ablation of Mushroom Bodies." *Science*
829 263 (5147): 692–95. https://doi.org/10.1126/science.8303280.
830 Berdnik, Daniela, Audrey P. Fan, Christopher J. Potter, and Liqun Luo. 2008.
831 "MicroRNA Processing Pathway Regulates Olfactory Neuron
832 Morphogenesis." *Current Biology* 18 (22): 1754–59.
833 https://doi.org/10.1016/j.cub.2008.09.045.
834 Bhandawat, Vikas, Shawn R. Olsen, Nathan W. Gouwens, Michelle L. Schlief,
835 and Rachel I. Wilson. 2007. "Sensory Processing in the Drosophila
836 Antennal Lobe Increases Reliability and Separability of Ensemble Odor
837 Representations." *Nature Neuroscience* 10 (11): 1474–82.
838 https://doi.org/10.1038/nn1976.
839 Brickley, S G, S G Cull-Candy, and M Farrant. 1996. "Development of a Tonic
840 Form of Synaptic Inhibition in Rat Cerebellar Granule Cells Resulting from
841 Persistent Activation of GABAA Receptors." *The Journal of Physiology* 497
842 (3): 753–59. https://doi.org/10.1113/JPHYSIOL.1996.SP021806.
843 Butcher, Nancy J., Anja B. Friedrich, Zhiyuan Lu, Hiromu Tanimoto, and Ian A.
844 Meinertzhagen. 2012. "Different Classes of Input and Output Neurons
845 Reveal New Features in Microglomeruli of the Adult Drosophila Mushroom

Body Calyx." *Journal of Comparative Neurology* 520 (10): 2185–2201. https://doi.org/10.1002/cne.23037.

Campbell, Robert A.A., Kyle S. Honegger, Hongtao Qin, Wanhe Li, Ebru Demir, and Glenn C. Turner. 2013a. "Imaging a Population Code for Odor Identity in the Drosophila Mushroom Body." *Journal of Neuroscience* 33 (25): 10568–81. https://doi.org/10.1523/JNEUROSCI.0682-12.2013.

———. 2013b. "Imaging a Population Code for Odor Identity in the Drosophila Mushroom Body." *Journal of Neuroscience* 33 (25): 10568–81. https://doi.org/10.1523/JNEUROSCI.0682-12.2013.

Caron, Sophie J.C., Vanessa Ruta, L. F. Abbott, and Richard Axel. 2013. "Random Convergence of Olfactory Inputs in the Drosophila Mushroom Body." *Nature* 497 (7447): 113–17. https://doi.org/10.1038/nature12063.

Cayco-Gajic, N. Alex, Claudia Clopath, and R. Angus Silver. 2017. "Sparse Synaptic Connectivity Is Required for Decorrelation and Pattern Separation in Feedforward Networks." *Nature Communications* 8 (1): 1–11. https://doi.org/10.1038/s41467-017-01109-y.

Cayco-Gajic, N. Alex, and R. Angus Silver. 2019. "Re-Evaluating Circuit Mechanisms Underlying Pattern Separation." *Neuron* 101 (4): 584–602. https://doi.org/10.1016/j.neuron.2019.01.044.

Cesana, Elisabetta, Katarzyna Pietrajtis, Céline Bidoret, Philippe Isope, Egidio D'Angelo, Stéphane Dieudonné, and Lia Forti. 2013. "Granule Cell Ascending Axon Excitatory Synapses onto Golgi Cells Implement a Potent Feedback Circuit in the Cerebellar Granular Layer." *Journal of Neuroscience* 33 (30): 12430–46. https://doi.org/10.1523/JNEUROSCI.4897-11.2013.

Chen, Tsai Wen, Trevor J. Wardill, Yi Sun, Stefan R. Pulver, Sabine L. Renninger, Amy Baohan, Eric R. Schreiter, et al. 2013a. "Ultrasensitive Fluorescent Proteins for Imaging Neuronal Activity." *Nature* 499 (7458): 295–300. https://doi.org/10.1038/nature12354.

———. 2013b. "Ultrasensitive Fluorescent Proteins for Imaging Neuronal Activity." *Nature* 499 (7458): 295–300. https://doi.org/10.1038/nature12354.

Clements, Jody, Tom Dolafi, Lowell Umayam, Nicole L. Neubarth, Stuart Berg, Louis K. Scheffer, and Stephen M. Plaza. 2020. "NeuPrint: Analysis Tools for EM Connectomics." *BioRxiv*. bioRxiv. https://doi.org/10.1101/2020.01.16.909465.

Clyne, Peter J., Coral G. Warr, Marc R. Freeman, Derek Lessing, Junhyong Kim, and John R. Carlson. 1999. "A Novel Family of Divergent Seven-Transmembrane Proteins: Candidate Odorant Receptors in Drosophila." *Neuron* 22 (2): 327–38. https://doi.org/10.1016/S0896-6273(00)81093-4.

Crittenden, Jill R., Efthimios M.C. Skoulakis, Kyung-An Han, Daniel Kalderon, and Ronald L. Davis. 1998. "Tripartite Mushroom Body Architecture Revealed by Antigenic Markers." *Learning & Memory* 5 (1): 38. /pmc/articles/PMC311260/.

D'Angelo, Egidio, and Chris I. de Zeeuw. 2009. "Timing and Plasticity in the Cerebellum: Focus on the Granular Layer." *Trends in Neurosciences* 32 (1): 30–40. https://doi.org/10.1016/J.TINS.2008.09.007.

Danielson, Nathan B., Gergely F. Turi, Max Ladow, Spyridon Chavlis, Panagiotis C. Petrantonakis, Panayiota Poirazi, and Attila Losonczy. 2017. "In Vivo

894 Imaging of Dentate Gyrus Mossy Cells in Behaving Mice." *Neuron* 93 (3):
895 552-559.e4. https://doi.org/10.1016/j.neuron.2016.12.019.
896 Delestro, Felipe, Lisa Scheunemann, Mélanie Pedrazzani, Paul Tchenio, Thomas
897 Preat, and Auguste Genovesio. 2020. "In Vivo Large-Scale Analysis of
898 Drosophila Neuronal Calcium Traces by Automated Tracking of Single
899 Somata." *Scientific Reports* 10 (1): 1–14. https://doi.org/10.1038/s41598-
900 020-64060-x.
901 Dubnau, Josh, Lori Grady, Toshi Kitamoto, and Tim Tully. 2001. "Disruption of
902 Neurotransmission in Drosophila Mushroom Body Blocks Retrieval but Not
903 Acquisition of Memory." *Nature* 411 (6836): 476–80.
904 https://doi.org/10.1038/35078077.
905 Duguid, Ian, Tiago Branco, Paul Chadderton, Charlotte Arlt, Kate Powell, and
906 Michael Häusser. 2015. "Control of Cerebellar Granule Cell Output by
907 Sensory-Evoked Golgi Cell Inhibition." *Proceedings of the National Academy*
908 *of Sciences of the United States of America* 112 (42): 13099–104.
909 https://doi.org/10.1073/pnas.1510249112.
910 Faul, Franz, Edgar Erdfelder, Albert Georg Lang, and Axel Buchner. 2007.
911 "G*Power 3: A Flexible Statistical Power Analysis Program for the Social,
912 Behavioral, and Biomedical Sciences." In *Behavior Research Methods*,
913 39:175–91. Psychonomic Society Inc.
914 https://doi.org/10.3758/BF03193146.
915 Frank, Dominic D., Genevieve C. Jouandet, Patrick J. Kearney, Lindsey J.
916 Macpherson, and Marco Gallio. 2015. "Temperature Representation in the
917 Drosophila Brain." *Nature 2015 519:7543* 519 (7543): 358–61.
918 https://doi.org/10.1038/nature14284.

Gao, Qian, Bingbing Yuan, and Andrew Chess. 2000. "Convergent Projections of Drosophila Olfactory Neurons to Specific Glomeruli in the Antennal Lobe." *Nature Neuroscience* 3 (8): 780–85. https://doi.org/10.1038/77680.

Gao, Shuying, Shin ya Takemura, Chun Yuan Ting, Songling Huang, Zhiyuan Lu, Haojiang Luan, Jens Rister, et al. 2008. "The Neural Substrate of Spectral Preference in Drosophila." *Neuron* 60 (2): 328–42. https://doi.org/10.1016/j.neuron.2008.08.010.

García-Sanchez, Marta, and Ramón Huerta. 2003. "Design Parameters of the Fan-out Phase of Sensory Systems." *Journal of Computational Neuroscience* 15 (1): 5–17. https://doi.org/10.1023/A:1024460700856.

GoodSmith, Douglas, Xiaojing Chen, Cheng Wang, Sang Hoon Kim, Hongjun Song, Andrea Burgalossi, Kimberly M. Christian, and James J. Knierim. 2017. "Spatial Representations of Granule Cells and Mossy Cells of the Dentate Gyrus." *Neuron* 93 (3): 677-690.e5. https://doi.org/10.1016/j.neuron.2016.12.026.

Gordon, Michael D., and Kristin Scott. 2009. "Motor Control in a Drosophila Taste Circuit." *Neuron* 61 (3): 373–84. https://doi.org/10.1016/j.neuron.2008.12.033.

Grabe, Veit, Amelie Baschwitz, Hany K.M. Dweck, Sofia Lavista-Llanos, Bill S. Hansson, and Silke Sachse. 2016. "Elucidating the Neuronal Architecture of Olfactory Glomeruli in the Drosophila Antennal Lobe." *Cell Reports* 16 (12): 3401–13. https://doi.org/10.1016/J.CELREP.2016.08.063.

Grimes, William N., Jun Zhang, Cole W. Graydon, Bechara Kachar, and Jeffrey S. Diamond. 2010. "Retinal Parallel Processors: More than 100

944 Independent Microcircuits Operate within a Single Interneuron." *Neuron* 65
945 (6): 873–85. https://doi.org/10.1016/J.NEURON.2010.02.028.
946 Groschner, Lukas N., Laura Chan Wah Hak, Rafal Bogacz, Shamik DasGupta,
947 and Gero Miesenböck. 2018. "Dendritic Integration of Sensory Evidence in
948 Perceptual Decision-Making." *Cell* 173 (4): 894-905.e13.
949 https://doi.org/10.1016/j.cell.2018.03.075.
950 Gruntman, Eyal, and Glenn C. Turner. 2013. "Integration of the Olfactory Code
951 across Dendritic Claws of Single Mushroom Body Neurons." *Nature*
952 *Neuroscience* 16 (12): 1821–29. https://doi.org/10.1038/nn.3547.
953 Hahnloser, Richard H.R., Alexay A. Kozhevnikov, and Michale S. Fee. 2002. "An
954 Ultra-Sparse Code Underlies the Generation of Neural Sequences in a
955 Songbird." *Nature* 419 (6902): 65–70.
956 https://doi.org/10.1038/nature00974.
957 Hallem, Elissa A., and John R. Carlson. 2006a. "Coding of Odors by a Receptor
958 Repertoire." *Cell* 125 (1): 143–60.
959 https://doi.org/10.1016/j.cell.2006.01.050.
960 ———. 2006b. "Coding of Odors by a Receptor Repertoire." *Cell* 125 (1): 143–
961 60. https://doi.org/10.1016/J.CELL.2006.01.050.
962 Hancock, Clare E., Florian Bilz, and André Fiala. 2019. "In Vivo Optical Calcium
963 Imaging of Learning-Induced Synaptic Plasticity in Drosophila
964 Melanogaster." *Journal of Visualized Experiments* 2019 (152): 60288.
965 https://doi.org/10.3791/60288.
966 Hayashi, Shigeo, Kei Ito, Yukiko Sado, Misako Taniguchi, Ai Akimoto, Hiroko
967 Takeuchi, Toshiro Aigaki, et al. 2002. "GETDB, a Database Compiling
968 Expression Patterns and Molecular Locations of a Collection of Gal4

969 Enhancer Traps." *Genesis* 34 (1–2): 58–61.
970 https://doi.org/10.1002/gene.10137.
971 Heisenberg, Martin, Alexander Borst, Sibylle Wagner, and Duncan Byers. 1985.
972 "Drosophila Mushroom Body Mutants Are Deficient in Olfactory Learning:
973 Research Papers." *Journal of Neurogenetics* 2 (1): 1–30.
974 https://doi.org/10.3109/01677068509100140.
975 Honegger, Kyle S., Robert A.A. Campbell, and Glenn C. Turner. 2011. "Cellular-
976 Resolution Population Imaging Reveals Robust Sparse Coding in the
977 Drosophila Mushroom Body." *Journal of Neuroscience* 31 (33): 11772–85.
978 https://doi.org/10.1523/JNEUROSCI.1099-11.2011.
979 Hong, Weizhe, Haitao Zhu, Christopher J. Potter, Gabrielle Barsh, Mitsuhiko
980 Kurusu, Kai Zinn, and Liqun Luo. 2009. "Leucine-Rich Repeat
981 Transmembrane Proteins Instruct Discrete Dendrite Targeting in an
982 Olfactory Map." *Nature Neuroscience* 12 (12): 1542–50.
983 https://doi.org/10.1038/nn.2442.
984 Huerta, Ramón, Thomas Nowotny, Marta García-Sanchez, H. D.I. Abarbanel,
985 and M. I. Rabinovich. 2004. "Learning Classification in the Olfactory
986 System of Insects." *Neural Computation* 16 (8): 1601–40.
987 https://doi.org/10.1162/089976604774201613.
988 Inada, Kengo, Yoshiko Tsuchimoto, and Hokto Kazama. 2017. "Origins of Cell-
989 Type-Specific Olfactory Processing in the Drosophila Mushroom Body
990 Circuit." *Neuron* 95 (2): 357-367.e4.
991 https://doi.org/10.1016/j.neuron.2017.06.039.
992 Jefferis, Gregory S.X.E., Christopher J. Potter, Alexander M. Chan, Elizabeth C.
993 Marin, Torsten Rohlfing, Calvin R. Maurer, and Liqun Luo. 2007.

"Comprehensive Maps of Drosophila Higher Olfactory Centers: Spatially Segregated Fruit and Pheromone Representation." *Cell* 128 (6): 1187–1203. https://doi.org/10.1016/J.CELL.2007.01.040.

Jortner, Ron A., S. Sarah Farivar, and Gilles Laurent. 2007. "A Simple Connectivity Scheme for Sparse Coding in an Olfactory System." *Journal of Neuroscience* 27 (7): 1659–69. https://doi.org/10.1523/JNEUROSCI.4171-06.2007.

Kakihara, Ken, Kaori Shinmyozu, Kagayaki Kato, Hosei Wada, and Shigeo Hayashi. 2008. "Conversion of Plasma Membrane Topology during Epithelial Tube Connection Requires Arf-like 3 Small GTPase in Drosophila." *Mechanisms of Development* 125 (3–4): 325–36. https://doi.org/10.1016/j.mod.2007.10.012.

Kanerva, Pentti. 1988. "Sparse Distributed Memory A Study of Psychologically Driven Storage." https://books.google.com/books?hl=it&lr=&id=I9tCr21-s-AC&oi=fnd&pg=PR11&dq=(1988)+Sparse+distributed+memory+(MIT,+Cambridge,+MA).&ots=QVtRYKxuLE&sig=lPrh_ybrezYEvJeWkt2-Ot4Pa8Q.

Kanichay, Roby T., and R. Angus Silver. 2008. "Synaptic and Cellular Properties of the Feedforward Inhibitory Circuit within the Input Layer of the Cerebellar Cortex." *Journal of Neuroscience* 28 (36): 8955–67. https://doi.org/10.1523/JNEUROSCI.5469-07.2008.

Laurent, Gilles. 2002. "Olfactory Network Dynamics and the Coding of Multidimensional Signals." *Nature Reviews Neuroscience* 3 (11): 884–95. https://doi.org/10.1038/nrn964.

1017 Lee, T., A. Lee, and L. Luo. 1999. "Development of the Drosophila Mushroom
1018 Bodies: Sequential Generation of Three Distinct Types of Neurons from a
1019 Neuroblast." *Undefined*.
1020 Lei, Zhengchang, Ke Chen, Hao Li, He Liu, and Aike Guo. 2013. "The GABA
1021 System Regulates the Sparse Coding of Odors in the Mushroom Bodies of
1022 Drosophila." *Biochemical and Biophysical Research Communications* 436
1023 (1): 35–40. https://doi.org/10.1016/j.bbrc.2013.05.036.
1024 Leiss, Florian, Claudia Groh, Nancy J. Butcher, Ian A. Meinertzhagen, and Gaia
1025 Tavosanis. 2009a. "Synaptic Organization in the Adult *Drosophila*
1026 Mushroom Body Calyx." *The Journal of Comparative Neurology* 517 (6):
1027 808–24. https://doi.org/10.1002/cne.22184.
1028 ———. 2009b. "Synaptic Organization in the Adult *Drosophila* Mushroom Body
1029 Calyx." *The Journal of Comparative Neurology* 517 (6): 808–24.
1030 https://doi.org/10.1002/cne.22184.
1031 Leitch, Beulah, and Gilles Laurent. 1996. "GABAergic Synapses in the Antenna1
1032 Lobe and Mushroom Body of the Locust Olfactory System." *THE JOURNAL*
1033 *OF COMPARATIVE NEUROLOGY* 372 (487): 514.
1034 https://doi.org/10.1002/(SICI)1096-9861(19960902)372:4.
1035 Li, Feng, Jack Lindsey, Elizabeth C. Marin, Nils Otto, Marisa Dreher, Georgia
1036 Dempsey, Ildiko Stark, et al. 2020a. "The Connectome of the Adult
1037 Drosophila Mushroom Body Provides Insights into Function." *ELife* 9
1038 (December): 1–217. https://doi.org/10.7554/eLife.62576.
1039 ———. 2020b. "The Connectome of the Adult Drosophila Mushroom Body
1040 Provides Insights into Function." *ELife* 9 (December): 1–217.
1041 https://doi.org/10.7554/eLife.62576.

1042 Li, Jinzhi, Brennan Dale Mahoney, Miles Solomon Jacob, and Sophie Jeanne
1043 Cécile Caron. 2020. "Visual Input into the Drosophila Melanogaster
1044 Mushroom Body." *Cell Reports* 32 (11): 108138.
1045 https://doi.org/10.1016/J.CELREP.2020.108138.
1046 Lin, Andrew C., Alexei M. Bygrave, Alix de Calignon, Tzumin Lee, and Gero
1047 Miesenböck. 2014. "Sparse, Decorrelated Odor Coding in the Mushroom
1048 Body Enhances Learned Odor Discrimination." *Nature Neuroscience* 17 (4):
1049 559–68. https://doi.org/10.1038/nn.3660.
1050 Lin, Hui-Hao, Jason Sih-Yu Lai, An-Lun Chin, Yung-Chang Chen, and Ann-Shyn
1051 Chiang. 2007. "A Map of Olfactory Representation in the Drosophila
1052 Mushroom Body." *Cell* 128 (6): 1205–17.
1053 https://doi.org/10.1016/J.CELL.2007.03.006.
1054 Litwin-Kumar, Ashok, Kameron Decker Harris, Richard Axel, Haim Sompolinsky,
1055 and L. F. Abbott. 2017. "Optimal Degrees of Synaptic Connectivity." *Neuron*
1056 93 (5): 1153-1164.e7. https://doi.org/10.1016/j.neuron.2017.01.030.
1057 Liu, Xu, and Ronald L. Davis. 2009. "The GABAergic Anterior Paired Lateral
1058 Neuron Suppresses and Is Suppressed by Olfactory Learning." *Nature*
1059 *Neuroscience* 12 (1): 53–59. https://doi.org/10.1038/nn.2235.
1060 Liu, Xu, William C. Krause, and Ronald L. Davis. 2007. "GABAA Receptor RDL
1061 Inhibits Drosophila Olfactory Associative Learning." *Neuron* 56 (6): 1090–
1062 1102. https://doi.org/10.1016/j.neuron.2007.10.036.
1063 Louis, Thierry, Aaron Stahl, Tamara Boto, and Seth M. Tomchik. 2017. "Cyclic
1064 AMP-Dependent Plasticity Underlies Rapid Changes in Odor Coding
1065 Associated with Reward Learning." *Proceedings of the National Academy of*
1066 *Sciences*, 201709037. https://doi.org/10.1073/pnas.1709037115.

Luo, Sean X., Richard Axel, and L. F. Abbott. 2010. "Generating Sparse and Selective Third-Order Responses in the Olfactory System of the Fly." *Proceedings of the National Academy of Sciences of the United States of America* 107 (23): 10713–18. https://doi.org/10.1073/pnas.1005635107.

Marin, Elizabeth C., Laurin Büld, Maria Theiss, Tatevik Sarkissian, Ruairí J.V. Roberts, Robert Turnbull, Imaan F.M. Tamimi, et al. 2020. "Connectomics Analysis Reveals First-, Second-, and Third-Order Thermosensory and Hygrosensory Neurons in the Adult Drosophila Brain." *Current Biology* 30 (16): 3167-3182.e4. https://doi.org/10.1016/J.CUB.2020.06.028.

Marr, David. 1969. "A Theory of Cerebellar Cortex." *The Journal of Physiology* 202 (2): 437–70. https://doi.org/10.1113/jphysiol.1969.sp008820.

Mayseless, Oded, Dominic S. Berns, Xiaomeng M. Yu, Thomas Riemensperger, André Fiala, and Oren Schuldiner. 2018. "Developmental Coordination during Olfactory Circuit Remodeling in Drosophila." *Neuron* 99 (6): 1204-1215.e5. https://doi.org/10.1016/j.neuron.2018.07.050.

McGuire, S. E., P. T. Le, and R. L. Davis. 2001. "The Role of Drosophila Mushroom Body Signaling in Olfactory Memory." *Science* 293 (5533): 1330–33. https://doi.org/10.1126/science.1062622.

McGuire, Sean E., Phuong T. Le, Alexander J. Osborn, Kunihiro Matsumoto, and Ronald L. Davis. 2003. "Spatiotemporal Rescue of Memory Dysfunction in Drosophila." *Science* 302 (5651): 1765–68. https://doi.org/10.1126/science.1089035.

Meier, Matthias, and Alexander Borst. 2019. "Extreme Compartmentalization in a Drosophila Amacrine Cell." *Current Biology* 29 (9): 1545-1550.e2. https://doi.org/10.1016/J.CUB.2019.03.070.

1092 Mitchell, Simon J., and R. Angus Silver. 2003. "Shunting Inhibition Modulates
1093 Neuronal Gain during Synaptic Excitation." *Neuron* 38 (3): 433–45.
1094 https://doi.org/10.1016/S0896-6273(03)00200-9.
1095 Münch, Daniel, and C. Giovanni Galizia. 2016. "DoOR 2.0 - Comprehensive
1096 Mapping of Drosophila Melanogaster Odorant Responses." *Scientific Reports*
1097 *2016 6:1* 6 (1): 1–14. https://doi.org/10.1038/srep21841.
1098 Olsen, Shawn R., Vikas Bhandawat, and Rachel I. Wilson. 2010. "Divisive
1099 Normalization in Olfactory Population Codes." *Neuron* 66 (2): 287–99.
1100 https://doi.org/10.1016/j.neuron.2010.04.009.
1101 Olsen, Shawn R., and Rachel I. Wilson. 2008. "Lateral Presynaptic Inhibition
1102 Mediates Gain Control in an Olfactory Circuit." *Nature* 452 (7190): 956–60.
1103 https://doi.org/10.1038/nature06864.
1104 Olshausen, Bruno A., and David J. Field. 2004. "Sparse Coding of Sensory
1105 Inputs." *Current Opinion in Neurobiology* 14 (4): 481–87.
1106 https://doi.org/10.1016/j.conb.2004.07.007.
1107 Papadopoulou, Maria, Stijn Cassenaer, Thomas Nowotny, and Gilles Laurent.
1108 2011. "Normalization for Sparse Encoding of Odors by a Wide-Field
1109 Interneuron." *Science* 332 (6030): 721–25.
1110 https://doi.org/10.1126/science.1201835.
1111 Parnas, Moshe, Andrew C. Lin, Wolf Huetteroth, and Gero Miesenböck. 2013.
1112 "Odor Discrimination in Drosophila: From Neural Population Codes to
1113 Behavior." *Neuron* 79 (5): 932–44.
1114 https://doi.org/10.1016/J.NEURON.2013.08.006.
1115 Pech, Ulrike, Natalia H. Revelo, Katharina J. Seitz, Silvio O. Rizzoli, and André
1116 Fiala. 2015. "Optical Dissection of Experience-Dependent Pre- and

Postsynaptic Plasticity in the Drosophila Brain." *Cell Reports* 10 (12): 2084–96. https://doi.org/10.1016/j.celrep.2015.02.065.

Perez Vicente, C. J., and D. J. Amit. 1989. "Optimised Network for Sparsely Coded Patterns." *Journal of Physics A: General Physics* 22 (5): 559–69. https://doi.org/10.1088/0305-4470/22/5/018.

Perez-Orive, Javier, Ofer Mazor, Glenn C. Turner, Stijn Cassenaer, Rachel I. Wilson, and Gilles Laurent. 2002. "Oscillations and Sparsening of Odor Representations in the Mushroom Body." *Science* 297 (5580): 359–65. https://doi.org/10.1126/science.1070502.

Pitman, Jena L., Wolf Huetteroth, Christopher J. Burke, Michael J. Krashes, Sen Lin Lai, Tzumin Lee, and Scott Waddell. 2011. "A Pair of Inhibitory Neurons Are Required to Sustain Labile Memory in the Drosophila Mushroom Body." *Current Biology* 21 (10): 855–61. https://doi.org/10.1016/j.cub.2011.03.069.

Quiroga, R. Quian, L. Reddy, G. Kreiman, C. Koch, and I. Fried. 2005. "Invariant Visual Representation by Single Neurons in the Human Brain." *Nature* 435 (7045): 1102–7. https://doi.org/10.1038/nature03687.

Raji, Joshua I., and Christopher J. Potter. 2021. "The Number of Neurons in Drosophila and Mosquito Brains." *PLOS ONE* 16 (5): e0250381. https://doi.org/10.1371/JOURNAL.PONE.0250381.

Ray, Subhasis, Zane N. Aldworth, and Mark A. Stopfer. 2020. "Feedback Inhibition and Its Control in an Insect Olfactory Circuit." *ELife* 9 (March). https://doi.org/10.7554/ELIFE.53281.

1140 Roberts, Alan, Brian M. H. Bush, and Society for Experimental Biology (Great
1141 Britain). Neurobiology Group. 1981. "Neurones without Impulses : Their
1142 Significance for Vertebrate and Invertebrate Nervous Systems," 290.
1143 Rolls, E. T., and M. J. Tovee. 1995. "Sparseness of the Neuronal Representation
1144 of Stimuli in the Primate Temporal Visual Cortex." *Journal of*
1145 *Neurophysiology* 73 (2): 713–26.
1146 https://doi.org/10.1152/jn.1995.73.2.713.
1147 Sahay, Amar, Donald A. Wilson, and René Hen. 2011. "Pattern Separation: A
1148 Common Function for New Neurons in Hippocampus and Olfactory Bulb."
1149 *Neuron*. Cell Press. https://doi.org/10.1016/j.neuron.2011.05.012.
1150 Santoro, Adam. 2013. "Reassessing Pattern Separation in the Dentate Gyrus."
1151 *Frontiers in Behavioral Neuroscience* 0 (JUL): 96.
1152 https://doi.org/10.3389/FNBEH.2013.00096.
1153 Scheffer, Louis K, C Shan Xu, Michal Januszewski, Zhiyuan Lu, Shin-ya
1154 Takemura, Kenneth J Hayworth, Gary B Huang, et al. 2020. "A Connectome
1155 and Analysis of the Adult Drosophila Central Brain." *ELife* 9: 1–73.
1156 https://doi.org/10.7554/elife.57443.
1157 Schindelin, Johannes, Ignacio Arganda-Carreras, Erwin Frise, Verena Kaynig,
1158 Mark Longair, Tobias Pietzsch, Stephan Preibisch, et al. 2012. "Fiji: An
1159 Open-Source Platform for Biological-Image Analysis." *Nature Methods*.
1160 Nature Publishing Group. https://doi.org/10.1038/nmeth.2019.
1161 Schweighofer, N., K. Doya, and F. Lay. 2001. "Unsupervised Learning of
1162 Granule Cell Sparse Codes Enhances Cerebellar Adaptive Control."
1163 *Neuroscience* 103 (1): 35–50. https://doi.org/10.1016/S0306-
1164 4522(00)00548-0.

Spruston, Nelson, Greg Stuart, and Michael Häusser. 2016. "Principles of Dendritic Integration."

Stocker, R. F., M. C. Lienhard, A. Borst, and K. F. Fischbach. 1990. "Neuronal Architecture of the Antennal Lobe in Drosophila Melanogaster." *Cell and Tissue Research* 262 (1): 9–34. https://doi.org/10.1007/BF00327741.

Stocker, Reinhard F., Gertrud Heimbeck, Nanaë Gendre, and J. Steven de Belle. 1997. "Neuroblast Ablation in Drosophila P[GAL4] Lines Reveals Origins of Olfactory Interneurons." *Journal of Neurobiology* 32 (5): 443–56. https://doi.org/10.1002/(SICI)1097-4695(199705)32:5<443::AID-NEU1>3.0.CO;2-5.

Sweeney, Sean T., Kendal Broadie, John Keane, Heiner Niemann, and Cahir J. O'Kane. 1995. "Targeted Expression of Tetanus Toxin Light Chain in Drosophila Specifically Eliminates Synaptic Transmission and Causes Behavioral Defects." *Neuron* 14 (2): 341–51. https://doi.org/10.1016/0896-6273(95)90290-2.

Tabuchi, Sawako, Jesse I. Gilmer, Karen Purba, and Abigail L. Person. 2019. "Pathway-Specific Drive of Cerebellar Golgi Cells Reveals Integrative Rules of Cortical Inhibition." *Journal of Neuroscience* 39 (7): 1169–81. https://doi.org/10.1523/JNEUROSCI.1448-18.2018.

Tseng, Qingzong, Eve Duchemin-Pelletier, Alexandre Deshiere, Martial Balland, Hervé Guilloud, Odile Filhol, and Manuel Théry. 2012. "Spatial Organization of the Extracellular Matrix Regulates Cell-Cell Junction Positioning." *Proceedings of the National Academy of Sciences of the United States of America* 109 (5): 1506–11. https://doi.org/10.1073/pnas.1106377109.

1189 Tsodyks, M. v., and M. v. Feigel'man. 1988. "The Enhanced Storage Capacity in
1190 Neural Networks with Low Activity Level." *EPL* 6 (2): 101–5.
1191 https://doi.org/10.1209/0295-5075/6/2/002.
1192 Turner, Glenn C., Maxim Bazhenov, and Gilles Laurent. 2008. "Olfactory
1193 Representations by Drosophila Mushroom Body Neurons." *Journal of*
1194 *Neurophysiology* 99 (2): 734–46. https://doi.org/10.1152/jn.01283.2007.
1195 Tyrrell, T., and D. Willshaw. 1992. "Cerebellar Cortex: Its Simulation and the
1196 Relevance of Marr's Theory." *Philosophical Transactions of the Royal Society*
1197 *of London. Series B, Biological Sciences* 336 (1277): 239–57.
1198 https://doi.org/10.1098/rstb.1992.0059.
1199 Vinje, William E., and Jack L. Gallant. 2000. "Sparse Coding and Decorrelation
1200 in Primary Visual Cortex during Natural Vision." *Science* 287 (5456): 1273–
1201 76. https://doi.org/10.1126/science.287.5456.1273.
1202 Vos, Bart P., Antonia Volny-Luraghi, and Erik de Schutter. 1999. "Cerebellar
1203 Golgi Cells in the Rat: Receptive Fields and Timing of Responses to Facial
1204 Stimulation." *European Journal of Neuroscience* 11 (8): 2621–34.
1205 https://doi.org/10.1046/j.1460-9568.1999.00678.x.
1206 Vosshall, Leslie B., Allan M. Wong, and Richard Axel. 2000. "An Olfactory
1207 Sensory Map in the Fly Brain." *Cell* 102 (2): 147–59.
1208 https://doi.org/10.1016/S0092-8674(00)00021-0.
1209 Wang, Guangxia, Bangyu Zhou, Shengxiong Wang, Kai Yang, Jianjian Zhao,
1210 Xing Yang, Yiming Li, and Lijun Shen. 2019. "The Reconstruction and
1211 Functional Mapping of a Recurrent Microcircuit in Drosophila Mushroom
1212 Body." *BioRxiv*, December, 819227. https://doi.org/10.1101/819227.

Wu, Chia Lin, Meng Fu Maxwell Shih, Pei Tseng Lee, and Ann Shyn Chiang. 2013. "An Octopamine-Mushroom Body Circuit Modulates the Formation of Anesthesia-Resistant Memory in Drosophila." *Current Biology* 23 (23): 2346–54. https://doi.org/10.1016/j.cub.2013.09.056.

Yasuyama, Kouji, Ian A. Meinertzhagen, and Friedrich-Wilhelm Schürmann. 2002a. "Synaptic Organization of the Mushroom Body Calyx in *Drosophila Melanogaster*." *Journal of Comparative Neurology* 445 (3): 211–26. https://doi.org/10.1002/cne.10155.

———. 2002b. "Synaptic Organization of the Mushroom Body Calyx in *Drosophila Melanogaster*." *Journal of Comparative Neurology* 445 (3): 211–26. https://doi.org/10.1002/cne.10155.

Zheng, Zhihao, J. Scott Lauritzen, Eric Perlman, Camenzind G. Robinson, Matthew Nichols, Daniel Milkie, Omar Torrens, et al. 2018. "A Complete Electron Microscopy Volume of the Brain of Adult Drosophila Melanogaster." *Cell* 174 (3): 730-743.e22. https://doi.org/10.1016/j.cell.2018.06.019.

Zheng, Zhihao, Feng Li, Corey Fisher, Iqbal Ali, Nadiya Sharifi, Steven Calle-Schuler, Joseph Hsu, et al. 2020. "Structured Sampling of Olfactory Input by the Fly Mushroom Body." *BioRxiv*, April, 2020.04.17.047167. https://doi.org/10.1101/2020.04.17.047167.

3.4 Summary

In this project, we focused on the inhibitory synapses provided by the APL neuron to MGs of the calyx and their role in supporting sparse odour representations at the KC layer. Via analysis of publicly available *Drosophila* whole brain connectomes (Scheffer et al., 2020a; Zheng et al., 2018), we showed that APL is highly involved in the microglomerular structure with reciprocal connections to both PN boutons and KC claws. Moreover, we found a positive correlation between the weight of APL synapses to either boutons or claws and the ones that the APL receives from these very same cells, suggesting an equilibrium between activation and inhibition in calycal microcircuits.

To clarify the role of inhibitory synapses on MGs, we performed *in vivo* calcium imaging experiments and showed that the APL response to odours varies among different stimuli and scales with the intensity of the response at the input population, the PNs. Nevertheless, postsynaptic odour-evoked activity measured in KC dendrites within MGs were more homogeneous in magnitude across odours, suggesting that APL might restrain part of the variability coming from the presynaptic PN boutons via proportional feed-forward inhibition. APL has been mainly described as a feedback neuron thus far (A. C. Lin et al. 2014; Lei et al. 2013; Amin et al. 2020), however, feedforward inhibition from the input population onto the next layer has been observed in other networks performing pattern separation such as the cerebellar granule layer (Cesana et al., 2013; Duguid et al., 2015; Kanichay & Silver, 2008; Tabuchi et al., 2019; Vos et al., 1999) and theorized in realistic computational models of insect´s mushroom bodies (Assisi et al., 2007; Luo et al., 2010).

We confirmed our hypothesis of APL normalizing dendritic claws activity by blocking APL output, which led to stronger and more variable responses in KC dendrites. Finally, volumetric calcium imaging showed that the APL inhibition is local within the MB calyx, similarly to what has been described in the *Drosophila* MB (Amin et al., 2020; G. Wang et al., 2019) as well as

in the APL´s homolog GGN in the locust (Leitch & Laurent, 1996; Ray et al., 2020). This finding is in line with the notion that local microcircuits allow even a single neuron to mimic the activity of several inhibitory interneurons, as described in both mammals and insects (Grimes et al., 2010; Meier & Borst, 2019). Additionally, localized inhibition is suggested to expand the dynamic range of inputs able to activate KCs (Ray et al., 2020).

In conclusion, we speculate that this localized, proportional APL inhibition makes KCs inputs integration combinatorial rather than strength-dependent, ensuring that KCs require the coactivation of multiple dendritic inputs in order to spike action potentials (Gruntman & Turner, 2013; Inada et al., 2017) and in turn maintaining KC odour representations sparse (Turner et al., 2008a). Hence, our analysis provides insights into how inhibition shapes sensory representations and assists stimuli discrimination in a brain region known to perform pattern separation.

4 Conclusion

The aim of this thesis was to understand how sensory information, in particular odours, are efficiently represented and discriminated in the brain and how these representations are then used to form and consolidate memories related to them.

Using *Drosophila melanogaster* as a model, I tackled both questions by investigating the structure and function of a neuropil known to participate in both stimuli representation and associative memory formation processes, the mushroom body (MB). In particular, I focused on the input region of the MB, the main calyx, where olfactory projection neurons (PNs) deliver sensory input to the intrinsic cells of the MB (Kenyon cells, KCs) via synaptic complexes known as microglomeruli (MGs). My attention to these synaptic microcircuits was driven by two main factors. First, the organization of the MGs supports the transformation of highly overlapping odour representations at the PN layer into sparse, decorrelated representations in KCs. However, the detailed mechanisms by which this is achieved are not known yet. Second, in the context of learning and memory formation the major attention has been paid to the MB output synapses. Nevertheless, several indications suggest that plasticity at the input synapses of the MB might play a role in memory consolidation as well.

Indeed, in chapter 2 of this thesis I show that after long term memory formation, the MGs specifically representing the stimulus used in the behavioural paradigm undergo structural changes. In particular, long-term memory formation led to an increase in the number of functional MGs, hence modifying the stimulus representation at the input region of the MB. The causality between memory formation and structural changes was also confirmed, as mutant flies known to be unable to form long-term memories did not show any conformational changes when subjected to the same behavioural paradigm. In the future, it will be interesting to test whether these additional MGs lead to the recruitment of new KCs in the odour representation, hence modifying the stimulus "code", or if the KC involved

are the same but their activation is somehow facilitated by additional inputs from the PNs. Taken together, in this chapter I reported stimulus-specific experience-induced structural modifications in a brain region fundamental for learning and memory.

In chapter 3, I focused on the aspect of stimuli representation in the calyx, and investigated the role of inhibitory synapses by the anterior paired lateral neuron (APL) on the microglomerular structures. First of all, I have found that the APL is highly involved in the majority of the MG complexes within the calyx, with synapses whose weight is proportional to the excitatory input of each MG. Second, by *in vivo* calcium imaging, I showed that APL normalizes odour-evoked activity in postsynaptic claws of the MGs by providing a local, feed-forward inhibition that scales with the PN input strength. Feedforward loops were not found in the MB calyx yet, though they have been described in homologous networks in other organisms such as rodents and humans. My hypothesis is that normalization of KC claws responses assists sparse odours representations by limiting the range of activation of each claw. In other words, APL ensures that a single strongly active claw will not be able to drive KC spikes, thereby allowing KCs to fire only when multiple claws are co-active. This hypothesis is confirmed by the fact that odour representations are not sparse in the absence of APL, and flies performs poorly compared to controls in an odour discrimination behavioural assay.

Taken together, in this thesis I have described two unknown features of sensory information processing at the level of MGs of the calyx. These data are of great value, as the input region of the mushroom body is often overlooked and thought as a rather passive synaptic layer. More generally, these data can be used to update current models of sensory processing and memory formation in the brain, and will bring us one step closer understanding how the brain is able to perform such complicated tasks.

5 References

Albus, J. S. (1971). A theory of cerebellar function. *Mathematical Biosciences*, *10*(1–2), 25–61. https://doi.org/10.1016/0025-5564(71)90051-4

Alivisatos, A. P., Chun, M., Church, G. M., Greenspan, R. J., Roukes, M. L., & Yuste, R. (2012). The Brain Activity Map Project and the Challenge of Functional Connectomics. In *Neuron* (Vol. 74, Issue 6, pp. 970–974). Cell Press. https://doi.org/10.1016/j.neuron.2012.06.006

ALTMAN, & J. (1997). Development of the Cerebellar System. *Relation to Its Evolution, Structure, and Functions.* https://ci.nii.ac.jp/naid/10006165950

Amin, H., Apostolopoulou, A. A., Suárez-Grimalt, R., Vrontou, E., & Lin, A. C. (2020). Localized inhibition in the Drosophila mushroom body. *ELife*, *9*, 1–31. https://doi.org/10.7554/elife.56954

Apps, R., & Garwicz, M. (2005). Anatomical and physiological foundations of cerebellar information processing. *Nature Reviews Neuroscience 2005 6:4*, *6*(4), 297–311. https://doi.org/10.1038/nrn1646

Arenz, A., Silver, R. A., Schaefer, A. T., & Margrie, T. W. (2008). The contribution of single synapses to sensory representation in vivo. *Science*, *321*(5891), 977–980. https://doi.org/10.1126/SCIENCE.1158391

Asahina, K., Louis, M., Piccinotti, S., & Vosshall, L. B. (2009). A circuit supporting concentration-invariant odor perception in Drosophila. *Journal of Biology 2009 8:1*, *8*(1), 1–19. https://doi.org/10.1186/JBIOL108

Aso, Y., Grübel, K., Busch, S., Friedrich, A. B., Siwanowicz, I., & Tanimoto, H. (2009). The Mushroom Body of Adult *Drosophila* Characterized by GAL4 Drivers. *Journal of Neurogenetics*, *23*(1–2), 156–172. https://doi.org/10.1080/01677060802471718

Aso, Y., Hattori, D., Yu, Y., Johnston, R. M., Iyer, N. A., Ngo, T. T. B., Dionne, H., Abbott, L. F., Axel, R., Tanimoto, H., & Rubin, G. M. (2014).

The neuronal architecture of the mushroom body provides a logic for associative learning. *ELife*, *3*, e04577. https://doi.org/10.7554/eLife.04577

Aso, Y., Sitaraman, D., Ichinose, T., Kaun, K. R., Vogt, K., Belliart-Guérin, G., Plaçais, P. Y., Robie, A. A., Yamagata, N., Schnaitmann, C., Rowell, W. J., Johnston, R. M., Ngo, T. T. B., Chen, N., Korff, W., Nitabach, M. N., Heberlein, U., Preat, T., Branson, K. M., … Rubin, G. M. (2014). Mushroom body output neurons encode valence and guide memory-based action selection in Drosophila. *ELife*, *3*, e04580. https://doi.org/10.7554/ELIFE.04580

Assisi, C., Stopfer, M., Laurent, G., & Bazhenov, M. (2007). Adaptive regulation of sparseness by feedforward inhibition. *Nature Neuroscience*, *10*(9), 1176–1184. https://doi.org/10.1038/nn1947

Babadi, B., & Sompolinsky, H. (2014). Sparseness and Expansion in Sensory Representations. *Neuron*, *83*(5), 1213–1226. https://doi.org/10.1016/j.neuron.2014.07.035

Bailey, C. H., & Chen, M. (1983). Morphological basis of long-term habituation and sensitization in aplysia. *Science*, *220*(4592), 91–93. https://doi.org/10.1126/SCIENCE.6828885

Baltruschat, L., Prisco, L., Ranft, P., Lauritzen, J. S., Fiala, A., Bock, D. D., & Tavosanis, G. (2021). Circuit reorganization in the Drosophila mushroom body calyx accompanies memory consolidation. *Cell Reports*, *34*(11), 108871. https://doi.org/10.1016/j.celrep.2021.108871

Bargmann, C. I. (2006). Comparative chemosensation from receptors to ecology. *Nature 2006 444:7117*, *444*(7117), 295–301. https://doi.org/10.1038/nature05402

Bates, A. S., Schlegel, P., Roberts, R. J. V., Drummond, N., Tamimi, I. F. M., Turnbull, R., Zhao, X., Marin, E. C., Popovici, P. D., Dhawan, S., Jamasb, A., Javier, A., Serratosa Capdevila, L., Li, F., Rubin, G. M., Waddell, S., Bock, D. D., Costa, M., & Jefferis, G. S. X. E. (2020). Complete Connectomic Reconstruction of Olfactory Projection Neurons

in the Fly Brain. *Current Biology*, *30*(16), 3183-3199.e6. https://doi.org/10.1016/j.cub.2020.06.042

Bello, B., Reséndez-Pérez, D., & Gehring, W. (1998). Spatial and temporal targeting of gene expression in Drosophila by means of a tetracycline-dependent transactivator system. *Undefined*.

Benton, R., Vannice, K. S., Gomez-Diaz, C., & Vosshall, L. B. (2009). Variant Ionotropic Glutamate Receptors as Chemosensory Receptors in Drosophila. *Cell*, *136*(1), 149–162. https://doi.org/10.1016/J.CELL.2008.12.001

Berridge, M. J. (1998). Neuronal Calcium Signaling. *Neuron*, *21*(1), 13–26. https://doi.org/10.1016/S0896-6273(00)80510-3

Bhandawat, V., Olsen, S. R., Gouwens, N. W., Schlief, M. L., & Wilson, R. I. (2007). Sensory processing in the Drosophila antennal lobe increases reliability and separability of ensemble odor representations. *Nature Neuroscience*, *10*(11), 1474–1482. https://doi.org/10.1038/nn1976

Billings, G., Piasini, E., Lorincz, A., Nusser, Z., & Silver, R. A. (2014). Network Structure within the Cerebellar Input Layer Enables Lossless Sparse Encoding. *Neuron*, *83*(4), 960–974. https://doi.org/10.1016/j.neuron.2014.07.020

Brand, A. H., & Perrimon, N. (1993). Targeted gene expression as a means of altering cell fates and generating dominant phenotypes. *Development*, *118*(2), 401–415. https://doi.org/10.1242/DEV.118.2.401

Brent, R., & Ptashne, M. (1985). A eukaryotic transcriptional activator bearing the DNA specificity of a prokaryotic repressor. *Cell*, *43*(3), 729–736. https://doi.org/10.1016/0092-8674(85)90246-6

Briggman, K. L., & Bock, D. D. (2012). Volume electron microscopy for neuronal circuit reconstruction. *Current Opinion in Neurobiology*, *22*(1), 154–161. https://doi.org/10.1016/J.CONB.2011.10.022

Brodal, A., & Kawamura, K. (1980). *The Olivocerebellar Projection*. 9–80. https://doi.org/10.1007/978-3-642-67775-5_3

Brooks, J. X., Carriot, J., & Cullen, K. E. (2015). Learning to expect the unexpected: rapid updating in primate cerebellum during voluntary self-motion. *Nature Neuroscience 2015 18:9*, *18*(9), 1310–1317. https://doi.org/10.1038/nn.4077

Bruyne, M. de, Clyne, P. J., & Carlson, J. R. (1999). Odor Coding in a Model Olfactory Organ: TheDrosophila Maxillary Palp. *Journal of Neuroscience*, *19*(11), 4520–4532. https://doi.org/10.1523/JNEUROSCI.19-11-04520.1999

Buckner, R. L. (2013). The Cerebellum and Cognitive Function: 25 Years of Insight from Anatomy and Neuroimaging. *Neuron*, *80*(3), 807–815. https://doi.org/10.1016/J.NEURON.2013.10.044

Butcher, N. J., Friedrich, A. B., Lu, Z., Tanimoto, H., & Meinertzhagen, I. A. (2012). Different classes of input and output neurons reveal new features in microglomeruli of the adult Drosophila mushroom body calyx. *Journal of Comparative Neurology*, *520*(10), 2185–2201. https://doi.org/10.1002/cne.23037

C H Bailey, and, & Kandel, E. R. (2003). Structural Changes Accompanying Memory Storage. *Http://Dx.Doi.Org/10.1146/Annurev.Ph.55.030193.002145*, *55*, 397–426. https://doi.org/10.1146/ANNUREV.PH.55.030193.002145

Cajal, S. R. y, & Ramón y Cajal, S. (1909). Histologie du système nerveux de l'homme & des vertébrés. In *Histologie du système nerveux de l'homme & des vertébrés.* Maloine,. https://doi.org/10.5962/bhl.title.48637

Campbell, R. A. A., Honegger, K. S., Qin, H., Li, W., Demir, E., & Turner, G. C. (2013). Imaging a population code for odor identity in the Drosophila mushroom body. *Journal of Neuroscience*, *33*(25), 10568–10581. https://doi.org/10.1523/JNEUROSCI.0682-12.2013

Cayco-Gajic, N. A., Clopath, C., & Silver, R. A. (2017). Sparse synaptic connectivity is required for decorrelation and pattern separation in feedforward networks. *Nature Communications*, *8*(1), 1–11. https://doi.org/10.1038/s41467-017-01109-y

Cayco-Gajic, N. A., & Silver, R. A. (2019). Re-evaluating Circuit Mechanisms Underlying Pattern Separation. *Neuron*, *101*(4), 584–602. https://doi.org/10.1016/j.neuron.2019.01.044

Cesana, E., Pietrajtis, K., Bidoret, C., Isope, P., D'Angelo, E., Dieudonné, S., & Forti, L. (2013). Granule cell ascending axon excitatory synapses onto Golgi cells implement a potent feedback circuit in the cerebellar granular layer. *Journal of Neuroscience*, *33*(30), 12430–12446. https://doi.org/10.1523/JNEUROSCI.4897-11.2013

Chang, F. L. F., & Greenough, W. T. (1984). Transient and enduring morphological correlates of synaptic activity and efficacy change in the rat hippocampal slice. *Brain Research*, *309*(1), 35–46. https://doi.org/10.1016/0006-8993(84)91008-4

Chen, T. W., Wardill, T. J., Sun, Y., Pulver, S. R., Renninger, S. L., Baohan, A., Schreiter, E. R., Kerr, R. A., Orger, M. B., Jayaraman, V., Looger, L. L., Svoboda, K., & Kim, D. S. (2013). Ultrasensitive fluorescent proteins for imaging neuronal activity. *Nature*, *499*(7458), 295–300. https://doi.org/10.1038/nature12354

Clements, J., Dolafi, T., Umayam, L., Neubarth, N. L., Berg, S., Scheffer, L. K., & Plaza, S. M. (2020). NeuPrint: Analysis Tools for EM Connectomics. In *bioRxiv* (p. 2020.01.16.909465). bioRxiv. https://doi.org/10.1101/2020.01.16.909465

Clyne, P. J., Warr, C. G., Freeman, M. R., Lessing, D., Kim, J., & Carlson, J. R. (1999). A novel family of divergent seven-transmembrane proteins: Candidate odorant receptors in Drosophila. *Neuron*, *22*(2), 327–338. https://doi.org/10.1016/S0896-6273(00)81093-4

Couto, A., Alenius, M., & Dickson, B. J. (2005). Molecular, Anatomical, and Functional Organization of the Drosophila Olfactory System. *Current Biology*, *15*(17), 1535–1547. https://doi.org/10.1016/J.CUB.2005.07.034

Davis, R. L. (2011). Traces of Drosophila Memory. *Neuron*, *70*(1), 8–19. https://doi.org/10.1016/J.NEURON.2011.03.012

de Belle, J. S., & Heisenberg, M. (1994). Associative odor learning in Drosophila abolished by chemical ablation of mushroom bodies. *Science*, *263*(5147), 692–695. https://doi.org/10.1126/science.8303280

Delestro, F., Scheunemann, L., Pedrazzani, M., Tchenio, P., Preat, T., & Genovesio, A. (2020). In vivo large-scale analysis of Drosophila neuronal calcium traces by automated tracking of single somata. *Scientific Reports*, *10*(1), 1–14. https://doi.org/10.1038/s41598-020-64060-x

Desmond, N. L., & Levy, W. B. (1983). Synaptic correlates of associative potentiation/depression: an ultrastructural study in the hippocampus. *Brain Research*, *265*(1), 21–30. https://doi.org/10.1016/0006-8993(83)91329-X

Ding, H., Smith, R. G., Poleg-Polsky, A., Diamond, J. S., & Briggman, K. L. (2016). Species-specific wiring for direction selectivity in the mammalian retina. *Nature 2016 535:7610*, *535*(7610), 105–110. https://doi.org/10.1038/nature18609

Dubnau, J., Grady, L., Kitamoto, T., & Tully, T. (2001). Disruption of neurotransmission in Drosophila mushroom body blocks retrieval but not acquisition of memory. *Nature*, *411*(6836), 476–480. https://doi.org/10.1038/35078077

Duguid, I., Branco, T., Chadderton, P., Arlt, C., Powell, K., & Häusser, M. (2015). Control of cerebellar granule cell output by sensory-evoked Golgi cell inhibition. *Proceedings of the National Academy of Sciences of the United States of America*, *112*(42), 13099–13104. https://doi.org/10.1073/pnas.1510249112

Durst, C., Eichmüller, S., & Menzel, R. (1994). Development and experience lead to increased volume of subcompartments of the honeybee mushroom body. *Behavioral and Neural Biology*, *62*(3), 259–263. https://doi.org/10.1016/S0163-1047(05)80025-1

Eccles, J. C., Llinás, R., & Sasaki, K. (1966). The mossy fibre-granule cell relay of the cerebellum and its inhibitory control by Golgi cells.

Experimental Brain Research 1966 1:1, *1*(1), 82–101. https://doi.org/10.1007/BF00235211

Engert, F., & Bonhoeffer, T. (1999). Dendritic spine changes associated with hippocampal long-term synaptic plasticity. *Nature 1999 399:6731*, *399*(6731), 66–70. https://doi.org/10.1038/19978

Esther A. Nimchinsky, Bernardo L. Sabatini, and, & Svoboda, K. (2003). Structure and Function of Dendritic Spines. *Http://Dx.Doi.Org/10.1146/Annurev.Physiol.64.081501.160008*, *64*, 313–353. https://doi.org/10.1146/ANNUREV.PHYSIOL.64.081501.160008

Falibene, A., Roces, F., & Rössler, W. (2015). Long-term avoidance memory formation is associated with a transient increase in mushroom body synaptic complexes in leaf-cutting ants. *Frontiers in Behavioral Neuroscience*, *0*(APR), 84. https://doi.org/10.3389/FNBEH.2015.00084

Fiala, A., Spall, T., Diegelmann, S., Eisermann, B., Sachse, S., Devaud, J. M., Buchner, E., & Galizia, C. G. (2002). Genetically Expressed Cameleon in Drosophila melanogaster Is Used to Visualize Olfactory Information in Projection Neurons. *Current Biology*, *12*(21), 1877–1884. https://doi.org/10.1016/S0960-9822(02)01239-3

Frank, D. D., Jouandet, G. C., Kearney, P. J., Macpherson, L. J., & Gallio, M. (2015). Temperature representation in the Drosophila brain. *Nature 2015 519:7543*, *519*(7543), 358–361. https://doi.org/10.1038/nature14284

French, A. S., Torkkeli, P. H., & Schuckel, J. (2011). Dynamic Characterization of Drosophila Antennal Olfactory Neurons Indicates Multiple Opponent Signaling Pathways in Odor Discrimination. *Journal of Neuroscience*, *31*(3), 861–869. https://doi.org/10.1523/JNEUROSCI.5243-10.2011

Gao, Q., Yuan, B., & Chess, A. (2000). Convergent projections of Drosophila olfactory neurons to specific glomeruli in the antennal lobe. *Nature Neuroscience*, *3*(8), 780–785. https://doi.org/10.1038/77680

Geinisman, Y., Berry, R. W., Disterhoft, J. F., Power, J. M., & Zee, E. A. van der. (2001). Associative Learning Elicits the Formation of Multiple-Synapse Boutons. *Journal of Neuroscience*, *21*(15), 5568–5573. https://doi.org/10.1523/JNEUROSCI.21-15-05568.2001

Gilmer, J. I., & Person, A. L. (2018). Theoretically Sparse, Empirically Dense: New Views on Cerebellar Granule Cells. *Trends in Neurosciences*, *41*(12), 874–877. https://doi.org/10.1016/J.TINS.2018.09.013

Glanzman, D. L., Kandel, E. R., & Schacher, S. (1990). Target-dependent structural changes accompanying long-term synaptic facilitation in Aplysia neurons. *Science*, *249*(4970), 799–802. https://doi.org/10.1126/SCIENCE.2389145

Grabe, V., Baschwitz, A., Dweck, H. K. M., Lavista-Llanos, S., Hansson, B. S., & Sachse, S. (2016). Elucidating the Neuronal Architecture of Olfactory Glomeruli in the Drosophila Antennal Lobe. *Cell Reports*, *16*(12), 3401–3413. https://doi.org/10.1016/J.CELREP.2016.08.063

Grimes, W. N., Zhang, J., Graydon, C. W., Kachar, B., & Diamond, J. S. (2010). Retinal Parallel Processors: More than 100 Independent Microcircuits Operate within a Single Interneuron. *Neuron*, *65*(6), 873–885. https://doi.org/10.1016/J.NEURON.2010.02.028

Groh, C., Lu, Z., Meinertzhagen, I. A., R€, W., & Library, W. O. (2012). Age-Related Plasticity in the Synaptic Ultrastructure of Neurons in the Mushroom Body Calyx of the Adult Honeybee Apis mellifera. *The Journal of Comparative Neurology | Research in Systems Neuroscience*, *520*, 3509–3527. https://doi.org/10.1002/cne.23102

Groh, C., & Rössler, W. (2014). *Environment-and Age-Dependent Plasticity of Synaptic Complexes in the Mushroom Bodies of Honeybee Queens Mushroom Body Microglomeruli View project Neuroethology of insect orientation behavior View project*. https://doi.org/10.1159/000092309

Gruntman, E., & Turner, G. C. (2013). Integration of the olfactory code across dendritic claws of single mushroom body neurons. *Nature Neuroscience*, *16*(12), 1821–1829. https://doi.org/10.1038/nn.3547

Hahnloser, R. H. R., Kozhevnikov, A. A., & Fee, M. S. (2002). An ultra-sparse code underlies the generation of neural sequences in a songbird. *Nature*, *419*(6902), 65–70. https://doi.org/10.1038/nature00974

Hallem, E. A., & Carlson, J. R. (2006a). Coding of Odors by a Receptor Repertoire. *Cell*, *125*(1), 143–160. https://doi.org/10.1016/j.cell.2006.01.050

Hallem, E. A., & Carlson, J. R. (2006b). Coding of Odors by a Receptor Repertoire. *Cell*, *125*(1), 143–160. https://doi.org/10.1016/J.CELL.2006.01.050

Hámori, J., & Somogyi, J. (1983). Differentiation of cerebellar mossy fiber synapses in the rat: A quantitative electron microscope study. *Journal of Comparative Neurology*, *220*(4), 365–377. https://doi.org/10.1002/CNE.902200402

Han, P. L., Levin, L. R., Reed, R. R., & Davis, R. L. (1992). Preferential expression of the drosophila rutabaga gene in mushroom bodies, neural centers for learning in insects. *Neuron*, *9*(4), 619–627. https://doi.org/10.1016/0896-6273(92)90026-A

Harvey, R. J., & Napper, R. M. A. (1991). Quantitatives studies on the mammalian cerebellum. *Progress in Neurobiology*, *36*(6), 437–463. https://doi.org/10.1016/0301-0082(91)90012-P

Hayashi-Takagi, A., Yagishita, S., Nakamura, M., Shirai, F., Wu, Y. I., Loshbaugh, A. L., Kuhlman, B., Hahn, K. M., & Kasai, H. (2015). Labelling and optical erasure of synaptic memory traces in the motor cortex. *Nature 2015 525:7569*, *525*(7569), 333–338. https://doi.org/10.1038/nature15257

Heisenberg, M. (2003). Mushroom body memoir: From maps to models. *Nature Reviews Neuroscience*, *4*(4), 266–275. https://doi.org/10.1038/nrn1074

Heisenberg, M., Borst, A., Wagner, S., & Byers, D. (1985). drosophila mushroom body mutants are deficient in olfactory learning: Research papers. *Journal of Neurogenetics*, *2*(1), 1–30. https://doi.org/10.3109/01677068509100140

Herculano-Houzel, S. (2010). Coordinated scaling of cortical and cerebellar numbers of neurons. *Frontiers in Neuroanatomy*, *0*(MARCH), 12. https://doi.org/10.3389/FNANA.2010.00012

Hige, T., Aso, Y., Rubin, G. M., & Turner, G. C. (2015). Plasticity-driven individualization of olfactory coding in mushroom body output neurons. *Nature*, *526*(7572), 258–262. https://doi.org/10.1038/nature15396

Hodos, W. (2009). Evolution of Cerebellum. *Encyclopedia of Neuroscience*, 1240–1243. https://doi.org/10.1007/978-3-540-29678-2_3124

Hourcade, B., Muenz, T. S., Sandoz, J.-C., Rössler, W., & Devaud, J.-M. (2010). Long-Term Memory Leads to Synaptic Reorganization in the Mushroom Bodies: A Memory Trace in the Insect Brain? *Journal of Neuroscience*, *30*(18), 6461–6465. https://doi.org/10.1523/JNEUROSCI.0841-10.2010

Hromádka, T., DeWeese, M. R., & Zador, A. M. (2008). Sparse Representation of Sounds in the Unanesthetized Auditory Cortex. *PLOS Biology*, *6*(1), e16. https://doi.org/10.1371/JOURNAL.PBIO.0060016

Huerta, R., Nowotny, T., García-Sanchez, M., Abarbanel, H. D. I., & Rabinovich, M. I. (2004). Learning classification in the olfactory system of insects. *Neural Computation*, *16*(8), 1601–1640. https://doi.org/10.1162/089976604774201613

Inada, K., Tsuchimoto, Y., & Kazama, H. (2017). Origins of Cell-Type-Specific Olfactory Processing in the Drosophila Mushroom Body Circuit. *Neuron*, *95*(2), 357-367.e4. https://doi.org/10.1016/j.neuron.2017.06.039

Isaacson, J. S. (2010). Odor representations in mammalian cortical circuits. *Current Opinion in Neurobiology*, *20*(3), 328–331. https://doi.org/10.1016/J.CONB.2010.02.004

Jarrell, T. A., Wang, Y., Bloniarz, A. E., Brittin, C. A., Xu, M., Thomson, J. N., Albertson, D. G., Hall, D. H., & Emmons, S. W. (2012). The connectome of a decision-making neural network. *Science*, *337*(6093), 437–444. https://doi.org/10.1126/SCIENCE.1221762

Jortner, R. A., Farivar, S. S., & Laurent, G. (2007). A simple connectivity scheme for sparse coding in an olfactory system. *Journal of Neuroscience*, *27*(7), 1659–1669. https://doi.org/10.1523/JNEUROSCI.4171-06.2007

Kanerva, P. (1988). *Sparse Distributed Memory A study of psychologically driven storage*. https://books.google.com/books?hl=it&lr=&id=I9tCr21-s-AC&oi=fnd&pg=PR11&dq=(1988)+Sparse+distributed+memory+(MIT,+Cambridge,+MA).&ots=QVtRYKxuLE&sig=lPrh_ybrezYEvJeWkt2-Ot4Pa8Q

Kanichay, R. T., & Silver, R. A. (2008). Synaptic and cellular properties of the feedforward inhibitory circuit within the input layer of the cerebellar cortex. *Journal of Neuroscience*, *28*(36), 8955–8967. https://doi.org/10.1523/JNEUROSCI.5469-07.2008

Kasthuri, N., Hayworth, K. J., Berger, D. R., Schalek, R. L., Conchello, J. A., Knowles-Barley, S., Lee, D., Vázquez-Reina, A., Kaynig, V., Jones, T. R., Roberts, M., Morgan, J. L., Tapia, J. C., Seung, H. S., Roncal, W. G., Vogelstein, J. T., Burns, R., Sussman, D. L., Priebe, C. E., … Lichtman, J. W. (2015). Saturated Reconstruction of a Volume of Neocortex. *Cell*, *162*(3), 648–661. https://doi.org/10.1016/J.CELL.2015.06.054

Kawato, M., Ohmae, S., Hoang, H., & Sanger, T. (2021). 50 Years Since the Marr, Ito, and Albus Models of the Cerebellum. *Neuroscience*, *462*, 151–174. https://doi.org/10.1016/J.NEUROSCIENCE.2020.06.019

Keene, A. C., & Waddell, S. (2007). Drosophila olfactory memory: single genes to complex neural circuits. *Nature Reviews Neuroscience 2007 8:5*, *8*(5), 341–354. https://doi.org/10.1038/nrn2098

Kremer, M. C., Christiansen, F., Leiss, F., Paehler, M., Knapek, S., Andlauer, T. F. M., Förstner, F., Kloppenburg, P., Sigrist, S. J., & Tavosanis, G. (2010). Structural long-term changes at mushroom body input synapses. *Current Biology*, *20*(21), 1938–1944. https://doi.org/10.1016/j.cub.2010.09.060

Kühn-Bühlmann, S., & Wehner, R. (2006). Age-dependent and task-related volume changes in the mushroom bodies of visually guided desert ants, Cataglyphis bicolor. *Journal of Neurobiology*, *66*(6), 511–521. https://doi.org/10.1002/NEU.20235

Larsson, M. C., Domingos, A. I., Jones, W. D., Chiappe, M. E., Amrein, H., & Vosshall, L. B. (2004). Or83b Encodes a Broadly Expressed Odorant Receptor Essential for Drosophila Olfaction. *Neuron*, *43*(5), 703–714. https://doi.org/10.1016/J.NEURON.2004.08.019

Laurent, G. (2002). Olfactory network dynamics and the coding of multidimensional signals. *Nature Reviews Neuroscience*, *3*(11), 884–895. https://doi.org/10.1038/nrn964

Lee, K. S., Schottler, F., Oliver, M., & Lynch, G. (1980). Brief bursts of high-frequency stimulation produce two types of structural change in rat hippocampus. *Https://Doi.Org/10.1152/Jn.1980.44.2.247*, *44*(2), 247–258. https://doi.org/10.1152/JN.1980.44.2.247

Lei, Z., Chen, K., Li, H., Liu, H., & Guo, A. (2013). The GABA system regulates the sparse coding of odors in the mushroom bodies of Drosophila. *Biochemical and Biophysical Research Communications*, *436*(1), 35–40. https://doi.org/10.1016/j.bbrc.2013.05.036

Leiss, F., Groh, C., Butcher, N. J., Meinertzhagen, I. A., & Tavosanis, G. (2009a). Synaptic organization in the adult *Drosophila* mushroom body calyx. *The Journal of Comparative Neurology*, *517*(6), 808–824. https://doi.org/10.1002/cne.22184

Leiss, F., Groh, C., Butcher, N. J., Meinertzhagen, I. A., & Tavosanis, G. (2009b). Synaptic organization in the adult *Drosophila* mushroom body calyx. *The Journal of Comparative Neurology*, *517*(6), 808–824. https://doi.org/10.1002/cne.22184

Leitch, B., & Laurent, G. (1996). GABAergic Synapses in the Antenna1 Lobe and Mushroom Body of the Locust Olfactory System. *THE JOURNAL OF COMPARATIVE NEUROLOGY*, *372*(487), 514. https://doi.org/10.1002/(SICI)1096-9861(19960902)372:4

Lent, D. D., Pintér, M., & Strausfeld, N. J. (2007). Learning with half a brain. *Developmental Neurobiology*, *67*(6), 740–751. https://doi.org/10.1002/DNEU.20374

Leuner, B., Falduto, J., & Shors, T. J. (2003). Associative Memory Formation Increases the Observation of Dendritic Spines in the Hippocampus. *Journal of Neuroscience*, *23*(2), 659–665. https://doi.org/10.1523/JNEUROSCI.23-02-00659.2003

Li, F., Lindsey, J., Marin, E. C., Otto, N., Dreher, M., Dempsey, G., Stark, I., Bates, A. S., Pleijzier, M. W., Schlegel, P., Nern, A., Takemura, S., Eckstein, N., Yang, T., Francis, A., Braun, A., Parekh, R., Costa, M., Scheffer, L., … Rubin, G. M. (2020a). The connectome of the adult drosophila mushroom body provides insights into function. *ELife*, *9*, 1–217. https://doi.org/10.7554/eLife.62576

Li, F., Lindsey, J., Marin, E. C., Otto, N., Dreher, M., Dempsey, G., Stark, I., Bates, A. S., Pleijzier, M. W., Schlegel, P., Nern, A., Takemura, S., Eckstein, N., Yang, T., Francis, A., Braun, A., Parekh, R., Costa, M., Scheffer, L., … Rubin, G. M. (2020b). The connectome of the adult drosophila mushroom body provides insights into function. *ELife*, *9*, 1–217. https://doi.org/10.7554/eLife.62576

Li, J., Mahoney, B. D., Jacob, M. S., & Caron, S. J. C. (2020). Visual Input into the Drosophila melanogaster Mushroom Body. *Cell Reports*, *32*(11), 108138. https://doi.org/10.1016/J.CELREP.2020.108138

Lichtman, J. W., Livet, J., & Sanes, J. R. (2008). A technicolour approach to the connectome. *Nature Reviews Neuroscience 2008 9:6*, *9*(6), 417–422. https://doi.org/10.1038/nrn2391

Lin, A. C., Bygrave, A. M., de Calignon, A., Lee, T., & Miesenböck, G. (2014). Sparse, decorrelated odor coding in the mushroom body enhances learned odor discrimination. *Nature Neuroscience*, *17*(4), 559–568. https://doi.org/10.1038/nn.3660

Litwin-Kumar, A., Harris, K. D., Axel, R., Sompolinsky, H., & Abbott, L. F. (2017). Optimal Degrees of Synaptic Connectivity. *Neuron*, *93*(5), 1153-1164.e7. https://doi.org/10.1016/j.neuron.2017.01.030

Liu, C., Plaaąais, P. Y., Yamagata, N., Pfeiffer, B. D., Aso, Y., Friedrich, A. B., Siwanowicz, I., Rubin, G. M., Preat, T., & Tanimoto, H. (2012). A subset of dopamine neurons signals reward for odour memory in Drosophila. *Nature*, *488*(7412), 512–516. https://doi.org/10.1038/nature11304

Liu, X., & Davis, R. L. (2009). The GABAergic anterior paired lateral neuron suppresses and is suppressed by olfactory learning. *Nature Neuroscience*, *12*(1), 53–59. https://doi.org/10.1038/nn.2235

Luo, S. X., Axel, R., & Abbott, L. F. (2010). Generating sparse and selective third-order responses in the olfactory system of the fly. *Proceedings of the National Academy of Sciences of the United States of America*, *107*(23), 10713–10718. https://doi.org/10.1073/pnas.1005635107

M, C., Y, T., G, E., WW, W., & DC, P. (1994). Green fluorescent protein as a marker for gene expression. *Science (New York, N.Y.)*, *263*(5148), 802–805. https://doi.org/10.1126/SCIENCE.8303295

Margulies, C., Tully, T., & Dubnau, J. (2005). Deconstructing Memory in Drosophila. *Current Biology*, *15*(17), R700–R713. https://doi.org/10.1016/J.CUB.2005.08.024

Marin, E. C., Büld, L., Theiss, M., Sarkissian, T., Roberts, R. J. V., Turnbull, R., Tamimi, I. F. M., Pleijzier, M. W., Laursen, W. J., Drummond, N., Schlegel, P., Bates, A. S., Li, F., Landgraf, M., Costa, M., Bock, D. D., Garrity, P. A., & Jefferis, G. S. X. E. (2020). Connectomics Analysis Reveals First-, Second-, and Third-Order Thermosensory and Hygrosensory Neurons in the Adult Drosophila Brain. *Current Biology*, *30*(16), 3167-3182.e4. https://doi.org/10.1016/J.CUB.2020.06.028

Marr, D. (1969). A theory of cerebellar cortex. *The Journal of Physiology*, *202*(2), 437–470. https://doi.org/10.1113/jphysiol.1969.sp008820

Masek, P., Worden, K., Aso, Y., Rubin, G. M., & Keene, A. C. (2015). A dopamine-modulated neural circuit regulating aversive taste memory in drosophila. *Current Biology*, *25*(11), 1535–1541. https://doi.org/10.1016/j.cub.2015.04.027

McGuire, S. E., Le, P. T., & Davis, R. L. (2001). The role of Drosophila mushroom body signaling in olfactory memory. *Science*, *293*(5533), 1330–1333. https://doi.org/10.1126/science.1062622

Meier, M., & Borst, A. (2019). Extreme Compartmentalization in a Drosophila Amacrine Cell. *Current Biology*, *29*(9), 1545-1550.e2. https://doi.org/10.1016/J.CUB.2019.03.070

Miyawaki, A., Llopis, J., Heim, R., McCaffery, J. M., Adams, J. A., Ikura, M., & Tsien, R. Y. (1997). Fluorescent indicators for Ca2+based on green fluorescent proteins and calmodulin. *Nature 1997 388:6645*, *388*(6645), 882–887. https://doi.org/10.1038/42264

Nakai, J., Ohkura, M., & Imoto, K. (2001). A high signal-to-noise Ca2+ probe composed of a single green fluorescent protein. *Nature Biotechnology 2001 19:2*, *19*(2), 137–141. https://doi.org/10.1038/84397

Ohyama, T., Schneider-Mizell, C. M., Fetter, R. D., Aleman, J. V., Franconville, R., Rivera-Alba, M., Mensh, B. D., Branson, K. M., Simpson, J. H., Truman, J. W., Cardona, A., & Zlatic, M. (2015a). A multilevel multimodal circuit enhances action selection in Drosophila. *Nature 2015 520:7549*, *520*(7549), 633–639. https://doi.org/10.1038/nature14297

Ohyama, T., Schneider-Mizell, C. M., Fetter, R. D., Aleman, J. V., Franconville, R., Rivera-Alba, M., Mensh, B. D., Branson, K. M., Simpson, J. H., Truman, J. W., Cardona, A., & Zlatic, M. (2015b). A multilevel multimodal circuit enhances action selection in Drosophila. *Nature 2015 520:7549*, *520*(7549), 633–639. https://doi.org/10.1038/nature14297

Okano, H., Hirano, T., & Balaban, E. (2000). Learning and memory. *Proceedings of the National Academy of Sciences*, *97*(23), 12403–12404. https://doi.org/10.1073/PNAS.210381897

Olsen, S. R., Bhandawat, V., & Wilson, R. I. (2010). Divisive normalization in olfactory population codes. *Neuron*, *66*(2), 287–299. https://doi.org/10.1016/j.neuron.2010.04.009

Olsen, S. R., & Wilson, R. I. (2008). Lateral presynaptic inhibition mediates gain control in an olfactory circuit. *Nature*, *452*(7190), 956–960. https://doi.org/10.1038/nature06864

Owald, D., Felsenberg, J., Talbot, C. B., Das, G., Perisse, E., Huetteroth, W., & Waddell, S. (2015). Activity of defined mushroom body output neurons underlies learned olfactory behavior in Drosophila. *Neuron*, *86*(2), 417–427. https://doi.org/10.1016/J.NEURON.2015.03.025

Papadopoulou, M., Cassenaer, S., Nowotny, T., & Laurent, G. (2011). Normalization for sparse encoding of odors by a wide-field interneuron. *Science*, *332*(6030), 721–725. https://doi.org/10.1126/science.1201835

Pech, U., Revelo, N. H., Seitz, K. J., Rizzoli, S. O., & Fiala, A. (2015). Optical dissection of experience-dependent pre- and postsynaptic plasticity in the Drosophila brain. *Cell Reports*, *10*(12), 2084–2096. https://doi.org/10.1016/j.celrep.2015.02.065

Perez Vicente, C. J., & Amit, D. J. (1989). Optimised network for sparsely coded patterns. *Journal of Physics A: General Physics*, *22*(5), 559–569. https://doi.org/10.1088/0305-4470/22/5/018

Perez-Orive, J., Mazor, O., Turner, G. C., Cassenaer, S., Wilson, R. I., & Laurent, G. (2002). Oscillations and sparsening of odor representations in the mushroom body. *Science*, *297*(5580), 359–365. https://doi.org/10.1126/science.1070502

Petersen, S. E., Fox, P. T., Posner, M. I., Mintun, M., & Raichle, M. E. (1988). Positron emission tomographic studies of the cortical anatomy of single-word processing. *Nature 1988 331:6157*, *331*(6157), 585–589. https://doi.org/10.1038/331585a0

Pitman, J. L., Huetteroth, W., Burke, C. J., Krashes, M. J., Lai, S. L., Lee, T., & Waddell, S. (2011). A pair of inhibitory neurons are required to sustain labile memory in the drosophila mushroom body. *Current Biology*, *21*(10), 855–861. https://doi.org/10.1016/j.cub.2011.03.069

Powell, K., Mathy, A., Duguid, I., & Häusser, M. (2015). Synaptic representation of locomotion in single cerebellar granule cells. *ELife*, *4*(JUNE2015). https://doi.org/10.7554/ELIFE.07290

Prisco, L., Deimel, S. H., Yeliseyeva, H., Fiala, A., & Tavosanis, G. (2021). The anterior paired lateral neuron normalizes odour-evoked activity at the mushroom body calyx. *BioRxiv*, 2021.09.20.461071. https://doi.org/10.1101/2021.09.20.461071

Quinn, W. G., Harris, W. A., & Benzer, S. (1974). Conditioned Behavior in Drosophila melanogaster. *Proceedings of the National Academy of Sciences*, *71*(3), 708–712. https://doi.org/10.1073/PNAS.71.3.708

Raji, J. I., & Potter, C. J. (2021). The number of neurons in Drosophila and mosquito brains. *PLOS ONE*, *16*(5), e0250381. https://doi.org/10.1371/JOURNAL.PONE.0250381

Ray, S., Aldworth, Z. N., & Stopfer, M. A. (2020). Feedback inhibition and its control in an insect olfactory circuit. *ELife*, *9*. https://doi.org/10.7554/ELIFE.53281

Rolls, E. T., & Tovee, M. J. (1995). Sparseness of the neuronal representation of stimuli in the primate temporal visual cortex. *Journal of Neurophysiology*, *73*(2), 713–726. https://doi.org/10.1152/jn.1995.73.2.713

Roostaei, T., Nazeri, A., Sahraian, M. A., & Minagar, A. (2014). The Human Cerebellum: A Review of Physiologic Neuroanatomy. *Neurologic Clinics*, *32*(4), 859–869. https://doi.org/10.1016/J.NCL.2014.07.013

Ryan, K., Lu, Z., & Meinertzhagen, I. A. (2016). The CNS connectome of a tadpole larva of Ciona intestinalis (L.) highlights sidedness in the brain of a chordate sibling. *ELife*, *5*(DECEMBER2016). https://doi.org/10.7554/ELIFE.16962

Sahay, A., Wilson, D. A., & Hen, R. (2011). Pattern Separation: A Common Function for New Neurons in Hippocampus and Olfactory Bulb. In *Neuron* (Vol. 70, Issue 4, pp. 582–588). Cell Press. https://doi.org/10.1016/j.neuron.2011.05.012

Santoro, A. (2013). Reassessing pattern separation in the dentate gyrus. *Frontiers in Behavioral Neuroscience*, *0*(JUL), 96. https://doi.org/10.3389/FNBEH.2013.00096

Scheffer, L. K., Xu, C. S., Januszewski, M., Lu, Z., Takemura, S., Hayworth, K. J., Huang, G. B., Shinomiya, K., Maitlin-Shepard, J., Berg, S., Clements, J., Hubbard, P. M., Katz, W. T., Umayam, L., Zhao, T., Ackerman, D., Blakely, T., Bogovic, J., Dolafi, T., … Plaza, S. M. (2020a). A connectome and analysis of the adult Drosophila central brain. *ELife*, *9*, 1–73. https://doi.org/10.7554/elife.57443

Scheffer, L. K., Xu, C. S., Januszewski, M., Lu, Z., Takemura, S. Y., Hayworth, K. J., Huang, G. B., Shinomiya, K., Maitin-Shepard, J., Berg, S., Clements, J., Hubbard, P. M., Katz, W. T., Umayam, L., Zhao, T., Ackerman, D., Blakely, T., Bogovic, J., Dolafi, T., … Plaza, S. M. (2020b). A connectome and analysis of the adult drosophila central brain. *ELife*, *9*, 1–74. https://doi.org/10.7554/ELIFE.57443

Schweighofer, N., Doya, K., & Lay, F. (2001). Unsupervised learning of granule cell sparse codes enhances cerebellar adaptive control. *Neuroscience*, *103*(1), 35–50. https://doi.org/10.1016/S0306-4522(00)00548-0

Shaner, N. C., Campbell, R. E., Steinbach, P. A., Giepmans, B. N. G., Palmer, A. E., & Tsien, R. Y. (2004). Improved monomeric red, orange and yellow fluorescent proteins derived from Discosoma sp. red fluorescent protein. *Nature Biotechnology 2004 22:12*, *22*(12), 1567–1572. https://doi.org/10.1038/nbt1037

Silver, R. A., Traynelis, S. F., & Cull-Candy, S. G. (1992). Rapid-time-course miniature and evoked excitatory currents at cerebellar synapses in situ. *Nature 1992 355:6356*, *355*(6356), 163–166. https://doi.org/10.1038/355163a0

Simpson, J. H. (2009). Chapter 3 Mapping and Manipulating Neural Circuits in the Fly Brain. *Advances in Genetics*, *65*, 79–143. https://doi.org/10.1016/S0065-2660(09)65003-3

Stocker, R. F., Lienhard, M. C., Borst, A., & Fischbach, K. F. (1990). Neuronal architecture of the antennal lobe in Drosophila melanogaster. *Cell and Tissue Research*, *262*(1), 9–34. https://doi.org/10.1007/BF00327741

Stopfer, M., Jayaraman, V., & Laurent, G. (2003). Intensity versus Identity Coding in an Olfactory System. *Neuron*, *39*(6), 991–1004. https://doi.org/10.1016/J.NEURON.2003.08.011

Sughrue, M. E. (2019). Novel approaches to brain mapping in the era of functional magnetic resonance imaging. *New Techniques for Management of "Inoperable" Gliomas*, 11–18. https://doi.org/10.1016/B978-0-12-813633-1.00003-7

Tabuchi, S., Gilmer, J. I., Purba, K., & Person, A. L. (2019). Pathway-specific drive of cerebellar golgi cells reveals integrative rules of cortical inhibition. *Journal of Neuroscience*, *39*(7), 1169–1181. https://doi.org/10.1523/JNEUROSCI.1448-18.2018

Takemura, S. ya, Nern, A., Chklovskii, D. B., Scheffer, L. K., Rubin, G. M., & Meinertzhagen, I. A. (2017). The comprehensive connectome of a neural substrate for 'ON' motion detection in Drosophila. *ELife*, *6*. https://doi.org/10.7554/ELIFE.24394

Tempel, B. L., Bonini, N., Dawson, D. R., & Quinn, W. G. (1983). Reward learning in normal and mutant Drosophila. *Proceedings of the National Academy of Sciences*, *80*(5), 1482–1486. https://doi.org/10.1073/PNAS.80.5.1482

The Mneme - Richard Wolfgang Semon, Louis Simon - Google Libri. (n.d.). Retrieved October 12, 2021, from https://books.google.de/books/about/The_Mneme.html?id=686StAEACAAJ&redir_esc=y

The structure of the nervous system of the nematode Caenorhabditis elegans. (1986). *Philosophical Transactions of the Royal Society of London. B, Biological Sciences*, *314*(1165), 1–340. https://doi.org/10.1098/RSTB.1986.0056

Tian, L., Hires, S. A., Mao, T., Huber, D., Chiappe, M. E., Chalasani, S. H., Petreanu, L., Akerboom, J., McKinney, S. A., Schreiter, E. R., Bargmann, C. I., Jayaraman, V., Svoboda, K., & Looger, L. L. (2009). Imaging neural activity in worms, flies and mice with improved GCaMP calcium indicators. *Nature Methods 2009 6:12*, *6*(12), 875–881. https://doi.org/10.1038/nmeth.1398

Tsodyks, M. v., & Feigel'man, M. v. (1988). The enhanced storage capacity in neural networks with low activity level. *EPL*, *6*(2), 101–105. https://doi.org/10.1209/0295-5075/6/2/002

Tully, T., & Quinn, W. G. (1985a). Classical conditioning and retention in normal and mutant Drosophila melanogaster. *Journal of Sensory, Comparative .e..., Arid Physiology A .~avio~*, *157*, 263–277.

Tully, T., & Quinn, W. G. (1985b). Classical conditioning and retention in normal and mutantDrosophila melanogaster. *Journal of Comparative Physiology A 1985 157:2*, *157*(2), 263–277. https://doi.org/10.1007/BF01350033

Turner, G. C., Bazhenov, M., & Laurent, G. (2008a). Olfactory representations by Drosophila mushroom body neurons. *Journal of Neurophysiology*, *99*(2), 734–746. https://doi.org/10.1152/jn.01283.2007

Turner, G. C., Bazhenov, M., & Laurent, G. (2008b). Olfactory representations by Drosophila mushroom body neurons. *Journal of Neurophysiology*, *99*(2), 734–746. https://doi.org/10.1152/jn.01283.2007

Tyrrell, T., & Willshaw, D. (1992). Cerebellar cortex: its simulation and the relevance of Marr's theory. *Philosophical Transactions of the Royal Society of London. Series B, Biological Sciences*, *336*(1277), 239–257. https://doi.org/10.1098/rstb.1992.0059

van Harreveld, A., & Fifkova, E. (1975). Swelling of dendritic spines in the fascia dentata after stimulation of the perforant fibers as a mechanism of post-tetanic potentiation. *Experimental Neurology*, *49*(3), 736–749. https://doi.org/10.1016/0014-4886(75)90055-2

Vinje, W. E., & Gallant, J. L. (2000). Sparse coding and decorrelation in primary visual cortex during natural vision. *Science*, *287*(5456), 1273–1276. https://doi.org/10.1126/SCIENCE.287.5456.1273

Vos, B. P., Volny-Luraghi, A., & de Schutter, E. (1999). Cerebellar Golgi cells in the rat: Receptive fields and timing of responses to facial stimulation. *European Journal of Neuroscience*, *11*(8), 2621–2634. https://doi.org/10.1046/j.1460-9568.1999.00678.x

Vosshall, L. B., Wong, A. M., & Axel, R. (2000). An olfactory sensory map in the fly brain. *Cell*, *102*(2), 147–159. https://doi.org/10.1016/S0092-8674(00)00021-0

Wang, G., Zhou, B., Wang, S., Yang, K., Zhao, J., Yang, X., Li, Y., & Shen, L. (2019). The reconstruction and functional mapping of a recurrent microcircuit in Drosophila mushroom body. *BioRxiv*, 819227. https://doi.org/10.1101/819227

Wang, Y., Guo, H.-F., Pologruto, T. A., Hannan, F., Hakker, I., Svoboda, K., & Zhong, Y. (2004). Stereotyped Odor-Evoked Activity in the Mushroom Body of Drosophila Revealed by Green Fluorescent Protein-Based Ca2+ Imaging. *Journal of Neuroscience*, *24*(29), 6507–6514. https://doi.org/10.1523/JNEUROSCI.3727-03.2004

Wanner, A. A., Genoud, C., Masudi, T., Siksou, L., & Friedrich, R. W. (2016). Dense EM-based reconstruction of the interglomerular projectome in the zebrafish olfactory bulb. *Nature Neuroscience 2016 19:6*, *19*(6), 816–825. https://doi.org/10.1038/nn.4290

Wilson, R. I., Turner, G. C., & Laurent, G. (2004). Transformation of Olfactory Representations in the Drosophila Antennal Lobe. *Science*, *303*(5656), 366–370. https://doi.org/10.1126/science.1090782

Withers, G. S., Fahrbach, S. E., & Robinson, G. E. (1993). Selective neuroanatomical plasticity and division of labour in the honeybee. *Nature 1993 364:6434*, *364*(6434), 238–240. https://doi.org/10.1038/364238a0

Wolfe, J., Houweling, A. R., & Brecht, M. (2010). Sparse and powerful cortical spikes. *Current Opinion in Neurobiology*, *20*(3), 306–312. https://doi.org/10.1016/J.CONB.2010.03.006

Wolpert, D. M., Miall, R. C., & Kawato, M. (1998). Internal models in the cerebellum. *Trends in Cognitive Sciences*, *2*(9), 338–347. https://doi.org/10.1016/S1364-6613(98)01221-2

Wu, C. L., Shih, M. F. M., Lee, P. T., & Chiang, A. S. (2013). An octopamine-mushroom body circuit modulates the formation of anesthesia-resistant memory in drosophila. *Current Biology*, *23*(23), 2346–2354. https://doi.org/10.1016/j.cub.2013.09.056

Yamagata, N., Ichinose, T., Aso, Y., Plaçais, P. Y., Friedrich, A. B., Sima, R. J., Preat, T., Rubin, G. M., & Tanimoto, H. (2015). Distinct dopamine neurons mediate reward signals for short- and long-term memories. *Proceedings of the National Academy of Sciences of the United States of America*, *112*(2), 578–583. https://doi.org/10.1073/pnas.1421930112

Yao, C. A., Ignell, R., & Carlson, J. R. (2005). Chemosensory Coding by Neurons in the Coeloconic Sensilla of the Drosophila Antenna. *Journal of Neuroscience*, *25*(37), 8359–8367. https://doi.org/10.1523/JNEUROSCI.2432-05.2005

Yasuyama, K., Meinertzhagen, I. A., & Schürmann, F.-W. (2002a). Synaptic organization of the mushroom body calyx in *Drosophila melanogaster*. *Journal of Comparative Neurology*, *445*(3), 211–226. https://doi.org/10.1002/cne.10155

Yasuyama, K., Meinertzhagen, I. A., & Schürmann, F.-W. (2002b). Synaptic organization of the mushroom body calyx in *Drosophila melanogaster*. *Journal of Comparative Neurology*, *445*(3), 211–226. https://doi.org/10.1002/cne.10155

Zheng, Z., Lauritzen, J. S., Perlman, E., Robinson, C. G., Nichols, M., Milkie, D., Torrens, O., Price, J., Fisher, C. B., Sharifi, N., Calle-Schuler, S. A., Kmecova, L., Ali, I. J., Karsh, B., Trautman, E. T., Bogovic, J. A., Hanslovsky, P., Jefferis, G. S. X. E., Kazhdan, M., … Bock, D. D. (2018).

A Complete Electron Microscopy Volume of the Brain of Adult Drosophila melanogaster. *Cell*, *174*(3), 730-743.e22. https://doi.org/10.1016/j.cell.2018.06.019

Zheng, Z., Li, F., Fisher, C., Ali, I., Sharifi, N., Calle-Schuler, S., Hsu, J., Masoodpanah, N., Kmecova, L., Kazimiers, T., Perlman, E., Nichols, M., Li, P., Jain, V., & Bock, D. (2020). Structured sampling of olfactory input by the fly mushroom body. *BioRxiv*, 2020.04.17.047167. https://doi.org/10.1101/2020.04.17.047167